

Multi-GNSS precise position, velocity, and acceleration determination for airborne gravimetry over Antarctica

vorgelegt von

M.Sc.

Min Li

ORCID: 0000-0003-3053-6669

an der Fakultät VI – Planen Bauen Umwelt
der Technischen Universität Berlin
zur Erlangung des akademischen Grades

Doktorin der Ingenieurwissenschaften

- Dr. -Ing. -

genehmigte Dissertation

Promotionsausschuss:

Vorsitzender: Prof. Dr. Harald Schuh

Gutachter: Prof. Dr. Frank Flechtner

Gutachter: Prof. Dr. Robert Weber (TU Wien)

Gutachter: Prof. Dr. Maorong Ge

Tag der wissenschaftlichen Aussprache: 10. September 2019

Berlin 2020

Abstract

The precise knowledge of aircraft position, velocity, and acceleration is a mandatory prerequisite for airborne gravimetry. For the determination of these quantities the Global Navigation Satellite System (GNSS) plays an important role. However, kinematic positioning over Antarctica is a challenging task which is different from positioning in low-latitude regions. The main reason is the sparse distribution of International GNSS Service (IGS) ground stations which is also difficult or impractical to be densified by setting up dedicated reference stations because of its hostile environment. Therefore, traditional double-differenced (DD) positioning using Global Positioning System (GPS) may be difficult to be applied. Precise Point Positioning (PPP) using a stand-alone receiver is recognized as a helpful tool for obtaining reliable and accurate trajectories of moving platforms based on precise orbit and clock products derived from a global reference network. On the one hand, the accuracy of real-time products cannot yet meet the requirement of trajectory recovery for airborne gravimetry, on the other hand the IGS final products still have day-boundary discontinuity and products of newly emerging systems is proved with regional biases which could contaminate the PPP integer ambiguity resolution considerably. Therefore, it is necessary to study the special characteristics of positioning over Antarctica and to exploit innovative and reliable approaches for precise position, velocity and acceleration determination. The core research topics and contributions to solve these questions within this thesis are summarized as follows:

An extended precise positioning method called Precise Orbit Positioning (POP), which was originally developed in Salazar et al. (2009), is further developed towards application with multi-GNSS data. This approach takes advantage of a widely spaced network of ground stations to estimate satellite clock offsets and drifts and only relies on precise orbit information. Within an experiment with 5 IGS stations over Antarctica, it turned out that the PPP solution is greatly affected by the discontinuities of IGS analysis center orbit and clock offsets (5 min and 30 s sampling, respectively) at the day boundaries, accompanied with biases as large as several decimeters in the vertical component. In contrast, the POP solution performs very robust with almost no large positioning errors and the accuracy is improved by about 50% in the North, East and Up coordinate components compared to the PPP solution. The advantage of being

independent of clock information is that POP can be applied for real-time performance using, i.e., the IGS ultra-rapid (predicted) products with an accuracy of about 5 cm. This is not only important for time-critical applications but also significant when applied to airborne gravimetry, as gravity results calculated from gravity measurements and GNSS solutions can be investigated in real time. Although the aircraft trajectories derived from traditional DD, PPP and POP generally agree at the decimeter level possibly because of the lack of observed satellites with elevation angles higher than 60° , it is illustrated that the decimeter level errors are mostly from the PPP solutions at the day boundaries, and POP has the potential to achieve centimeter-level accuracy for the vertical component with sparse distributed reference stations.

As is well known, PPP and its related integer ambiguity fixing performance can be much degraded by satellite orbits and clocks of poor quality, such as that of current Geostationary Earth Orbit (GEO) satellites of the Chinese BeiDou Navigation Satellite System (BDS), due to temporal variation of orbit errors that cannot be fully absorbed by ambiguities. To overcome this problem, the POP approach was implemented and compared with PPP in terms of integer ambiguity fixing and trajectory accuracy. In a simulation test, multi-GNSS observations from 136 globally distributed receivers of the IGS Multi-GNSS Experiment (MGEX) network were used and four of them in Antarctica were processed in kinematic mode as moving stations. The result shows that POP can improve the ambiguity fixing of dual- and four-system combinations and significant improvement is found especially for the BDS solution due to its large orbit errors. The GPS+GLONASS+Galileo+BDS ambiguity fixed solution enables the highest 3D position accuracy of about 3.0 cm compared to 4.3 cm of the GPS-only solution. Within a real flight experiment over Antarctica, it is also confirmed that POP ambiguity fixing performs better and can considerably reduce the fluctuations and noises in estimated trajectories and can also speed up (re-)convergence of the solution compared to that of PPP solutions. It becomes significant when ambiguity fixing is applied to airborne kinematic positioning over Antarctica since the continuous tracking time is usually short compared to that in other regions.

The aforesaid POP method is extended further to derive reliable and high accurate velocity and acceleration which are more important than position for

airborne gravimetry. A GPS+GLONASS+Galileo+BDS four-system model is presented and proper weighting of different types of observations is investigated. The PPP solutions are also calculated with multi-GNSS observations for comparison. The results show that compared to an Equivalent Weight Ratio (EWR), it is more appropriate and efficient to assign the weights using a Posteriori Weight Ratio (PWR). During static tests over Antarctica, it was found that POP derived velocity and acceleration tend to have much lower noise than the PPP solutions. Moreover, the addition of GLONASS, Galileo and BDS data can increase the accuracy of velocity and acceleration estimates by 32% and 43% with POP compared to a GPS-only solution when using data of 30-second sampling interval and the improvements are 28% and 31% with respect to the PPP solutions.

For the purpose of airborne gravimetry, the L1 observable is suggested for acceleration determination because of its lower observation noise. Within processing of two real flight data sets, it was found that the baseline length is also critical for velocity and acceleration determination using the traditional DD method. Biases as large as several cm/s could appear in velocity estimates when the baseline length reaches several hundred kilometers. However, the POP velocity results turned out to be still robust showing almost no biases or outliers. The derived vertical accelerations were found to be at the 1 mGal level and thus sufficient to separate the disturbing kinematic accelerations affecting the airborne platform from the gravity measurements.

Keywords: PPP; double-difference; position; velocity; acceleration; ambiguity fixing; global network; orbit error; clock offsets and drifts; airborne gravimetry; Antarctica; GPS; GLONASS; Galileo; BDS

Zusammenfassung

Die genaue Kenntnis der Flugzeugposition, -geschwindigkeit und -beschleunigung ist eine zwingende Voraussetzung für die gravimetrische Vermessung aus der Luft. Für die Bestimmung dieser Größen spielt das Global Navigation Satellite System (GNSS) eine wichtige Rolle. Die kinematische Positionierung über der Antarktis ist jedoch eine anspruchsvolle Aufgabe, die sich von der Positionierung in Regionen mit niedriger Breite unterscheidet. Der Hauptgrund ist die spärliche Verteilung der Bodenstationen des Internationalen GNSS-Dienstes (IGS), die zudem aufgrund der widrigen Bedingungen in der Antarktis nur sehr schwierig durch die Einrichtung spezieller Referenzstationen verdichtet werden kann. Daher ist es schwierig, die traditionelle Doppeldifferenzmessung (DD) mit dem Global Positioning System (GPS) anzuwenden. Die präzise Punktpositionierung (PPP) mit einem eigenständigen Empfänger ist als hilfreiche Methode zur Erzielung zuverlässiger und genauer Trajektorien von bewegten Plattformen auf der Grundlage von präzisen Orbit- und Uhrenprodukten aus einem globalen Referenznetzwerk anerkannt. Einerseits kann die Genauigkeit von Echtzeitprodukten die Anforderung an die Trajektoriengewinnung für die luftgestützte Gravimetrie noch nicht erfüllen, andererseits weisen die IGS-Endprodukte noch eine tagesgebundene Diskontinuität auf. Zudem wurden bei Produkten neuerer GNSS-Systeme regionale Verzerrungen nachgewiesen, die die ganzzahlige Mehrdeutigkeitsauflösung der PPP erheblich verschlechtern können. Daher ist es notwendig, die besonderen Eigenschaften der Positionierung über der Antarktis zu untersuchen und innovative und zuverlässige Ansätze zur präzisen Positions-, Geschwindigkeits- und Beschleunigungsbestimmung zu entwickeln. Die Forschungsschwerpunkte und Beiträge zur Lösung dieser Fragen innerhalb dieser Arbeit sind wie folgt zusammengefasst:

Eine erweiterte präzise Positionierungsmethode namens Precise Orbit Positioning (POP), die ursprünglich in Salazar et al. (2009) entwickelt wurde, wurde in Richtung der Anwendung mit Multi-GNSS-Daten weiterentwickelt. Dieser Ansatz nutzt ein weit verzweigtes Netz von Bodenstationen, um Versatz und Drift der Satellitenuhren zu schätzen und stützt sich nur auf präzise Orbitinformationen. In einem Experiment mit 5 IGS-Stationen über der Antarktis stellte sich heraus, dass die PPP-Lösung stark von den Diskontinuitäten der IGS-Analysezentrumsbahn und der Uhrenversätze (5

Minuten bzw. 30 Sekunden Sampling) an den Tagesgrenzen beeinflusst wird, begleitet von Biasen bis zu mehreren Dezimetern in der vertikalen Komponente. Im Gegensatz dazu arbeitet die POP-Lösung sehr robust und weist fast keine großen Positionierungsfehler auf. Die Genauigkeit wird bei den Nord-, Ost- und Vertikal-Koordinatenkomponenten um etwa 50% gegenüber der PPP-Lösung verbessert. Der Vorteil der Unabhängigkeit von Uhreninformationen besteht darin, dass POP für Echtzeitlösungen z.B. mit den ultra-schnellen (vorhergesagten) IGS-Produkten mit einer Genauigkeit von ca. 5 cm eingesetzt werden kann. Dies ist nicht nur für zeitkritische Anwendungen wichtig, sondern auch für die Fluggravimetrie, da die Schwerefeldergebnisse, berechnet aus Schwerebeobachtungen und GNSS-Lösungen, in Echtzeit untersucht werden können. Obwohl die Flugbahnen, die von traditionellen DD, PPP und POP abgeleitet werden, im Allgemeinen nur auf Dezimeterskalen übereinstimmen, möglicherweise aufgrund des Fehlens beobachteter Satelliten mit Elevationswinkeln über 60° , wird veranschaulicht, dass die Dezimeterfehler größtenteils von den PPP-Lösungen an den Tagesgrenzen stammen und POP dagegen das Potenzial hat, eine Zentimetergenauigkeit für die vertikale Komponente mit spärlich verteilten Referenzstationen zu erreichen.

Bekanntlich können PPP und die damit verbundene Fähigkeit der ganzzahligen Mehrdeutigkeitsfixierung durch ungenaue Satellitenbahnen und -uhren, wie die der geostationären Satelliten (GEO) des chinesischen BeiDou-Navigationssatellitensystems (BDS), aufgrund zeitlicher Schwankungen von Orbitfehlern, die von Mehrdeutigkeiten nicht vollständig absorbiert werden können, erheblich beeinträchtigt werden. Um dieses Problem zu lösen, wurde der POP-Ansatz implementiert und mit PPP in Bezug auf die ganzzahlige Mehrdeutigkeitsfixierung und Trajektoriengenauigkeit verglichen. In einem Simulationstest wurden Multi-GNSS-Beobachtungen von 136 weltweit verteilten Empfängern des IGS Multi-GNSS Experiment (MGEX)-Netzes verwendet und vier davon in der Antarktis kinematisch als bewegliche Stationen verarbeitet. Das Ergebnis zeigt, dass POP die Mehrdeutigkeitsfixierung von Zwei- und Vier-Systemkombinationen verbessern kann und insbesondere für die BDS-Lösung aufgrund ihrer großen Orbitfehler erhebliche Verbesserungen erzielt werden. Die mehrdeutigkeitsfixierte GPS+GLONASS+Galileo+BDS Lösung ermöglicht die höchste 3D-Positionsgenauigkeit von ca. 3,0 cm gegenüber 4,3 cm der reinen GPS-Lösung.

Im Rahmen eines realen Flugexperiments über der Antarktis wird zudem bestätigt, dass die POP-Mehrdeutigkeitsfixierung besser funktioniert, da die Fluktuationen und das Rauschen in den geschätzten Trajektorien erheblich reduziert werden kann und auch die (Re-)Konvergenz der Lösung im Vergleich zu PPP-Lösungen beschleunigt werden kann. Die Methode wird signifikant, wenn die Mehrdeutigkeitsfixierung bei der luftgestützten kinematischen Positionierung über der Antarktis angewendet wird, da die kontinuierliche Trackingzeit im Vergleich zu anderen Regionen in der Regel kurz ist.

Die vorgenannte POP-Methode wurde weiter ausgebaut, um zuverlässige und hochpräzise Geschwindigkeit und Beschleunigung abzuleiten, die für die luftgestützte Gravimetrie wichtiger sind als die Position. Ein GPS+GLONASS+Galileo+BeiDou Viersystemmodell wird vorgestellt und die richtige Gewichtung verschiedener Arten von Beobachtungen untersucht. Die PPP-Lösungen werden auch mit Multi-GNSS-Beobachtungen zum Vergleich berechnet. Die Ergebnisse zeigen, dass es im Vergleich zu einem Äquivalentgewichtsverhältnis (EWR) sinnvoller und effizienter ist, die Gewichte mit einem Posteriori Weight Ratio (PWR) zuzuordnen. Bei statischen Tests über der Antarktis wurde festgestellt, dass die von POP abgeleitete Geschwindigkeit und Beschleunigung tendenziell viel weniger verrauscht sind als die PPP-Lösungen. Darüber hinaus kann die Hinzufügung von GLONASS-, Galileo- und BDS-Daten die Genauigkeit der Geschwindigkeits- und Beschleunigungsschätzungen um 32% bzw. 43% gegenüber einer reinen GPS-Lösung bei Verwendung von Daten mit einem Abtastintervall von 30 Sekunden erhöht werden. Die Verbesserungen liegen dann bei 28% bzw. 31% gegenüber den PPP-Lösungen.

Für die luftgestützte Gravimetrie wird die Verwendung der L1-Beobachtung aufgrund ihres geringeren Beobachtungsrauschens zur Beschleunigungsbestimmung vorgeschlagen. Bei der Verarbeitung von zwei realen Flugdatensätzen wurde festgestellt, dass die Basislänge zwischen den verwendeten Bodenstationen auch für die Bestimmung von Geschwindigkeit und Beschleunigung mit der traditionellen DD-Methode entscheidend ist. Verzerrungen von bis zu mehreren cm/s können bei Geschwindigkeitsschätzungen auftreten, wenn die Grundlinienlänge mehrere hundert Kilometer erreicht. Die POP-Geschwindigkeitsergebnisse erwiesen sich jedoch als noch robust und zeigten fast keine Verzerrungen oder Ausreißer. Die abgeleiteten

Vertikalbeschleunigungen lagen auf dem Niveau von 1 mGal und reichen damit aus, um die störenden kinematischen Beschleunigungen, die das Flugzeug beeinflussen, von den Schwerkraftmessungen zu trennen.

Stichworte: PPP; Doppeldifferenz; Position; Geschwindigkeit; Beschleunigung; Mehrdeutigkeiten-Fixierung; Globales Netz; Bahnfehler; Uhrenoffsets und -driften; Fluggravimetrie; Antarktis; GPS; GLONASS; Galileo; BDS

Table of contents

Abstract	i
Zusammenfassung	iv
Table of contents	vii
List of Acronyms	x
List of Related Publications	xii
1 Introduction	1
1.1 Motivation.....	1
1.2 Background.....	2
1.2.1 Airborne gravimetry.....	2
1.2.2 GNSS applied in airborne gravimetry.....	5
1.2.3 Basic principle of airborne gravimetry.....	7
1.3 Challenges and research objectives.....	7
1.4 Overview of dissertation.....	12
2 Precise Orbit Positioning with GPS and GLONASS data	14
2.1 GNSS observation model.....	14
2.2 Antarctica data processing.....	17
2.2.1 Validation with the static data.....	18
2.2.2 Validation with the real flight kinematic data.....	24
2.2.3 POP real-time performance.....	27
2.3 Conclusions.....	28
3 Multi-GNSS PPP and POP ambiguity fixing	30
3.1 Ambiguity fixing.....	31
3.2 BDS ambiguity fixing.....	32
3.3 Validation with IGS data.....	35
3.3.1 Data description.....	35
3.3.2 Performance of Ambiguity Fixing.....	37
3.3.3 Performance of positioning.....	39
3.4 Result of a real flight experiment.....	42
3.5 Conclusions.....	46
4 Precise velocity and acceleration determination	48
4.1 GPS/GLONASS/Galileo/BDS velocity estimation procedures.....	50
4.2 Combination of different types of observations.....	55
4.3 Static experiments over Antarctica.....	56
4.3.1 Data description.....	56
4.3.2 Performance assessment of the POP method using GPS data.....	57

4.3.3 Performance assessment of the POP and PPP methods using multi-GNSS data	59
4.4 A real flight experiment.....	63
4.4.1 The first data set processing.....	63
4.4.2 The second data set processing.....	68
4.5 Conclusions.....	72
5 Miscellanea of velocity and acceleration determination.....	75
5.1 Real-time velocity and acceleration determination.....	75
5.2 Differentiator design.....	77
5.3 Receiver clock reset.....	79
5.4 Summary.....	82
6 Conclusions and outlooks.....	83
References.....	86
Acknowledgments.....	94

List of Acronyms

BDS	the Chinese BeiDou Navigation Satellite System
BKG	Bundesamt für Kartographie und Geodäsie (i.e., Federal Agency for Cartography and Geodesy, Germany)
CASERTZ	Corridor Aerogeophysics of the Southeast Ross Transect Zone
CODE	Centre for Orbit Determination in Europe
CSNO	China Satellite Navigation Office
DD	Double-Difference
ECC	Eccentric satellites
ECEF	the Earth centered Earth fixed reference frame
EIGEN-6C4	the European Improved Gravity model of the Earth by New techniques
ESA	European Space Agency
EWR	Equivalent Weight Ratio
FDMA	Frequency Division Multiple Access
FFT	Fast Fourier Transform
FOC	Full Operational Capability
Galileo	the European Union navigation satellite system
GEO	Geostationary Earth Orbit
GEOHALO	the German GEOScience High Altitude and LONG range research project
GFZ	Deutsches GeoForschungsZentrum (the German Research Centre for Geosciences)
GIOVE	Galileo In-Orbit Validation Element
GLONASS	the Russian GLOBal Navigation Satellite System
GNSS	Global Navigation Satellite System
GOCE	Gravity field and steady-state Ocean Circulation Explorer
GPS	Global Positioning System
GPSTk	GPS Tool kit
GRACE	the Gravity Recovery and Climate Experiment satellite
HDOP	Horizontal Dilution Of Precision
HMW	the Hatch-Melbourne-Wübbena wide-lane combination

IGS	International GNSS Service
IGSO	Inclined Geo-synchronous Orbit
IOV	In-Orbit Validation
IFB	Inter-frequency Bias
ISB	Inter-system Bias
LC	Ionosphere-free Linear Combination
LEO	Low Earth Orbit
MGEX	the IGS Multi-GNSS Experiment
MEO	Medium altitude Earth Orbit
NL	Narrow-Lane
NOAA	National Oceanic and Atmospheric Administration
NRC	the US National Research Council
NRL	the US Naval Research Laboratory
PNT	Positioning, Navigation, and Timing
POP	Precise Orbit Positioning
PPP	Precise Point Positioning
PWR	Posteriori Weight Ratio
RMS	Root Mean Square
RTK	Real-Time Kinematic
RTPP	the IGS Real-Time Pilot Project
SP3	Standard Product 3
STD	Standard deviation
SV	Space Vehicle
TEC	Total Electron Content
UD	Un-differenced
UPD	Uncalibrated Phase Delay
UTC	Universal Time Coordinated
VADASE	Variometric Approach for Displacements Analysis with Stand-alone Engine
VDOP	Vertical Dilution of Precision
WL	Wide-Lane

List of Related Publications

1. Li, M., T. Xu, B. Lu, and K. He (2019), Multi-GNSS Precise Orbit Positioning for airborne gravimetry over Antarctica, *GPS Solut.*, 23(2), doi:10.1007/s10291-019-0848-9.
2. Li, M., K.H. Neumayer, F. Flechtner, B. Lu, C. Förste, K. He, T. Xu (2018), Performance assessment of multi-GNSS precise velocity and acceleration determination over Antarctica, *Journal of Navigation*, 72(1), 1-18, doi:10.1017/S0373463318000656.
3. Li, M., T. Xu, F. Flechtner, C. Förste, B. Lu, K. He (2019), Improving the performance of multi-GNSS ambiguity fixing for airborne kinematic positioning over Antarctica, *remote sensing*, 11(8), 992, doi:10.3390/rs11080992.

The paper 1 contributed to the Chapter 2; The paper 3 contributed to the Chapter 3; The papers 1 and 2 contributed to the Chapter 4.

1 Introduction

1.1 Motivation

The Earth's gravity field and its temporal variations are very important for many scientific and economic applications, such as geodesy (Montenbruck and Gill, 2000; Bock et al., 2003), geophysics explorations (Forsberg and Sideris, 1993; Novák et al., 2003), geologic applications (Forsberg et al., 1997; Bell et al., 1999; Neumeyer et al., 2006), etc. Airborne gravimetry plays a significant role to acquire medium and high-resolution information about the Earth's gravity field to close the gap between the terrestrial gravity field measurements on the ground, e.g. from gravimeters, and the global gravity models based on the satellite gravimetry.

The trajectory and attitude of a moving platform are indispensable information for analyzing airborne gravimetry data. The acceleration is used to separate the kinematic disturbing information affecting the platform from the gravity measurements. Therefore, precise position, velocity and acceleration are all crucial for airborne gravimetry (Christian and Guenter, 2003; Forsberg and Olesen, 2010).

Nowadays, the Global Navigation Satellite System (GNSS) is widely used to obtain precise position, velocity and acceleration information. However, the determination of GNSS based precise position and velocity faces the following special challenges in Antarctica. First, the conventional differential positioning is difficult to apply over Antarctica since there is a sparse distribution of reference stations of the International GNSS Service (IGS), and their inter-station distances can be up to thousands of kilometers which is beyond the range of single-baseline differential positioning. It is also very difficult to set up a reference station due to the critical weather conditions and the adamant soil layers. Second, the satellites observed over Antarctica are usually tracked at lower elevation because of the orbit inclination that may degrade the accuracy of the position and velocity estimates in the vertical component. Additionally, the relatively shorter continuous observation periods may cause difficulties for integer ambiguity resolution which can usually improve the positioning accuracy significantly. Third, the velocity estimates may be easily contaminated by the frequent ionospheric fluctuations over the polar regions, while its impact on the acceleration is not yet clearly studied, although twice time-derivatives of the carrier

phase measurements can reduce such effect. Thus, the effect of ionospheric fluctuations on both velocity and acceleration estimation still requires thorough investigation when performed over Antarctica. Finally, multi-GNSS can improve the positioning accuracy and reliability considerably compared to a single system. However, further investigation is still required for multi-GNSS kinematic positioning over Antarctica, especially under highly dynamic flight conditions. Therefore, the research motivation of this thesis is to develop and evaluate reliable and practical approaches to overcome the above specific problems of positioning, velocity and acceleration determination over Antarctica for airborne gravimetry.

1.2 Background

1.2.1 Airborne gravimetry

The gravity field is important and valuable in many scientific applications, such as to define geoid heights, to reflect the Earth's interior, or to study the movement of water in the oceans. Gravity measurement techniques have progressed from terrestrial point measurement, to shipborne gravimetry, to deriving gravity from the perturbations of satellite orbits, and most recently to airborne gravimetry (Kennedy, 2002a; Schlamminger, 2018). Airborne gravimetry is a comparatively economical and efficient measurement technique, which can be applied anywhere an aircraft can fly over. One advantage of airborne gravimetry is that it enables fast acquisition of gravity data. Another is that it can be applied in large, inaccessible and remote areas, such as coastal, polar and mountains regions, where gravity observation gaps are often left by other measurement techniques. When airborne gravimetry was first attempted in the 1960s (LaCoste, 1967), it had been demonstrated capable of meeting many medium resolution requirements such as local and regional geological studies and sub-ice topography (Bell et al., 1999), geoid and coastal oceanography (Forsberg et al, 2001), or geophysics exploration applications (Salychev and Schwarz, 1995; Ferguson and Hammada, 2000), just to name a few examples. It was concluded in these experiments that airborne gravimetry is able to measure gravity with a standard deviation between 0.5 and 3 mGal (10^{-5} m/s²) at a spatial resolution of about 10 km. The resolution here is defined as the minimum recoverable half wavelength of the gravity signal.

In the last decade, a dedicated airborne gravimetry campaign was carried out during the GEOHALO (GEOscience High Altitude and LOng range research project) mission over Italy. The gravimetry sensors were mounted on a business jet G550 aircraft (Figure 1.1, upper left) which flew at a high speed of about 450 km/h along the survey tracks. The final gravity results after extracting the disturbing GNSS accelerations (applying a low-pass) are comparable with the global gravity field model EIGEN-6C4 with an agreement of 1.94 mGal in terms of root mean square (RMS) of the residuals at a resolution of about 20 km (He, 2015).

Airborne gravimetry over polar regions had already been carried out several times since the 1990s. The US Naval Research Laboratory (NRL) together with the National Oceanic and Atmospheric Administration (NOAA), and the Danish National Survey carried out gravity surveys between 1992 and 1999 covering large parts of the Arctic Ocean, with an accuracy level of around 2 mGal at 15 km resolution (Brozena et al., 1996). An Orion P-3 aircraft (Figure 1.1, upper right) was used to conduct this high altitude (~4.1 km), high speed (~400 km/h) and long range experiment.

An aero-geophysical survey over the West Antarctica ice sheet was performed to recover the free-air gravity anomalies over the West Antarctica area (Bell et al., 1999). The geophysical survey covered a 300,000 km² region in West Antarctica over the course of five field seasons. Finally, the free-air gravity anomaly was determined at an accuracy of 1.39 mGal RMS after crossover adjustment. The gravity data from this survey reveal the major geologic structures of the West Antarctica rift system, including the mountains, basins, ridges and domes.

Airborne gravity surveys were also carried out over Antarctica, such as the CASERTZ (Corridor Aerogeophysics of the Southeast Ross Transect Zone) Antarctica Program (Bell et al., 1990). In this campaign, a small kind of aircraft like the Twin-Otter (Figure 1.1, lower left) was used because of its excellent performance of low dynamics at low air speed. With high quality gravity measurements at a typical resolution of 4-6 km, the estimated gravity anomaly can be achieved with an accuracy of 1-2 mGal RMS.



Figure 1.1 The GEOHALO aircraft (upper left), the Orion P-3 aircraft (upper right) and the Twin-Otter aircraft (lower left and right).

One recent airborne gravimetry, the ESA PolarGAP gravity field campaign, was carried out in the period between December 7, 2015 and January 19, 2016 using also a Twin-Otter aircraft (Figure 1.1, lower right). The primary objective of this campaign was to fill the Southern polar gap of the ESA gravity field mission GOCE (Gravity field and steady-state Ocean Circulation Explorer), which is beyond the coverage of the GOCE orbit up to South of 83.5° in latitude (Jordan et al., 2016). With the successful completion of this campaign, the final airborne gravity solutions with an overall accuracy of about 2 mGal are useful to overcome the GOCE polar gap problem (Lu et al., 2019).

In recent years, new gravity acceleration sensors such as the Fugro airborne gravity system and multi-GNSS combined processing have resulted in airborne survey accuracy of 1 mGal or less at a resolution of several kilometers when operated over small regions (Williams and MacQueen, 2001; Olesen, 2002; Mogren, 2019), or at a resolution of tens of kilometers in a large area of continental scale (Jordan et al., 2016; Lu et al., 2017).

1.2.2 GNSS applied in airborne gravimetry

When the United States Global Positioning System (GPS) was first applied in the late 1980s, its applicability for airborne gravimetry became recognized. In the early studies, the differential GPS technique had always been proven as the key to derive the trajectory and velocity. During 1980–1990s, GPS pseudorange observations were mainly used in airborne experiments which was not sufficient for most airborne applications (Brozena et al., 1989). The development of the differential technique using carrier phase observations started from the 1990s, when the accuracy of positions and velocities have reached a useful level and air- and shipborne gravimetry could actually be carried out with a higher accuracy and resolution. Since then, a vast of researches reported that an accuracy of about 0.1 m position in the vertical component can be obtained (Cannon et al., 1997; Han, 1997; Han and Rizos, 1999; Castleden et al., 2005). The vertical accelerations were then calculated based on twice time derivatives of these vertical positions (Brozena et al., 1989; Kleusberg, 1990; van Dierendonck et al., 1994). However, the derived accelerations are strongly dependent on the position accuracy, and discontinuities may be introduced by gaps in the positional series (Bruton, 2000). Additionally, such accelerations tend to have a large noise even if they are calculated carefully with proper differentiators.

In Kleusberg and Wells (1990) and Jekeli and Garcia (1997), the accelerations were calculated in an alternative way which is directly estimated from the epoch-differenced carrier phase measurements. The benefit of this method is that some critical issues for precise position estimation are no longer required, i.e., the integer ambiguity resolution. Kennedy et al. (2001) first made a comparison of the carrier phase derived accelerations with that from the position differentiation and showed preliminary promising results of this method for being better suited for acceleration estimation in airborne gravimetry. Since then, the carrier phase method had always been used for acceleration determination for high accuracy and high resolution airborne gravimetry (Kennedy, 2002b; van Graas and Soloviev, 2004; Mostafa, 2005; Zhang et al., 2017).

Besides the differential technique, the undifferenced technique using a standalone receiver has also been applied in airborne gravimetry. Zhang and Forsberg (2007) analyzed the Precise Point Positioning (PPP) kinematic positioning errors in a large area with an operation distance of thousands of kilometers by comparison with

airborne laser altimetry and satellite altimetry and the potential of PPP for generating 10 cm level kinematic heights over a large area was illustrated. Gerlach et al. (2010) calculated the gravity disturbances by combining GNSS accelerations calculated from float PPP solutions and quantities derived from an inertial measurement. The resulting standard deviation (STD) of the differences of the gravity disturbance estimates was 3.3 mGal at 24 crossover points.

Colosimo et al. (2011) proposed the Variometric Approach for Displacements Analysis with Stand-alone Engine (VADASE), in which the change of position (delta position) between two adjacent epochs is determined by single-differencing of the carrier phase observations. It is regarded that the delta position over a certain time is basically equivalent to a velocity, and therefore it can also be applied in aero-gravimetry. In fact, this approach is theoretically equivalent to PPP for deriving the velocity since the essentials of both approaches are differentiation of the carrier phase measurements and no reference stations are required for both of them. This approach can sense real-time velocities with accuracy of 1 cm/s in horizontal and 2 cm/s in vertical. Zhang et al. (2017) applied this approach to an airborne gravimetry campaign carried out in central China in 2015. First the aircraft velocities were estimated and then the accelerations were calculated from the velocities by using a Taylor approximation differentiator. It was found that the accelerations have almost the same accuracy of that calculated from double-difference (DD) positioning and PPP approaches. The accuracy of the gravity results was approximately 3–4 mGal with respect to in-situ terrestrial gravity data.

A network based approach named Precise Orbit Positioning (POP) (Salazar et al., 2009) was applied in airborne kinematic positioning and velocity determination. POP aims at overcoming the shortcomings of the baseline limitations of the differential technique. Its positioning performance has been assessed in a network in Southern Europe with baselines of hundreds of kilometers. A 3D RMS error of 0.046 m was obtained for kinematic PPP, whereas POP produced a comparable accuracy of 0.049 m (Salazar et al., 2009). The POP method was also applied for precise velocity and acceleration determination in a low dynamic flight over Spain and showed similar performance as the RTK (Real-Time Kinematic) method (Salazar et al., 2011). When applied to a network in equatorial South America with baselines longer than 1,770 km,

the results showed its clear advantages in long-range scenarios when compared with the RTK solutions.

1.2.3 Basic principle of airborne gravimetry

In principle, in an airborne gravimetry mission, the total accelerations are measured by a gravimeter along the travelling trajectory. Accelerations due to the movement of the aircraft are measured by GNSS. The difference between these two accelerations is the effect of the gravity field (Kennedy, 2002a; Schaller et al., 2019).

Generally, the scalar gravimetry is most common. We therefore define the measurement model of scalar airborne gravimetry in an inertial system (Schwarz and Li, 1997) as

$$\delta g = \dot{v} - f_u + (f_0 - f_b) + \delta g_E - \gamma \quad (1.1)$$

where δg is the gravity disturbance; \dot{v} is the vertical acceleration component of the aircraft calculated from the time derivative of the velocity; f_u denotes the superposition of all vertical accelerations measured by the gravimeter; f_0 is the gravity measured by the gravimeter at the base station, i.e. the airport; f_b represents the reference gravity value at the base station; δg_E contains all kinds of error corrections, including the Eötvös correction (Moritz, 1980), horizontal acceleration correction (LaCoste, 1967) and free-air correction (Olesen, 2002), etc; γ is the normal gravity at sea level (Forsberg and Olesen, 2010).

In order to achieve high accuracy gravity at high resolutions for some geophysical exploration applications such as the petroleum prospecting, an often-quoted requirement is 1 mGal accuracy at 1 km resolution (NRC, 1995; Kennedy, 2002a). To meet this requirement, the accuracy of GNSS derived vertical position and velocity is required at the cm, and mm/s level, respectively. Since this is still a big challenge, it is regarded that the GNSS vertical acceleration has become the dominant error source in airborne gravimetry.

1.3 Challenges and research objectives

The traditional differential technique faces new challenges when applied in airborne kinematic positioning over Antarctica. First, there is a sparse distribution of IGS

stations in Antarctica and their baselines can be up to thousands of kilometers, which is beyond the range of differential positioning. The adamant soil layers and harsh weather conditions (ultra-low temperatures and strong winds) in Antarctica make it difficult to establish and maintain a continuously operating reference station network to meet adequate and remarkable relative positioning performance. To reduce expenses, usually only one reference station would be installed with an operating radius of several hundred kilometers. For such a long baseline, the single-baseline differential positioning is not always reliable (He et al., 2016; Yalvac et al., 2018). As the length of the baseline increases, the number of available DD observations decreases and distance-dependent problems such as reliable carrier phase ambiguity resolution may appear. In addition, compared to positioning in low-latitude regions, the relatively short continuous observation time would not be beneficial to the estimation of the carrier phase ambiguities. These all make differential positioning over Antarctica meet great challenges.

PPP (Malys and Jensen, 1990; Zumberge et al., 1997; Kouba and Heroux, 2001) is a flexible, cost-effective technique that has been widely used in geodesy and geodynamical applications. It has powerful capabilities for airborne kinematic positioning (Zhang and Forsberg, 2007). During the last decade, it had been demonstrated that PPP opened up an alternative way for the trajectory recovery of long range flights.

However, PPP requires precise orbit and clock information, and its related ambiguity resolution can be contaminated by the region-dependent biases in the products, especially for the newly emerged GNSS systems. Additionally, the IGS final orbits and clocks are daily products and PPP will also be severely affected by the orbit and clock discontinuities at the day boundaries when processing the airborne data covering two consecutive days, some large errors will appear in the positional results. Moreover, the clock drifts derived from time differentiation tend to be noisier than that from estimation, which will affect the PPP based velocity determination.

The VADASE approach (see Section 1.2.2) proposed by Colosimo et al. (2011) is an effective way to get high-precision epoch-wise displacements based on integration of the change of position (delta position). It can also be used for precise velocity determination since the delta position over time is basically equivalent to a velocity. However, this approach cannot be used to obtain absolute positions and the estimated

velocity and acceleration are also dependent on external orbit and clock information as PPP.

The POP approach (see Section 1.2.2) is different from PPP, because the satellite clock offsets and drifts are estimated using a global or large regional network. Thus, it is independent of the clock information and free of interpolation errors of the satellite clock offsets. It also allows the use of various types of IGS products, such as the broadcast ephemeris, the final, rapid, ultra-rapid (observed), and ultra-rapid (predicted) orbits. This is reasonable because the ultra-rapid orbits have an accuracy of 5 cm and are sufficient for precise POP performance. By using IGS real-time observation data and its ultra-rapid orbits, POP approach can be applied in real time. It is also sufficient for precise velocity and acceleration determination for airborne gravimetry and the effectiveness is confirmed in both a low dynamic flight experiment and a wide network test with baselines of thousands of kilometers (Salazar et al., 2011). In this contribution, its performance in Antarctica will be evaluated, and it is extended to not only GPS, but also multi-GNSS data.

There are also some other challenges for positioning over Antarctica besides the sparse distributed reference stations. First, the satellites observed over Antarctica tend to have low elevations and therefore the vertical position and velocity will be worse than that derived in other regions. Second, the relatively short continuous observation time and occasionally losing track and regain of satellites may degrade the positioning accuracy, and it will also bring difficulties for integer ambiguity resolution. Third, the frequent fluctuations of ionosphere during the day time may severely affect the estimated velocity, and the effect of remaining ionospheric errors on the acceleration estimation still needs further investigation even the ionosphere effect can be significantly reduced after the second-order time derivative of the carrier-phase measurements.

Currently, the GPS and GLONASS are already offering a global positioning, navigation and timing (PNT) service. The Galileo system is now in the transition phase to full operational capability (FOC) and is expected to consist of 30 available satellites in the Medium altitude Earth Orbit (MEO) planes by 2020. As of March 2019, there are 24 active Galileo satellites, as shown in Table 1.1. These satellites are divided into three groups: four In-Orbit Validation (IOV) satellites, two highly eccentric (ECC) satellites and twenty-one FOC satellites. Eight active satellites will

occupy each of three orbital planes inclined at an angle of 56° to the equator. Such an inclination of orbits was chosen to ensure good coverage of polar latitudes, which are poorly served by the GPS system (https://www.esa.int/Our_Activities/Navigation/Galileo/Galileo_a_constellation_of_navigation_satellites).

At the same time, the Chinese BeiDou navigation satellite system (BDS) has evolved from the demonstration navigation satellite system (BDS-1) to the regional navigation system (BDS-2). The BDS-3 started in 2009 and aimed at providing a global service by launching 30 satellites. By December 2018, the BDS consisted of a space segment of 5 Geostationary Earth Orbit (GEO), 7 Inclined Geo-Synchronous Orbit (IGSO), and 21 MEO satellites (CSNO, 2018). The IGSO and MEO satellites hold an inclination (mean longitude) of 55° to the equatorial plane and also have a good coverage over the polar regions as well as the Galileo satellites. Table 1.2 summarizes the deployment status of BDS-2 and BDS-3, including the transmitted signal types and the number of available satellites. It is worthwhile to notice that the observation quality of the BDS-3 signal is comparable to that of GPS L1/L2/L5 and Galileo E1/E5a/E5b signals, and the elevation-dependent code biases which is identified in the code observations of BDS-2 satellites are not notable in the new signals of the BDS-3 satellites (Zhang et al., 2017; Li et al., 2018). However, the orbit quality of BDS-2 GEO satellites is still very poor as they maintain almost stationary with respect to the Earth and can degrade the performance of PPP and its ambiguity fixing (Montenbruck et al., 2017; Liu et al., 2018).

Table 1.1 Constellation status of Galileo satellite system as of March 2019.
(<https://www.gsc-europa.eu/system-status/Constellation-Information>)

Satellite	SV ¹ ID	Status
GIOVE ²	A, B	Retired
IOV	E11, E12, E19	Operational
	E20	Unavailable
FOC	E18, E14	Launched into wrong orbit, denoted as “ECC” satellites, for testing only
	E22	Unavailable
	E21, E25, E27, E31	Commissioning ³

E24, E30, E07, E08, E09, Operational (15)
 E01, E02, E03, E04, E05,
 E26, E36, E13, E15, E33

¹Space Vehicle (SV) identifier is the Galileo satellite ranging code identifier. ²Galileo In-Orbit Validation Element (GIOVE). ³Commissioning means the satellite is under In-Orbit test phase.

Table 1.2 Deployment status of the BDS-2 and BDS-3 as of December 2018

System	Blocks	Signals	Number of satellites
BDS-2	GEO	B1I, B2I, B3I	5+1 ^a
	IGSO	B1I, B2I, B3I	5
	MEO	B1I, B2I, B3I	4
BDS-3	IGSO	B1I, B3I, B1C, B2a/b	2
	MEO	B1I, B3I, B1C, B2a/b	16+1 ^a

^aNon-operational satellite

The fusion of multi-GNSS constellations will allow a large number of satellites under different elevations to be observed by a receiver. This has helped considerably in improving the reliability of positioning under critical conditions, e.g., in urban canyons and polar regions. For airborne long-range kinematic positioning, a sufficient number of visible satellites can help to achieve reliable differential as well as undifferenced positioning performance. Therefore, all available observations should be fully used to enhance the performance of the vertical component with the aim of generating reliable and comparative solutions for all approaches, and reliable multi-GNSS data processing algorithms should be developed with the especial consideration of the BDS GEO orbit error.

Based on the consideration of the special characteristics of positioning over Antarctica analyzed above, the objective of this thesis is to derive the optimal position, velocity and acceleration solutions for airborne gravimetry by comparing and evaluating the results calculated from DD, PPP and POP approaches.

1.4 Overview of dissertation

In this thesis, the GNSS data processing approaches for precise position, velocity and acceleration for airborne gravimetry over Antarctica are comprehensively studied and evaluated. It is organized in six chapters.

Chapter 1 is an introduction to the research of this thesis. The motivation and background of this study are discussed and the challenges and objectives are specified, then the contributions of this research are addressed.

Chapter 2 is based on my paper: Li et al. (2019), Multi-GNSS Precise Orbit Positioning for airborne gravimetry over Antarctica, *GPS Solut.*, 23(2), doi: 10.1007/s10291-019-0848-9, and presents the observation model of multi-GNSS POP processing and analyzes its typical application in airborne kinematic positioning with IGS data. The POP real-time performance is also assessed. By processing one set of data from a real flight experiment, the positions derived from DD, PPP and POP approaches are compared and evaluated under dynamic conditions.

Chapter 3 is based on my paper: Li et al. (2019), Improving the performance of multi-GNSS ambiguity fixing for airborne kinematic positioning over Antarctica, *remote sensing*, 11(8), 992, doi:10.3390/rs11080992, and introduces the basic algorithms of DD-level ambiguity fixing and some special analyses are given to the GLONASS and BDS. Afterwards, with the processing of IGS Multi-GNSS Experiment (MGEX) data and a data set from a real flight experiment over Antarctica, the performance of single-, dual- and four-system PPP and POP ambiguity fixing as well as kinematic positioning are compared and analyzed. The results, conclusions and perspectives are finally summarized.

Chapter 4 is based on my paper: Li et al. (2019), Performance assessment of multi-GNSS precise velocity and acceleration determination over Antarctica, *Journal of Navigation*, 72(1), 1-18, doi:10.1017/S0373463318000656, and presents a multi-GNSS combination model as well as a combination strategy for precise velocity and acceleration determination. Two kinds of static experiments are performed. The first assesses the POP performance using the IGS network of different sizes with ionosphere-free linear combination (LC) and L1 observations. The second demonstrates and compares the PPP and POP derived velocity and acceleration estimates with multi-GNSS data. With two sets of real flight data processed, the

velocity and acceleration results calculated from DD, PPP and POP approaches are carefully compared and analyzed, the low frequency disturbing signals affecting the platform are finally extracted and investigated for gravimetry.

Chapter 5 describes miscellaneous aspects of velocity and acceleration determination including real-time performance, differentiator design and receiver clock reset, together with the treatments and solutions regarding these issues.

Finally, **Chapter 6** summarizes the primary results achieved in the previous chapters, and illustrates the final conclusions and recommendations for future work.

2 Precise Orbit Positioning with GPS and GLONASS data

Since the DD and PPP approaches have been reported not always being reliable for precise kinematic positioning over Antarctica (see Section 1.2.2), we will investigate the POP approach in terms of its capability of kinematic positioning in this chapter. The airborne flight experiment often covers two consecutive days, PPP can be greatly affected by the orbit and clock interpolation errors at the day boundaries, whereas POP is applied to deal with this problem since it is independent of the clock information. First, the multi-GNSS positioning model is presented. Then, the performance of kinematic PPP and POP are evaluated using the IGS data, the POP real-time performance is also assessed. By processing one set of data from a real flight experiment, the kinematic positions derived from the DD, PPP and POP approaches are compared and some useful conclusions are obtained.

2.1 GNSS observation model

For multi-GNSS positioning, the observation equations for undifferenced carrier phase L and pseudorange P can be expressed as follows:

$$\begin{aligned} L_r^s &= \rho_r^s + c(dt_r - dt^s) + \lambda(b_{r,s} - b^s) + \lambda N_r^s + T_r^s - \alpha_f I_r^s + \varepsilon_r^s \\ P_r^s &= \rho_r^s + c(dt_r - dt^s) + c(d_{r,s} - d^s) + \alpha_f I_r^s + T_r^s + e_r^s \end{aligned} \quad (2.1)$$

where r denotes the receiver, s is the satellite, λ is the wavelength of the carrier phase, c is the speed of light in a vacuum, ρ_r^s is the geometric distance between the satellite position vector at the signal emission time and the receiver position vector at the signal arrival time, dt_r and dt^s are the receiver and satellite clock biases, $b_{r,s}$ and b^s are the receiver- and satellite-dependent uncalibrated phase delays (UPDs) (Ge et al., 2008), $d_{r,s}$ and d^s are the code biases for the receiver and satellite, N_r^s is the integer ambiguity, T_r^s is the zenith total tropospheric delay, I_r^s is the ionospheric delay, α_f means the ionospheric delay is a function of the frequency f , and ε_r^s , e_r^s are the sum of the multipath effect error and measurement noise for the carrier phase and pseudorange observations, respectively. Furthermore, the relativistic delay and phase wind-up error must be corrected with

proper models (Kouba, 2009; Leick et al., 2015), although they are not included in the equations. The first-order ionospheric delay can be eliminated by the ionosphere-free combination of the code and carrier phase observations. The carrier phase L_r^s and pseudorange P_r^s indicated in the following equations are by default the ionosphere-free combined observations.

Let us introduce G and R to denote the GPS and GLONASS systems, respectively. Because of the different frequencies and signal structures of the individual GNSS, the receiver-dependent code $d_{r,s}$ and phase delays $b_{r,s}$ are different for different systems. Their differences are called inter-system biases (ISB) for code and phase observations. As GLONASS satellites emit signals on individual frequencies, frequency-dependent biases occur in the receivers. For a GLONASS satellite with k different frequency factors, the phase delays b_{r,R_k} are different. Their differences are usually called inter-frequency biases (IFB) (Wang et al., 2001; Wanninger, 2012).

The inter-system and inter-frequency biases should be considered in a combined analysis of multi-GNSS data. Consequently, the corresponding parameters have to be established for multi-GNSS data processing: one bias is set-up for the code and carrier phase measurements (each frequency for GLONASS) of each system. If we do not consider the integer ambiguity resolution, the satellite- and receiver-dependent carrier phase hardware delay biases b^s and $b_{r,s}$ usually remain stable over time, and can be absorbed by the ambiguity parameters (Defraigne et al., 2007; Geng et al., 2012; Li et al., 2015). Therefore, the ISB parameters for phase measurements are assimilated into the ambiguity parameters. The satellite and receiver code biases d^s and $d_{r,s}$ are absorbed by the clock parameters dt^s and dt_r , giving $d\bar{t}^s$ and $d\bar{t}_r$, respectively. Thus, combining $\lambda(b_{r,s} - b^s)$ and λN_r^s to give $\lambda \bar{N}_r^s$, Equation (2.1) can be rewritten using the inter-system parameters (actually the ISB parameters for the code measurements), then the following equations are obtained:

$$\begin{aligned}
L_r^G &= \rho_r^G + c(d\bar{t}_r - d\bar{t}^G) + \lambda_G \bar{N}_r^G + T_r^G + \varepsilon_r^G \\
L_r^R &= \rho_r^R + c(d\bar{t}_r - d\bar{t}^R) + ISB_G^{R_k} + \lambda_R \bar{N}_r^R + T_r^R + \varepsilon_r^R \\
P_r^G &= \rho_r^G + c(d\bar{t}_r - d\bar{t}^G) + T_r^G + e_r^G \\
P_r^R &= \rho_r^R + c(d\bar{t}_r - d\bar{t}^R) + ISB_G^{R_k} + T_r^R + e_r^R
\end{aligned} \tag{2.2}$$

where $d\bar{t}_r = dt_r + d_{r,s}$, $d\bar{t}^s = dt^s + d^s$, $\lambda_s \bar{N}_r^s = \lambda_s N_r^s + \lambda_s (b_{r,s} - b^s) - c(d_{r,s} - d^s)$, and ISB_G^{Rk} is the inter-system bias of GLONASS with frequency factor k with respect to GPS, which is in fact the IFB parameters.

For the POP method, we have to estimate the receiver and satellite clock offsets. For this purpose, a reference clock dt_0 is typically introduced as a reference for all other clocks (including GLONASS satellite clocks with all frequencies and other receiver clocks) (Salazar et al., 2011). Hence,

$$\begin{aligned} d\tau_r &= d\bar{t}_r - dt_0 \\ d\tau^s &= d\bar{t}^s - dt_0 \end{aligned} \quad (2.3)$$

For different satellite systems, we have

$$d\tau^G = d\bar{t}^G - dt_0, \quad d\tau^R = d\bar{t}^R - dt_0 \quad (2.4)$$

Then, the following equations are obtained:

$$\begin{aligned} L_r^G &= \rho_r^G + c(d\tau_r - d\tau^G) + \lambda_G \bar{N}_r^G + T_r^G + \varepsilon_r^G \\ L_r^R &= \rho_r^R + c(d\tau_r - d\tau^R) + ISB_G^{Rk} + \lambda_R \bar{N}_r^R + T_r^R + \varepsilon_r^R \\ P_r^G &= \rho_r^G + c(d\tau_r - d\tau^G) + T_r^G + e_r^G \\ P_r^R &= \rho_r^R + c(d\tau_r - d\tau^R) + ISB_G^{Rk} + T_r^R + e_r^R \end{aligned} \quad (2.5)$$

Because the receiver and satellite clock offsets in Equation (2.5) have to be solved synchronously, the singularity has to be treated. Therefore, we choose a master station r_0 from which the reference clock is taken for the network. Thus, for the master station, considering that its coordinates are fixed, Equation (2.5) becomes

$$\begin{aligned} l_{r_0}^G &= -cd\tau^G + \lambda_G \bar{N}_{r_0}^G + \delta T_{r_0}^G + \varepsilon_{r_0}^G \\ l_{r_0}^R &= -cd\tau^R + ISB_G^{Rk} + \lambda_R \bar{N}_{r_0}^R + \delta T_{r_0}^R + \varepsilon_{r_0}^R \\ p_{r_0}^G &= -cd\tau^G + \delta T_{r_0}^G + e_{r_0}^G \\ p_{r_0}^R &= -cd\tau^R + ISB_G^{Rk} + \delta T_{r_0}^R + e_{r_0}^R \end{aligned} \quad (2.6)$$

where l and p are the ‘‘observed minus computed’’ phase and pseudorange measurements, respectively, and δT is the wet tropospheric delay. For those reference stations, denoted by the number k , that have fixed or tightly constrained coordinates, their clock offsets are estimated with respect to the master station r_0 .

Therefore,

$$\begin{aligned}
l_{r_k}^G &= c(d\tau_{r_k} - d\tau^G) + \lambda_G \bar{N}_{r_k}^G + \delta T_{r_k}^G + \varepsilon_{r_k}^G \\
l_{r_k}^R &= c(d\tau_{r_k} - d\tau^R) + ISB_G^{R_k} + \lambda_R \bar{N}_{r_k}^R + \delta T_{r_k}^R + \varepsilon_{r_k}^R \\
p_{r_k}^G &= c(d\tau_{r_k} - d\tau^G) + \delta T_{r_k}^G + e_{r_k}^G \\
p_{r_k}^R &= c(d\tau_{r_k} - d\tau^R) + ISB_G^{R_k} + \delta T_{r_k}^R + e_{r_k}^R
\end{aligned} \tag{2.7}$$

For the rover, the estimated parameters are the position and the satellite and receiver clock offsets with respect to the master station:

$$\begin{aligned}
l_r^G &= -\mathbf{e}_r^G \cdot \mathbf{x}_r + c(d\tau_r - d\tau^G) + \lambda_G \bar{N}_r^G + \delta T_r^G + \varepsilon_r^G \\
l_r^R &= -\mathbf{e}_r^R \cdot \mathbf{x}_r + c(d\tau_r - d\tau^R) + ISB_G^{R_k} + \lambda_R \bar{N}_r^R + \delta T_r^R + \varepsilon_r^R \\
p_r^G &= -\mathbf{e}_r^G \cdot \mathbf{x}_r + c(d\tau_r - d\tau^G) + \delta T_r^G + e_r^G \\
p_r^R &= -\mathbf{e}_r^R \cdot \mathbf{x}_r + c(d\tau_r - d\tau^R) + ISB_G^{R_k} + \delta T_r^R + e_r^R
\end{aligned} \tag{2.8}$$

where \mathbf{e}_r^s is the unit vector in the direction from the receiver r to the satellite s , and \mathbf{x}_r is the correction of the a priori position vector. The equations for the master, references, and rover are connected by the estimation of the satellite clock offsets. Due to this manipulation, these equations become solvable in a unique manner.

2.2 Antarctica data processing

In this section, the available Antarctica IGS data are described and a real flight experiment is introduced. The positioning performances of the PPP and POP methods using IGS static data and a reference station installed at the South Pole are assessed. The kinematic positions and velocities of a receiver mounted on an aircraft are then analyzed using the DD, PPP, and POP approaches, and the results are compared.

Kinematic data were obtained from the ESA PolarGAP gravity field campaign, which was conducted from December 7, 2015 to January 19, 2016. The primary objective of this campaign was to perform an airborne gravity survey over the southern polar gap of the ESA's satellite gravity field mission GOCE (Jordan et al. 2016). A Twin-Otter aircraft was used (Figure 1.1, bottom right). Figure 2.1 shows two typical flights, P26 and P36. In this section, we use P26 for analysis (conducted on January 8, 2016, from 18:30 to 06:00 the next day). Three receivers named AIR2,

0158 and SPAN were installed on the airplane to collect the kinematic data. However, only the observation data of AIR2 on that day is available at the moment. A reference station SP2X was installed at the South Pole so that the aircraft could fly from the South Pole along the operation radius to the end point, and then fly back; such a performance is also beneficial for efficient DD processing as usually only one base station is installed. The flight radius can be as long as 500 km.

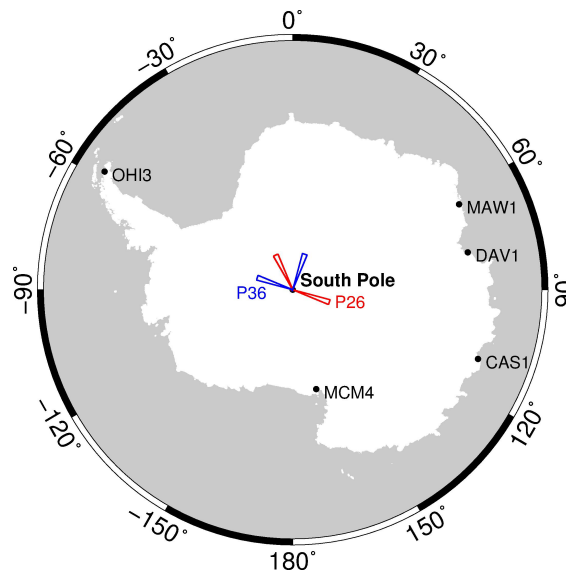


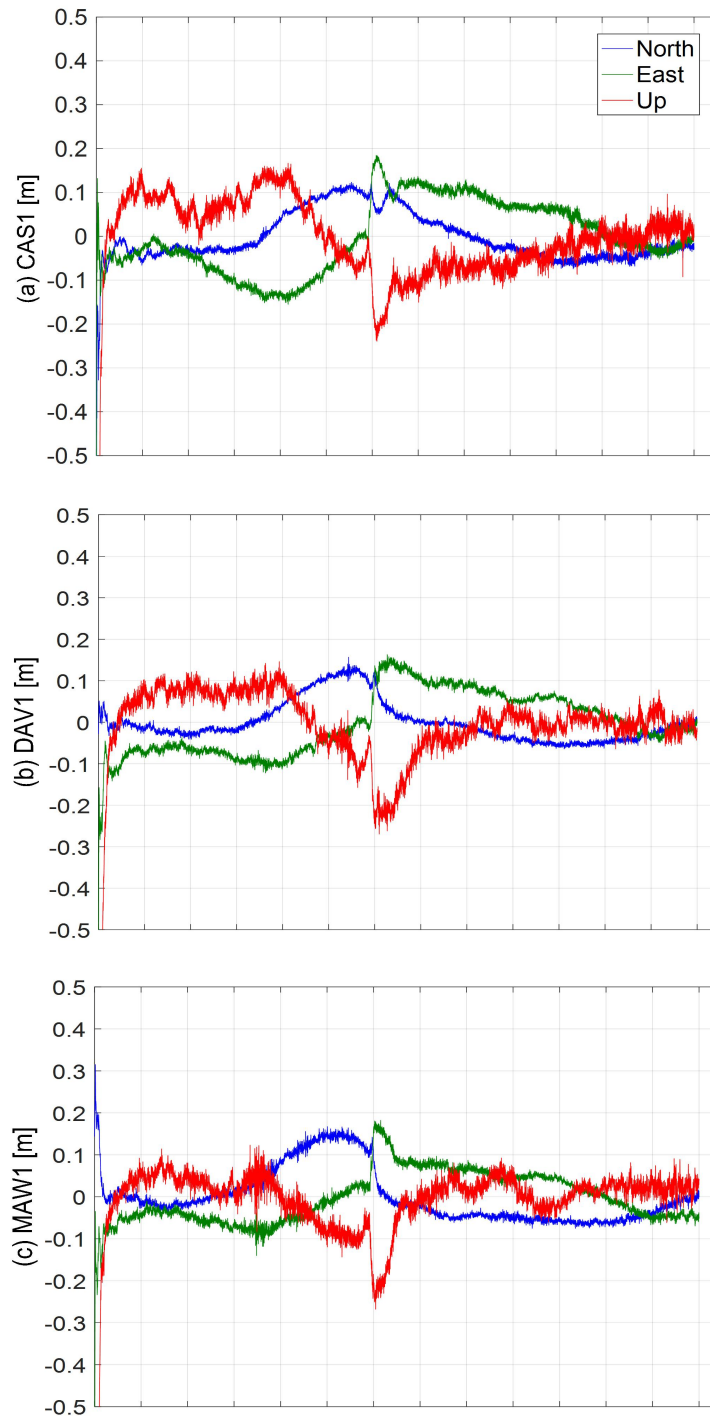
Figure 2.1 Four sets of flight trajectories. The reference station SP2X is installed at the South Pole. The points around the coast are the IGS stations. All receivers including the rover AIR2 observe GPS and GLONASS data. P26 (red) and P36 (blue) each include two flights.

2.2.1 Validation with the static data

As there is no “reference solution” to evaluate the kinematic trajectories derived from the three methods, the performance of the PPP and POP methods were first evaluated with IGS data. DD was not calculated in this stage, because the available reference stations are too far away.

The positions of the four IGS stations (CAS1, DAV1, MAW1, and OHI3) and the reference station SP2X were calculated in kinematic mode. The sampling interval was 1 s. As these IGS stations are also used for independent POP calculation purposes for AIR2, their data spans ranged from 18:00 to 07:00 the next day in an attempt to cover the time span of AIR2. Figures 2.2 and 2.3 show the positional differences between the solutions from PPP and POP regarding the IGS nominal position (weekly position solution) in a local (north, east, and up) coordinate system. As there is no “true” value

for SP2X, the reference position for the two methods is taken from their individual static solutions. Figure 2.4 shows the corresponding statistics of the RMS values.



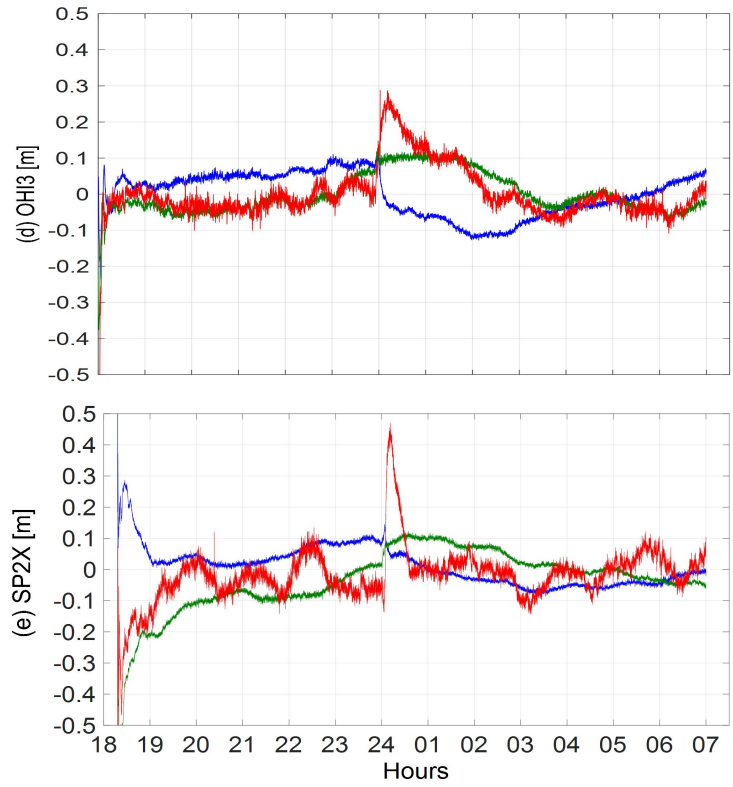
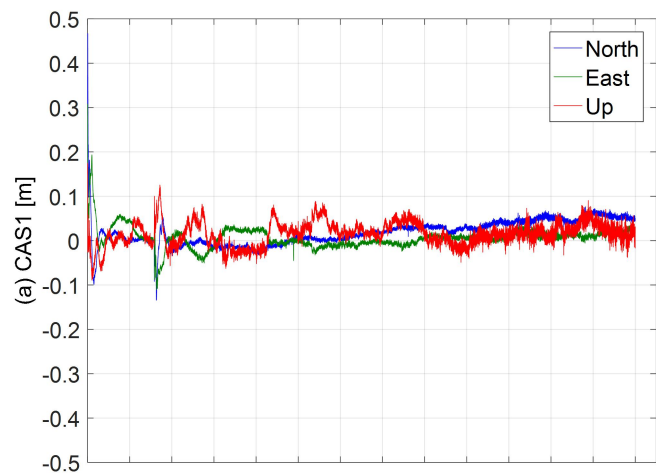


Figure 2.2 PPP positional differences of the four IGS stations regarding the IGS nominal position and SP2X regarding its static solution. (a)–(e) are for stations CAS1, DAV1, MAW1, OHI3, and SP2X, respectively.



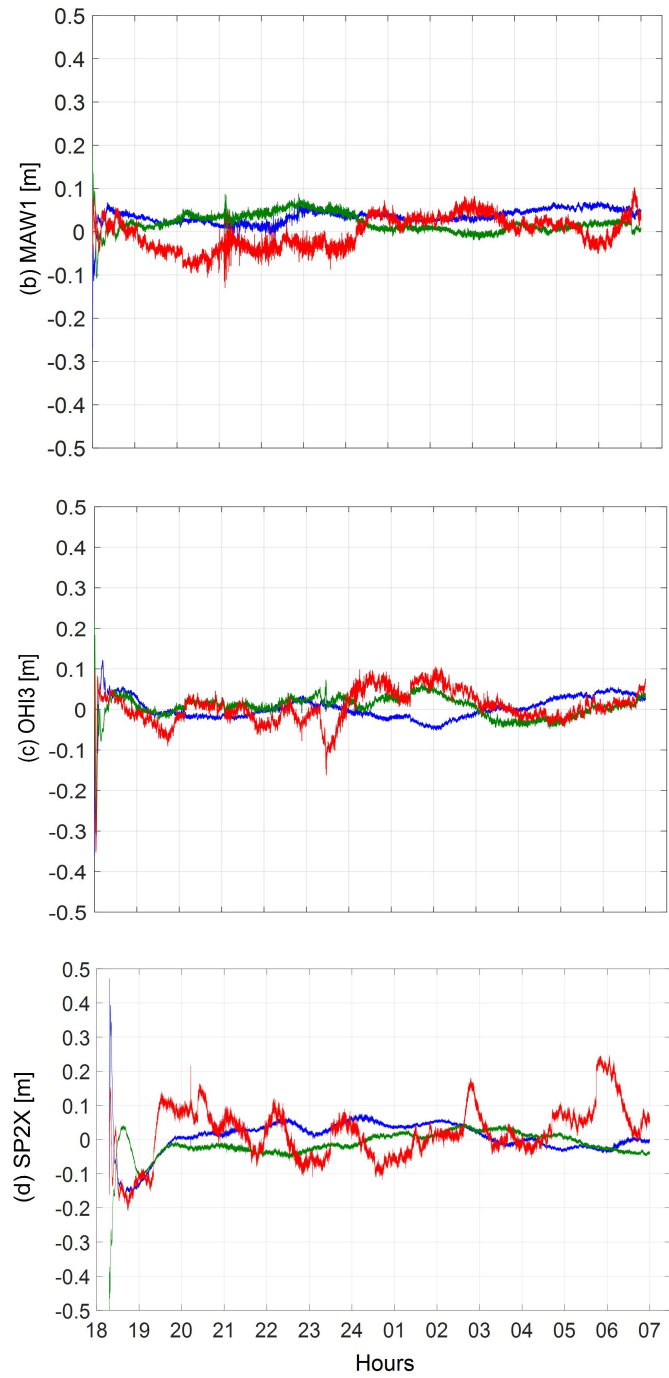


Figure 2.3 POP positional differences of the three IGS stations (DAV1 is not included as it is taken as the master station) regarding the IGS nominal position and SP2X regarding its static solution. (a)–(d) are for stations CAS1, MAW1, OHI3, and SP2X, respectively.

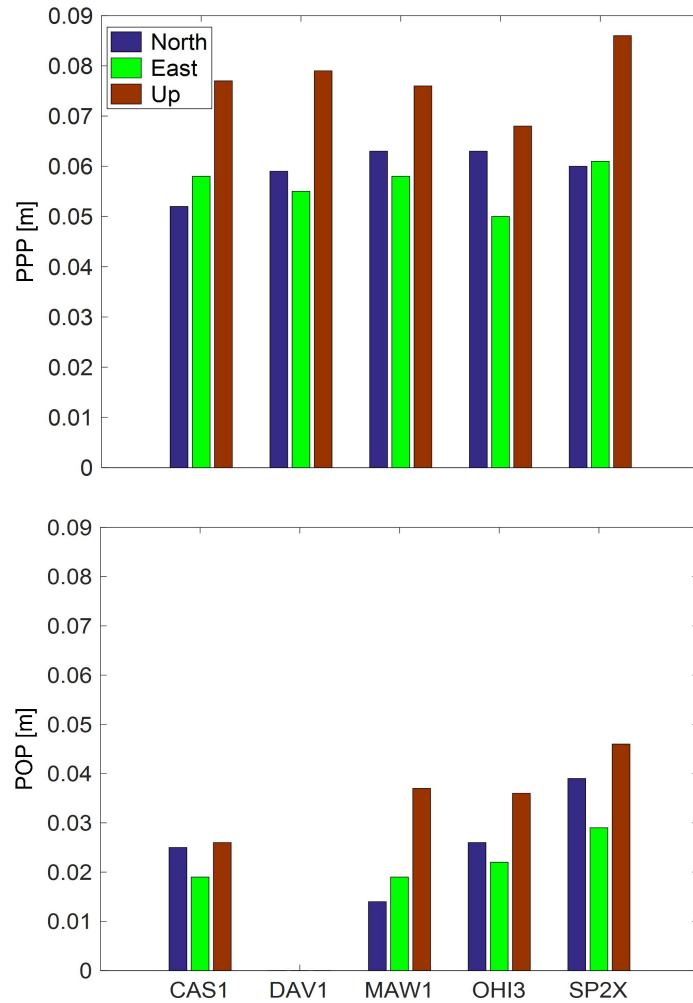


Figure 2.4 RMS values of positional estimates of PPP and POP for the five reference stations

The PPP solutions were calculated with the GFZ (German Research Centre for Geosciences) analysis center final products, using orbit- and clock-rates of 5 min and 30 s, respectively. The CODE (Centre for Orbit Determination in Europe) analysis center actually provides high-rate (5 s) clocks and should be used for high-sampling-rate data processing. However, only the GPS high-rate clock was available at the time of the PolarGAP campaign, so the positioning errors with GPS-only observations are sometimes more significant than the influence caused by the clock-rate. Therefore, the GFZ 30 s clock was applied instead. As the IGS products are daily solutions, the orbits and clocks are not consistent at the day boundaries. The interpolation errors of orbits and clock offsets at the boundary epochs of two consecutive days may result in jumps in the positioning results. We can see from Figure 2.2 that large positioning errors occur from around 23:00 to 01:00 for the five stations. For the POP method, the satellite clock offsets are estimated

“on-the-fly” and the interpolation errors of orbits at the boundary epochs may have been absorbed by the clock estimates. Almost no large positioning errors can be seen at those boundary epochs in Figure 2.3, and the results are much more robust than the PPP solutions. When we compare the RMS values of their positioning errors in Figure 2.4, there is an average improvement of 56%, 61%, and 53% for the north, east, and up components, respectively. Overall, this illustrates the potential of the POP method in generating centimeter-level kinematic vertical positions over long baselines.

As for SP2X, the PPP and POP individual static solutions after convergence can reach millimeter-level accuracy, and can be taken as references to evaluate their inner accuracies. We can see the fluctuations around their reference solutions in Figures 2.2(e) and 2.3(d). The accuracy of the vertical position of SP2X is worse than that of the four IGS stations. This is because no satellites with elevation angles larger than 60° can be observed at SP2X (Figure 2.5, left), whereas for the other four IGS stations (Figure 2.5, right) located along the Antarctica coast, high-elevation satellites (even up to 90°) can still be observed. This may account for the better positioning accuracy in the upward component of the IGS stations than SP2X, which is located at the South Pole.

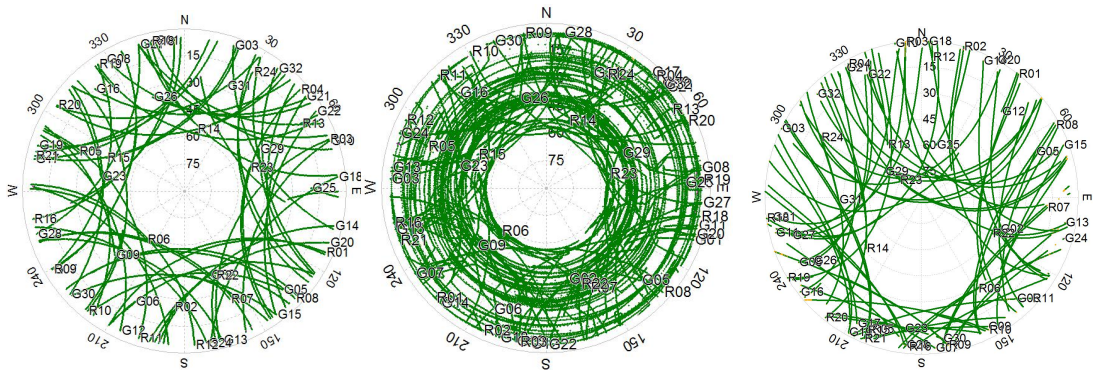


Figure 2.5 Sky plots (azimuth vs. elevation) of GPS and GLONASS with L1/2 observations for stations SP2X (left), AIR2 (middle), and OHI3 (right) on January 8 and 9, 2016.

As for the discontinuities of the orbits and clocks over two consecutive days, we can generate a new orbit and clock product over the time period from 12:00 to 12:00 the next day, but this would require globally distributed IGS stations. In this study, we only need five reference stations to obtain the desired results with the POP method. This is much more convenient and efficient.

We also analyzed the convergence time of the PPP and POP solutions since they can both be applied in real-time. Here, a converged solution means that the 3D positional accuracy is better than 0.1 m. The statistical results in terms of convergence time are presented in Table 2.1. We can see that the PPP method usually requires a convergence time of about 30 min. However, POP can shorten the convergence time to less than 15 min. One exception is the SP2X station, which requires more than 1 h to converge for PPP and 40 min for POP. This is mainly because of the low elevation angles of the observed satellites. Even after convergence, the accuracy of the upward component can still be worse than 0.1 m in some epochs.

Table 2.1 Convergence time of the PPP and POP solutions for the five stations

(unit: minutes)

Convergence Time	CAS1	DAV1	MAW1	OHI3	SP2X
PPP	38.2	29.6	22.5	22.1	70.2
POP	13.2	-	7.4	13.8	40.5

2.2.2 Validation with the real flight kinematic data

Finally, the kinematic position of the rover AIR2 was calculated with the three methods. Usually, the DD solution can be regarded as reference. However, for a baseline as long as several hundred kilometers (see Figure 2.6), the DD solution may be vulnerable to common errors that cannot be completely eliminated by differential processing. Therefore, in this case the DD solution is not sufficiently robust to be considered as the reference. It is difficult to evaluate the performance of long-range kinematic positioning. Here, we consider the positional differences of the three solutions. The results are shown in Figure 2.7, and the STD values are given in Table 2.2.

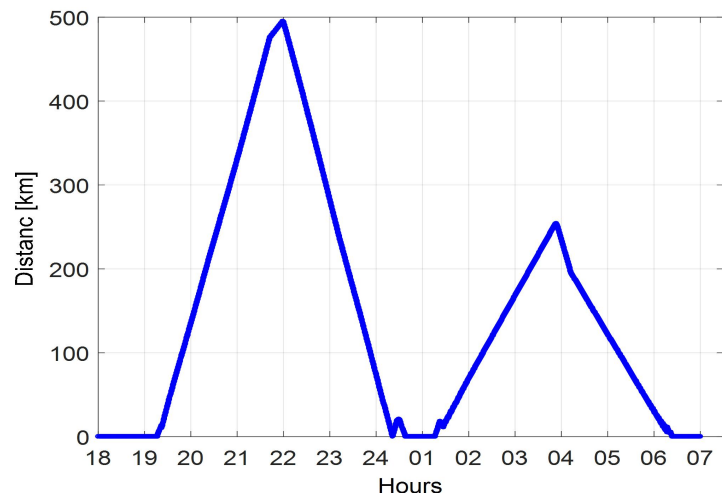
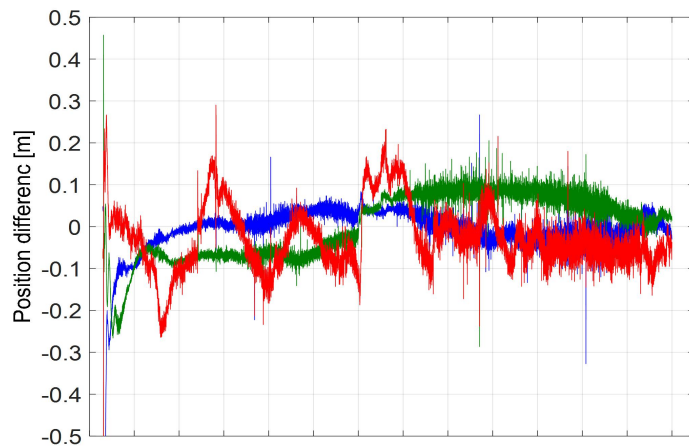
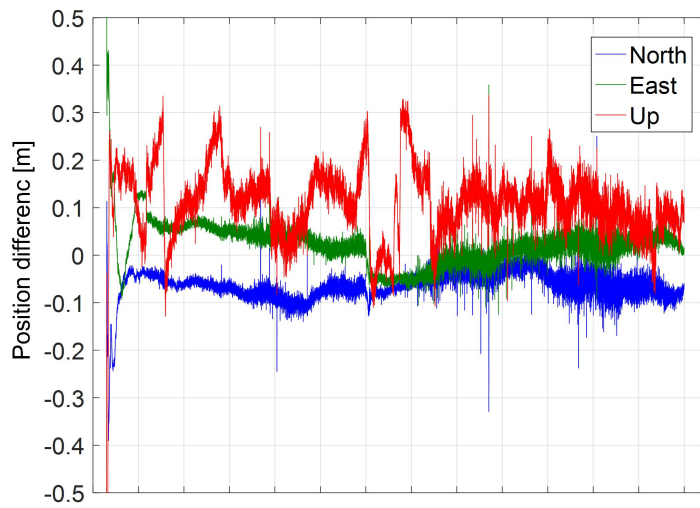


Figure 2.6 Baseline length between the rover AIR2 and the reference station SP2X



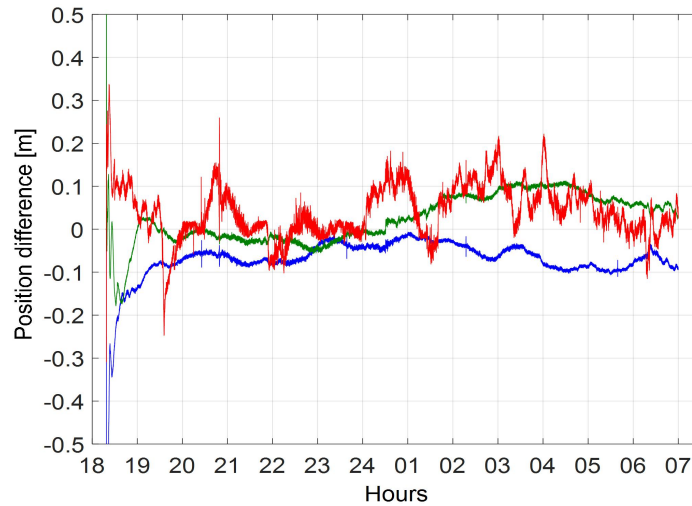


Figure 2.7 Positional differences between different solutions for AIR2. Top: DD minus PPP, middle: POP minus PPP, bottom: POP minus DD.

Table 2.2 Statistics of positional differences between different solutions for AIR2

STD (m)	North	East	Up
DD - PPP	0.028	0.035	0.076
POP - PPP	0.026	0.034	0.068
POP - DD	0.024	0.029	0.060

Figure 2.7 displays the positional differences between DD, PPP, and POP. Comparisons among different solutions do not suggest a clear preference for any one, with the heights generally showing decimeter-level agreement. Again, similar to the solutions using IGS data (Figure 2.2), significant jumps appear in the differences between PPP and the other solutions from 24:00 to 01:00 (the top and middle panels in Figure 2.7). These jumps are likely to come from the orbit and clock discontinuities in the PPP solutions, because the DD and POP methods can get rid of such effect. However, there are also some other large discrepancies among the positional estimates in the vertical direction. In fact, none of the individual upward solutions is robust, and there two main reasons for this. The first is the fact that no satellites with elevation angles greater than 60° can be observed for SP2X and AIR2 (Figure 2.5, top and middle subplots), and therefore the vertical position may not be reliably estimated.

The second reason is that, under highly dynamic conditions, frequent losing track and regain of satellites is not beneficial for the estimation of the carrier phase ambiguities.

The top and middle panels in Figure 2.7 also provide a visual impression that the differences between PPP and the other methods tend to be noisier than those between DD and POP, which indicates that the large noise most likely comes from the PPP solution. The behavior of the clock makes it hard to interpolate without losing accuracy. The noise mainly comes from interpolation errors of the satellite clock offsets at the day boundaries or with a large interval (e.g., 5 min). The STD statistics in Table 2.2 indicate a typical agreement of about 3 cm (horizontal) and 6 cm (vertical) between the DD and POP solutions, which is the best agreement among the three solutions. It can be concluded that these two methods are independent of the clock information and thus are not affected by clock discontinuities and interpolation errors.

2.2.3 POP real-time performance

For the results presented so far, only the GFZ final products have been applied. Since the POP method is independent of the clock information, it is possible to use different types of IGS products, including the ultra-rapid (predicted orbit). This indicates that POP can be potentially applied in real time. Since the accuracy of the ultra-rapid (predicted) satellite clock is 3 ns, the requirement for real-time PPP applications cannot be satisfied. Fortunately, the IGS Real-Time Pilot Project (RTPP) (<http://www.rtigs.net>) provides real-time orbits with an accuracy of 5 cm and a clock accuracy of 0.3 ns which is almost the same accuracy as the IGS ultra-rapid (observed) products (3 cm for orbit and 0.15 ns for clock). The real-time observation data, orbits, and clock corrections can be broadcasted to users through the Ntrip Broadcaster. After registration and authorization on the client server, users can access the data and then carry out real-time precise positioning. In this study, we obtained the archived real-time orbits, clocks, and observation data for January 8 and 9, 2016, from the Federal Agency for Cartography and Geodesy (BKG) data center in a simulated real-time mode. The orbit and clock sampling are the same as for the final products. The kinematic positions of station CAS1 were calculated by the PPP and POP methods, and the results are shown in Figure 2.8.

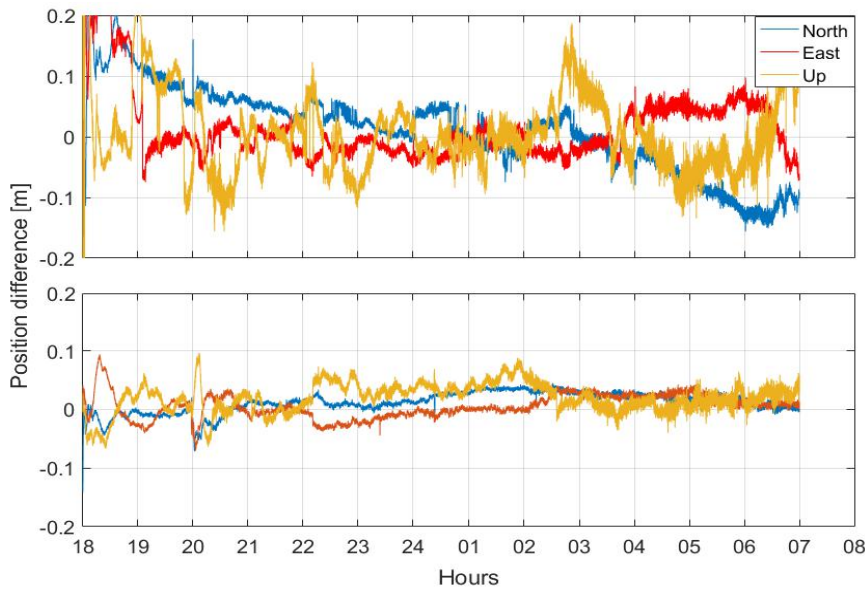


Figure 2.8 CAS1 positional differences derived from PPP (top) and POP (bottom) solutions relative to the IGS nominal position using the RTPP products

Figure 2.8 indicates that the PPP results are still robust at the day boundaries when using the real-time products, this is mainly due to the fact that the real-time orbits and clocks are consistent at each day. However, the PPP solutions tend to be worse than that of POP, the RMS values of positional differences using PPP are 0.060, 0.058, and 0.085 m for the north, east, and up components, respectively, whereas they are 0.021, 0.021, and 0.032 m for the POP solution. However, POP is free of such effects, and the real-time solutions are comparable with that based on the final products. The robust POP real-time solutions make it feasible to check the gravity results in real time by calculating the gravity measurements together with the GNSS solutions.

2.3 Conclusions

In this chapter, we have applied the DD, PPP and POP approaches to obtain precise kinematic position of the aircraft for airborne gravimetry. The time period of flying covers two consecutive days, during which time the PPP-derived position may be vulnerable to interpolation errors of the satellite orbit and clock offsets, especially around the discontinuities at the day boundaries. In contrast, the POP method estimates the satellite clock offsets and drifts “on-the-fly” and is, therefore, independent of the effect of the clock behavior. Studies with Antarctica IGS data

show that there are large positioning biases in the PPP solutions at the day boundaries, whereas POP produces robust positional estimates of the four IGS stations. Compared with PPP, the POP obtains an average improvement in position of about 50% in the three coordinate components. Comparisons of the three types of positional solutions during a real flight experiment do not suggest a clear preference for any one, with the heights generally showing decimeter-level agreement. This discrepancy is mainly due to the low elevation angles observed at the rover AIR2 and the reference station SP2X located at the South Pole. As well as for post-processing, POP can also be applied in real-time using the ultra-rapid (predicted) orbits and the results are comparable with those using the final products.

3 Multi-GNSS PPP and POP ambiguity fixing

It is known to us that the PPP approach is applied with precise orbit and clock products and observations of a stand-alone receiver. It usually takes about 30 min for initialization to achieve centimeter-level positioning accuracy and can be improved significantly by the carrier phase ambiguity resolution technique (Ge et al., 2008; Collins et al., 2008; Laurichesse et al., 2009).

Satellites observed over Antarctica are usually tracked at lower elevation and over a shorter continuous period, due to the GNSS constellation with inclined orbit planes. Both observations of short period and at lower elevation bring difficulties in integer ambiguity resolution which is expected to improve the horizontal accuracy on one hand, on the other hand they also degrade the accuracy in height component. Therefore, further investigation is still required for PPP and its integer ambiguity resolution applied to the polar regions and especially under highly dynamic conditions, although they have been well demonstrated elsewhere (Teunissen and Verhagen, 2009; Verhagen, 2016).

Nowadays with the construction of global coverage of the Galileo and BDS navigation satellite systems, the multi-GNSS, including GPS, GLONASS, Galileo and BDS, can provide a great number of satellites for positioning. That means, the poor accuracy of the vertical position due to the lower tracking elevation over Antarctica can be improved considerably. The GPS, GLONASS and Galileo final orbit and clock products turn out to be at the same level of accuracy since their MGEX tracking stations are globally and evenly distributed whereas there are only about 71 stations with BDS observations mainly distributed in Europe and Asia-pacific area and only two stations named CAS1 and DAV1 in Antarctica. Because of the insufficiently well distributed stations and a poorly developed solar radiation pressure model (Kazmierski et al., 2018), the accuracy of BDS satellite orbits is relatively low compared to that of the other GNSS satellites, particularly for the BDS GEO satellites. The positioning and ambiguity fixing of BDS PPP will be greatly affected since it is dependent of the orbit and clock products. Li et al. (2017) and Liu et al. (2018) illustrated that the impact of BDS GEO orbit errors is similar for all stations in a regional network as the directions of the satellite to all receivers are almost the same and thus can be assimilated into the UPDs. However, the impact difference gets larger

for a global network from station to station and is regarded as a main obstacle for ambiguity fixing.

As the POP approach is in principle a network solution with fixed satellite orbits where satellite clock offsets are estimated with a global or large regional reference network instead of a few nearby reference stations. According to Douša (2010), 96% of the orbit error in the radial direction can be compensated by the satellite clock in such a network processing mode. Including more stations will improve clock estimation especially when the tracking stations are rather sparse over the interesting region. Furthermore, fixing ambiguities with respect to nearby reference stations is in principle easier than PPP ambiguity fixing with possibly contaminated UPDs. Therefore, this approach can achieve a higher positioning performance as well as ambiguity fixing compared to PPP when processing BDS observations.

In this chapter, we concentrate on the comprehensive study of the PPP and POP in the aspects of ambiguity fixing and multi-GNSS impact and their improvement in positioning performance for their applications in the polar regions.

The rest of the chapter is organized as follows. After the introduction of the basic observation model of multi-GNSS data processing, algorithms of DD-ambiguity fixing is introduced for complexity with some special analyses for GLONASS and BDS. Afterwards, with the data of IGS MGEX network and data of a real flight experiment over Antarctica, the performance of single-, dual- and four-system PPP and POP ambiguity fixing as well as kinematic positioning are analyzed and investigated. The results, conclusions and perspectives are finally summarized.

3.1 Ambiguity fixing

The GNSS observation equations with pseudorange and carrier phase measurements can be referred to Equation (2.1) in Chapter 2. During POP processing, the whole equations are connected by the estimation of satellite clocks in a network mode, therefore, the ambiguity fixing can be easily made on DD-level for POP. For comparison, the PPP ambiguity fixing is also made on DD-level in this study.

For DD ambiguity fixing using ionosphere-free observations, a DD ambiguity is usually expressed as the combination of wide- and narrow-lane (WL and NL) ambiguity for fixing

$$N_{\text{IF},r,r'}^{s,s'} = \frac{f_i}{f_i + f_j} N_{nr,r'}^{s,s'} + \frac{f_i f_j}{f_i^2 - f_j^2} N_{wr,r'}^{s,s'} \quad (3.1)$$

where r and r' , s and s' represent two receivers and two satellites, respectively. N_{IF} is the ionosphere-free DD ambiguity, N_n and N_w is the DD WL and NL ambiguity, respectively. i and j indicate frequency number, f_i and f_j mean the corresponding frequency. In this chapter, the L1 and L2 signals are used for GPS and GLONASS, E1 and E5a for Galileo, B1 and B2 for BDS.

The WL ambiguity can be estimated by taking the time average of the Hatch-Melbourne-Wübbena (HMW) (Hatch, 1982; Melbourne, 1985; Wübbena, 1985) combination of the pseudorange and carrier phase observations. Then the DD WL ambiguity can be fixed according to its probability by rounding to its nearest integer (Dong and Bock, 1989; Ge et al., 2008; Ruan et al., 2019).

After WL fixing, the NL ambiguity can be derived with the fixed WL and the float ionosphere-free ambiguity, and fixed in the same way as WL. A DD integer ambiguity can be reconstructed only when both the related WL and NL are fixed, and then as a constraint imposed on the normal equations with original UD ambiguities (Ge et al., 2005).

It should be mentioned that for GLONASS, because of its frequency-division multiple-access (FDMA) strategy, the receiver code hardware delay $d_r^{R_k}$ as well as the phase delay $b_r^{R_k}$ are different for satellites with different frequency factors k , referred as to IFB for code and carrier phase, respectively (Reussner and Wanninger, 2011; Teunissen and Khodabandeh, 2019). Therefore, they cannot be removed by forming DD ambiguity unless, homogeneous receivers, i.e. the same type of receivers, are used (Wanninger, 2012; Geng et al., 2019). Since the code and carrier phase IFBs of a particular satellite is the same for all involved receivers, they can be eliminated while forming difference between homogeneous receivers. Through this classification, the IFB causes no effect on WL fixing. By the way, IFBs can also be estimated and calibrated for integer ambiguity resolution (Tian et al., 2015).

3.2 BDS ambiguity fixing

The temporal variation of BDS satellite-induced code bias is identified in its code

observations. Although it has minor impact on positioning since the code measurements are assigned a much lower weight compared to the carrier phase measurements, the precision and consistence of the WL ambiguity derived from the HMW combination observations are severely affected. The variation of this bias is elevation dependent and can be corrected with an empirical correction model for IGSO and MEO satellites (Wanninger and Beer, 2014) and also for GEO satellites (Lou et al., 2017). Due to the slight difference in satellite elevation for regional networks, such code bias is almost identical for all receivers and can be absorbed by the WL UPDs at the satellite side (Li et al., 2017). However, when applied in a global network in this study, they can neither be eliminated by DD nor assimilated into the UPDs. Therefore, the code biases of BDS satellites should be corrected before ambiguity fixing. The impact of the correction is shown in Figure 3.1 where the corrected code observation residuals show a typical behaviour of elevation-dependence, the higher the elevation angles, the smaller the residuals.

Besides the satellite-induced code bias, the poor orbit quality of BDS GEO satellites will also affect the estimation of the float ambiguity as well as the kinematic position significantly. The geometric orbit error $d\rho_r^s$ for BDS GEO satellites can be expressed as

$$d\rho_r^s = (\alpha_r^s, \beta_r^s, \delta_r^s) \cdot (dx^s, dy^s, dz^s) \quad (3.2)$$

where $(\alpha_r^s, \beta_r^s, \delta_r^s)$ is the direct cosine unit vector at the direction from the receiver r to the satellite s , (dx^s, dy^s, dz^s) is the orbit error in radial, cross and along directions. Li et al. (2017) and Liu et al. (2018) both use a regional network to force the orbit error to be absorbed by the NL UPDs. However, it is not practical for a global network as the unit vector is different from a GEO satellite to global receivers. In the UPD estimation for PPP ambiguity fixing, the coordinates of reference stations, orbits and clocks are fixed, the orbit errors will be mostly absorbed by the ionosphere-free ambiguities. Since the orbit bias is changing with time, its effect is different on the estimated ionosphere-free ambiguities depending on the continuous tracking time of each ambiguity besides the station location. This will consequently result in inaccurate UPD estimates and finally the fixing performance of ambiguity fixing at rover stations. However, the temporal varying orbit error can more likely be assimilated into the satellite clock estimates rather than the float ambiguities in POP

where the satellite clock parameters are estimated which will lead to a better ambiguity fixing and positioning performance.

According to the IGS processing convention, the satellite clock offset products of GPS, GLONASS, Galileo and BDS may be biased with a constant since the satellite code hardware bias is absorbed by the satellite clock (Ge et al., 2012). According to our experimental analysis, when applying such multi-GNSS clock product, the constant bias will be mostly assimilated into the code observation residuals. Here we take the observation data of MGEX station CAS1 for analysis. The PPP and POP are processed with ionosphere-free pseudorange and carrier phase measurements and only the code observation residuals are analyzed. For GPS, even though different satellites have different elevation angles, they generally show a behaviour of elevation-dependence, the higher the elevation angles, the smaller the residuals. Therefore, the code residuals of all GPS satellites are ranged according to their elevation angles in ascending order. These code residuals are lumped together to calculate the RMS values with a sampling step size of 0.1 degrees. Such calculations of the RMS values from the code residuals hold for GLONASS, Galileo and BeiDou satellites. Figure 3.1 shows the RMS of elevation dependent ionosphere-free code residuals. It can be seen that there exists a constant bias in the code residuals of PPP but not POP. That is because when we estimate the satellite clocks in POP, the code bias is not assimilated into the code residuals but into the satellite clocks. What can be concluded here is that the code bias inside the satellite clocks will contribute to the estimation of the float ambiguity and the NL ambiguity fixing since the clocks are involved in the PPP adjustment. Therefore, the estimated UPD should be used together with the corresponding orbit and clock for PPP ambiguity fixing. What can also be found from the POP results is that the code observation residuals are at the same level for each system, therefore, we set equal weights to the code observations of each system.

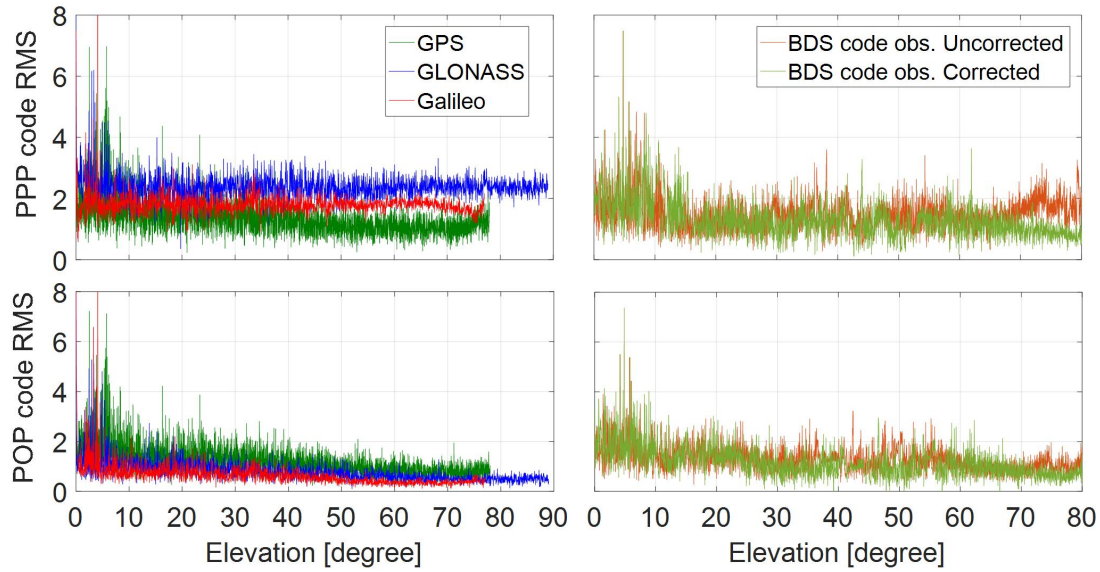


Figure 3.1 The RMS values of ionosphere-free code residuals of PPP and POP solutions. For each system, the code residuals of all involved satellites are lumped together to calculate the RMS values (unit: m). The BDS code observations before and after corrected with the satellite-induced code bias are shown in the right two subplots.

For multi-GNSS ambiguity fixing, the DD ambiguity can be fixed within each system. Since BDS does not have a good coverage outside the Asia-Pacific area and only 3 to 6 Galileo satellites can be tracked by Antarctica stations, therefore, in order to overcome the limitation of the number of valid satellites, GLONASS, Galileo and BDS are processed together with GPS, respectively.

3.3 Validation with IGS data

3.3.1 Data description

In order to verify the performance of PPP and POP ambiguity fixing, 136 global multi-GNSS reference stations are selected among which seven (CAS1, DAV1, MAW1, MCM4, OHI3, OHI2 and SYOG) are located in Antarctica. One reason why we use a global network is that the Galileo and BDS satellite clocks cannot be estimated well with a sparse distribution of IGS network around Antarctica. The other is that such a regional network is not sufficient for GLONASS ambiguity fixing since there are not enough exactly the same type of receivers as those in Antarctica. The distribution of these multi-GNSS stations is shown in Figure 3.2.

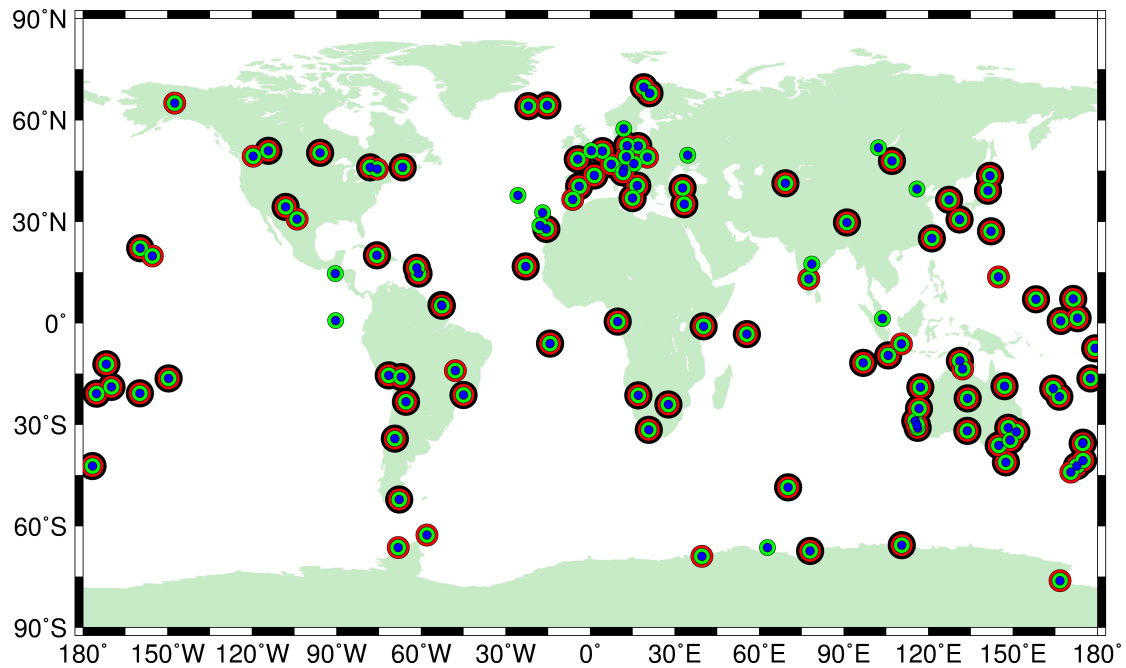


Figure 3.2 The distribution of global multi-GNSS network used in this study. The colors represent the tracked GNSS systems on a station, GPS in blue, GLONASS in green, Galileo in red and BDS in black.

The coordinates of these reference stations are fixed to the IGS weekly solutions. The GFZ analysis center final orbit and clock products are used for PPP whereas the satellite clock offsets are estimated with the network in Figure 3.2 for POP.

The PPP and POP ambiguity resolution performance in terms of fixing rate and positioning accuracy of solutions of GPS, GPS+GLONASS, GPS+Galileo, GPS+BDS and all four systems GPS+GLONASS+Galileo+BDS are analyzed.

During the data processing, we found that the observations of the Antarctica stations MAW1 and SYOG cannot be processed properly because of a lot of outliers in the positional estimates and OHI2 and OHI3 are collocated stations. Therefore, only stations CAS1, DAV1, OHI3 and MCM4 are processed in kinematic mode as they observe the most GNSS systems. Observation data from day of year 1 to 14, 2018 are processed.

In the ambiguity fixing, all possible DD ambiguities between a kinematic station and all the static stations are defined as candidates and are checked for fixing according to their fixing probability. For the GLONASS fixing, there are quite a few receivers of the same type and with exactly the same firmware and antennas as the

receivers in Antarctica used as rover in the experiment. Therefore, we ignore the differences in the firmware versions of receivers. Four types of most commonly used receivers for GLONASS ambiguity fixing, namely SEPT POLARX5, TRIMBLE NETR9, JAVAD TRE_G3TH DELTA and LEICA GR25, are selected each for one rover station, respectively. Their distributions are shown in Figure 3.3.

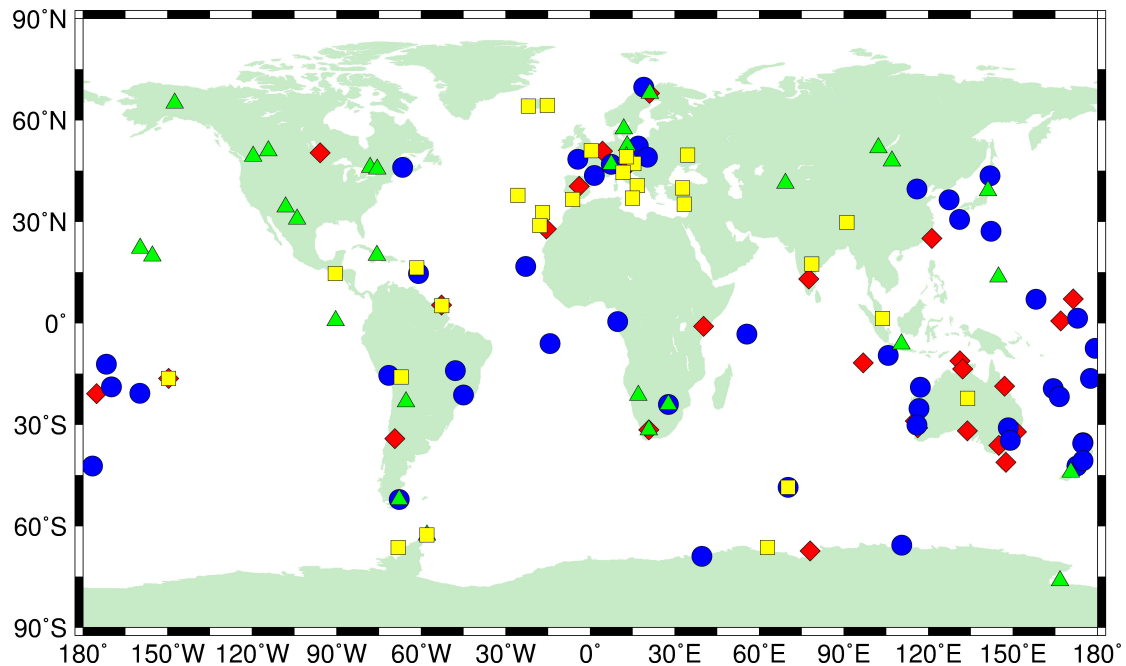


Figure 3.3 The distribution of GLONASS stations selected for integer ambiguity fixing. The red diamonds denote the SEPT POLARX5 receivers, the blue dots denote the TRIMBLE NETR9 receivers, the yellow squares denote the JAVAD TRE_G3TH DELTA receivers and the green triangles denote the LEICA GR25 receivers. The firmware versions for different types of receivers are ignored in this study.

3.3.2 Performance of Ambiguity Fixing

In this section, the DD ambiguity candidates are defined over baselines shorter than a distance of 3500 km and at least with 15 min common observations. For reliable fixing, we excluded DD ambiguities with a STD larger than 0.15 cycles or a fractional part larger than 0.25 cycles. The fixed rate, defined as the ratio of the number of the fixed and that of all independent DD ambiguities, can be a very efficient indicator to judge the fixing performance. There is an average of 35013, 51145, 43662, 39810 and 65505 daily independent DD ambiguity candidates can be used with GPS, GR, GE, GC and GREC observations, respectively. We can see that the addition of GLONASS, Galileo and BDS can enhance the estimation of the float solutions, therefore a higher

fixing rate can be achieved.

Obviously the WL fixing does not have any differences for PPP and POP since it is independent of the analysis model and only code and carrier phase observations are applied. Therefore, we only compare the performance of NL fixing.

The fixing percentages with single-, dual- and four-system observations are analyzed. The results are displayed in Figure 3.4. The average fixing percentage of PPP is 88.4% with GPS-only observations which is generally lower than that of the static processing (Ge et al., 2005, Li et al., 2017) because kinematic stations are involved for fixing. The fixing percentages of POP with GPS, GLONASS and Galileo observations are slightly higher than the corresponding PPP solutions, while the improvement is significant with the BDS observations because of the reduced impact of the orbit errors.

With the addition of other GNSS observations, a higher fixing rate can be achieved than the GPS-only solution most likely because multi-GNSS enhances the float solution. The average fixing percentages of PPP GC and GREC solutions are only about 86.8 and 89.5%, which are even 5.0 and 2.3% lower than its GR solutions. The major reason is the poor fixing of BDS because of its relatively poor orbit and clock quality. However, the POP is free from such effect, while its GR, GE and GC solutions show almost the same fixing percentage which is higher than that of GPS-only and its GREC solution represents the highest fixing rate of about 92.7%.

Comparing the ambiguity fixing of PPP and POP solutions using GC or GREC observations, the advantage of the POP approach is confirmed that the orbit biases can be absorbed by clock parameters for better estimates of float ambiguities and consequently better fixing performance.

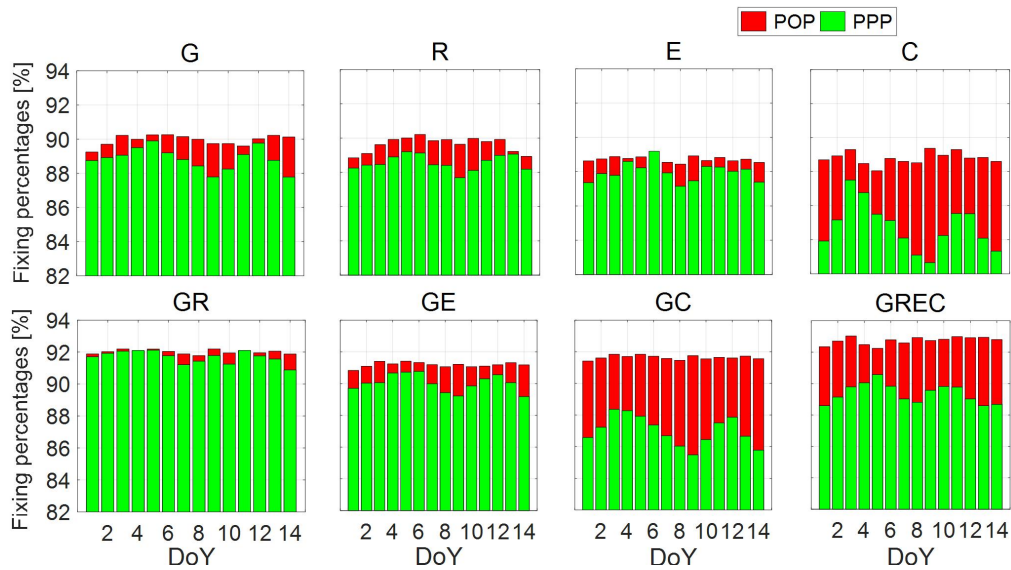


Figure 3.4 The fixing percentages of PPP and POP ambiguity resolution with 14 days of single-, dual- and four-system observations. By doing a chi-squared distribution test with a 0.05 level of significance, it is shown that the p -value that indicates the significance-level for the differences between PPP and POP calculated with observations from R, E, C, GR, GE, GC and GREC is 0.062, 0.078, 0.0030, 0.25, 0.09, 0.0036 and 0.019, respectively, with respect to GPS-only. We can see there are significant differences between the PPP and POP results with C, GC, and GREC observations.

3.3.3 Performance of positioning

For the four stations CAS1, DAV1, OHI3 and MCM4, their PPP and POP solutions with integer ambiguity fixing were established. The position differences of the float and fixed solutions regarding the IGS estimated coordinates for station CAS1 are shown in Figures 3.5 and 3.6 for PPP and POP approach, respectively. The average RMS values of the station coordinates over 14 days are calculated for each station to assess the performance of PPP and POP float as well as fixed solutions, the statistical results are shown in Figure 3.7.

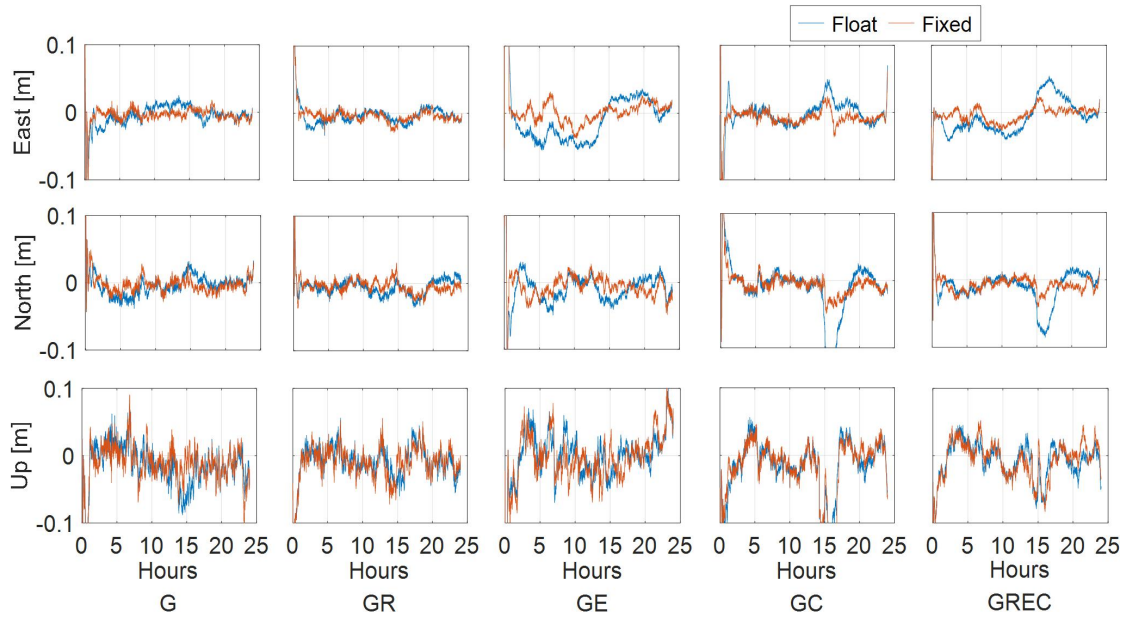


Figure 3.5 The single-, dual- and four-system PPP float and fixed solutions with respect to the IGS nominal position for station CAS1 on DOY 1, 2018

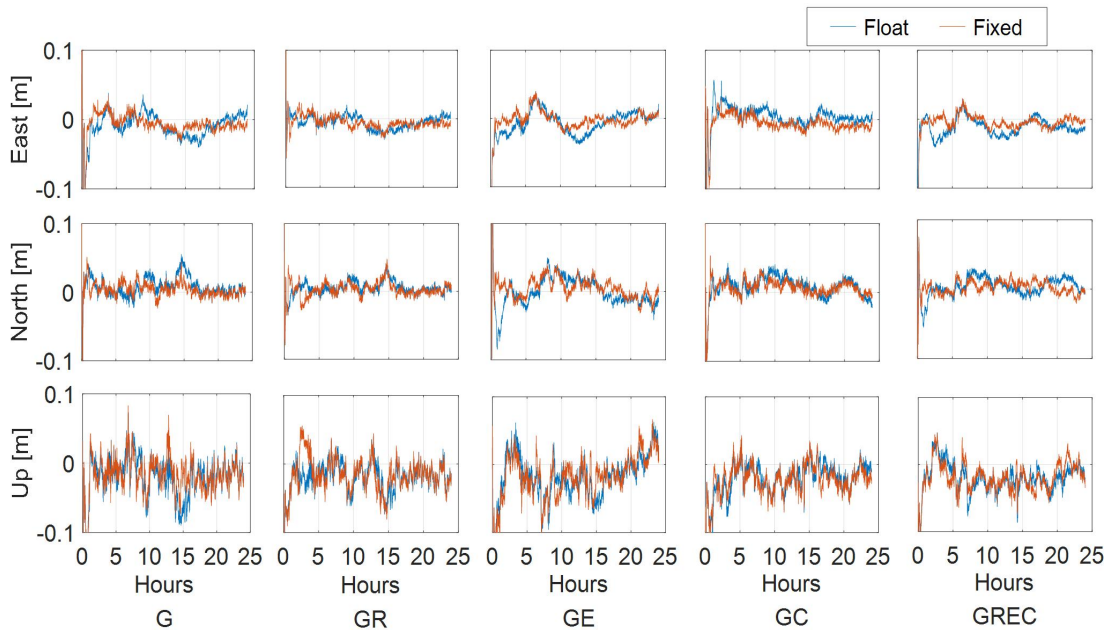


Figure 3.6 The single-, dual- and four-system POP float and fixed solutions with respect to the IGS nominal position for station CAS1 on DOY 1, 2018

Figures 3.5 and 3.6 give us a visual impression that the POP approach has on average a better performance than PPP for GE, GC and GREC solutions. Some fluctuations appear in the PPP GE position differences in Figure 3.5 which may due to the short-term fluctuations in the Galileo satellite clocks. The influence of BDS orbits and clocks on PPP GC and GREC kinematic positioning is significant. Some large

positioning errors appear between 14:00 and 16:00. The fixed solutions can improve the accuracy in the horizontal directions, the RMS value of GC solutions is reduced by 8 and 17% for the east and north components, respectively. However, in the POP solutions most of the orbit biases are compensated by the clock parameters, the positioning errors caused by the remaining orbit errors are below 5 cm for all components as shown in Figure 3.6. Moreover, the POP ambiguity resolution can further improve the positioning performance in the east component and the accuracy is improved by 14%. The differences of PPP and POP positioning results are not significant with GPS and GR observations, which is mainly due to their stable orbit and clock quality derived from globally well distributed stations.

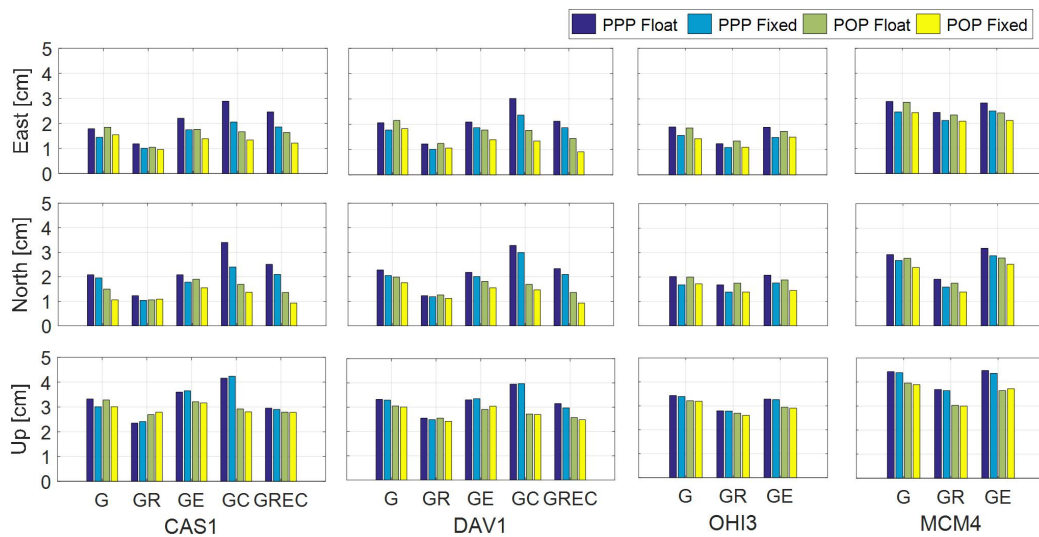


Figure 3.7 The average RMS values of kinematic PPP and POP solutions after convergence for stations CAS1, DAV1, OHI3 and MCM4 with different types of observations in the east, north and up components

Figure 3.7 shows the average RMS values of PPP and POP kinematic positioning results regarding the IGS reference over the 14 days. The positioning results of stations CAS1 and DAV1 indicate that the accuracy of the GC and GREC float PPP solutions are relatively poor, and even worse than the corresponding GPS-only solution. It is mainly caused by the poor quality of BDS orbits. The GE solution shows almost no improvement because of the limited number of available Galileo satellites. Meanwhile the GR solution represents an average improvement of 31.3, 33.1 and 18.5% compared to the GPS-only solution for the east, north and up components, respectively. The PPP fixed solutions can improve the accuracy in the

east and north components, i.e., an average improvement of 13.1, 9.5, 16.9, 29.7 and 20.0% with G, GR, GE, GC and GREC observations, respectively.

The POP single-, dual- and four-system float solutions are more stable and can achieve higher accuracy than the corresponding PPP float solutions of the four stations, i.e., the average improvements are 12.7, -2.4, 21.0, 28.1 and 6.3% with G, GR, GE, GC and GREC observations for the up component. Moreover, the POP GR, GE and GC solutions are all better than its GPS-only solution, while its GREC fixed solutions enables the highest average positioning accuracy of 1.2, 1.1 and 2.5 cm compared to that of its GPS-only fixed solution of 2.0, 1.8 and 3.3 cm for the east, north and up component, respectively.

3.4 Result of a real flight experiment

The real flight data is also from the ESA PolarGAP airborne gravimetry campaign which was introduced in Section 2.2. Here, we choose the data collected on day 19 December 2015 for analysis, which covers about 10.5 hours from 10:30 to 21:00 (UTC, Universal Time Coordinated). The GNSS data collected by the three receivers AIR2, 0158 and SPAN mounted on the Twin-Otter aircraft are all available on day December 19 and therefore can be used in this section. The trajectory is shown in Figure 3.8 with a radius about 750 km around the South Pole. As no observation data from the dedicated reference station SP2X was available on that day we used data of another reference station (FD83) which was installed in a tented field camp (Figure 3.8).

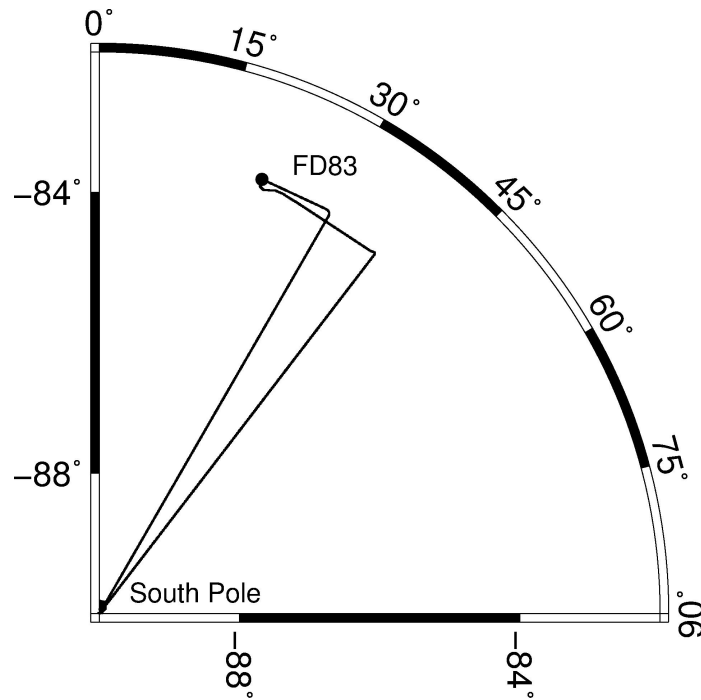


Figure 3.8 The trajectory of this flight and the location of the other reference station FD83.
The aircraft flew from the camp FD83 to the South Pole and then back to the camp.

As the observed satellites on these kinematic receivers are at low elevation angles (less than 60°), a cut-off angle of 7° is applied to fully use all satellites. Since AIR2 observes GR data, 0158 and SPAN observe GPS data, only GPS data is processed for the three antennas in DD, PPP and POP mode for validation. For DD processing only one reference station FD83 is used, while 42 IGS reference stations around Australia are included for PPP and POP processing. The sampling interval of the receivers in the experiment is 1 second.

Unfortunately, it is very difficult to evaluate the positional results of the three approaches, since no “true” or accurate trajectory is available as reference. As the three onboard antennas are fixed on the aircraft, the inter-antenna distance should remain constant during the flight. It should be pointed out that special attention must be paid to the different signal receiving time for the two receivers of a baseline, although they are programmed to receive the signal at the same epoch. The difference could reach up to more than 1 milliseconds due to online clock steering which usually shows up in the observations as millisecond jumps, for example JAVAD DELTA G3T receiver on AIR2. This is a problem mainly for receivers moving with high speed but not for static or kinematic station of moderate speed. The positions are

interpolated to the same nominal epoch time to get rid of such influence.

The time series of baseline length of the three processing approaches are calculated and shown in Figure 3.9. Be aware of that the DD estimates of the first one hour are not shown, because the reference station FD83 was moved during that time period.

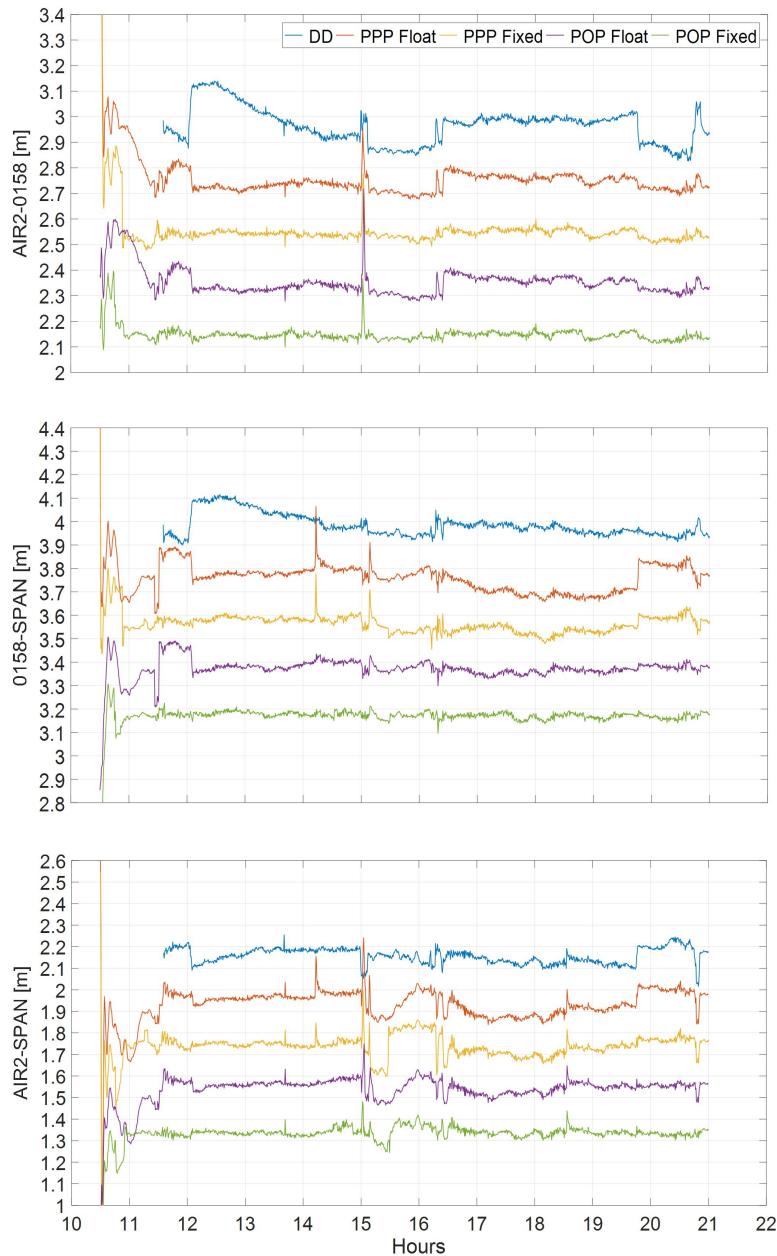


Figure 3.9 The time series of baseline length of the three antennas derived from DD, PPP and POP approaches. Both the float as well as fixed solutions are shown for PPP and POP. For clarity, the DD, PPP float, PPP fixed and POP float results are shifted by 0.2, 0.4, 0.6 and 0.8 m, respectively.

In general, there are two time periods of baseline results with larger variations, i.e.,

15:00–16:30 and 20:00–21:00 for almost all solutions besides the initialization at the beginning. The variations are more obvious in the two baselines with AIR2 than the baseline 0158–SPAN. This indicates that data quality of AIR2 might be the reason. The major reason is that in airborne kinematic positioning over Antarctica, the receivers occasionally losing track and gain of satellites observed simultaneously by the ground station and the rover is not beneficial for the estimation of the carrier phase ambiguities. This can be seen in the satellite visibility in Figure 3.10 that the continuous tracking time of one satellite is usually shorter than that in other regions. Therefore, there will be less DD observations at each epoch for the three baselines. It seems that the aforesaid fluctuations are most likely caused by the insufficient number of DD observations at AIR2 station, especially during the time 20:00–21:00, which can be seen in Figure 3.11.

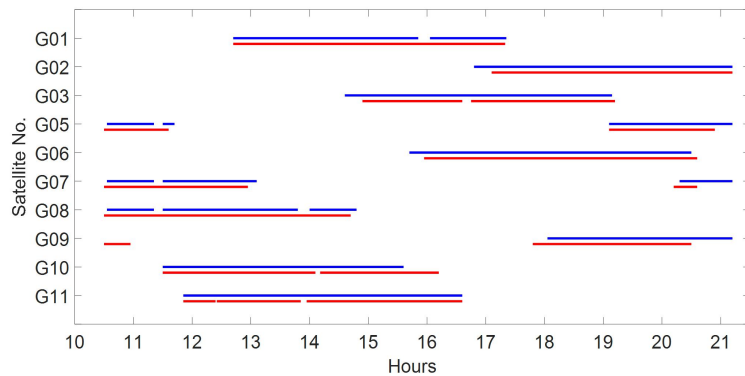


Figure 3.10 The satellite visibility tracked by the reference station FD83 (blue) and the rover AIR2 (red). Only 10 satellites are shown here.

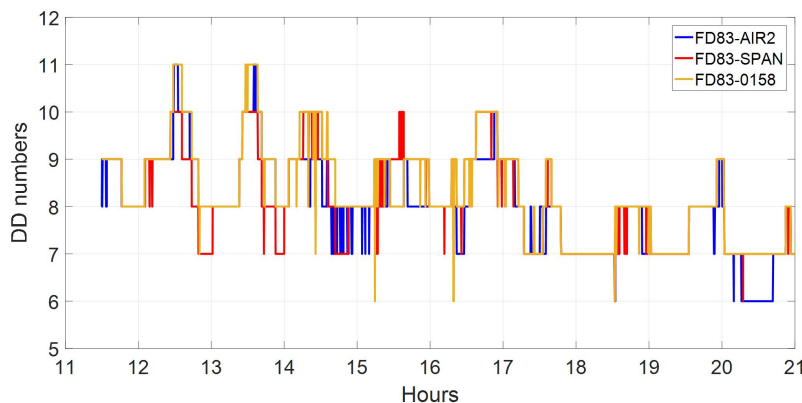


Figure 3.11 The number of DD observations used in the processing for the three baselines.

The STD values of the three baselines calculated with DD, PPP and POP float and

fixed solutions are shown in Figure 3.12. It is clearly visible that the DD approach does not work well because only a single reference station is used for such a large region which is on average worse than PPP. The POP generally shows a better performance than PPP both in float and fixed solutions, especially in the results of 0158–SPAN, and the errors in the baseline results are almost within 10 cm. Comparing the STD of float and fixed solutions, ambiguity fixing indeed improved the position accuracy significantly. The time series of the fixed solutions shown in Figure 3.9 are much flatter than their float solutions and most of the fluctuations and jumps in the float solutions disappeared. This is also a proof that the fluctuations and jumps are caused by poor observation quality of the rovers. From the beginning, it is very clear that ambiguity fixing can also considerably reduce the convergence time, in this case from 1 hour to an half hour on average.

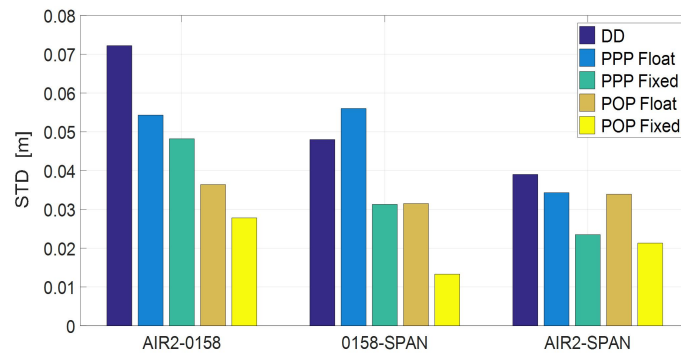


Figure 3.12 Statistics of the distances between the three antennas derived from the five types of solutions

Overall, the POP fixed solution has the best performance with a STD of 1-3 cm for the three baseline results. The ambiguity fixing is very important for airborne kinematic positioning in the polar regions to overcome fluctuations and jumps caused by poor data quality since the continuous tracking time is usually short and more signal interruptions could occur due to the high dynamical movement.

3.5 Conclusions

This chapter focuses on PPP and POP ambiguity fixing for improving the kinematic positioning performance over Antarctica with multi-GNSS observations. The multi-GNSS PPP and its ambiguity fixing are demonstrated severely influenced by the poor orbit quality of the BDS GEO satellites. A network-based approach named

POP is implemented to overcome such effect. Its ambiguity fixing performance is investigated and compared with PPP.

With data collected from a global network of 136 stations over 14 days, it is demonstrated that the BDS involved PPP solutions are not reliable, some positioning errors larger than 10 cm appear in the horizontal and vertical components with GC observations. However, the orbit errors can be mostly compensated by the satellite clocks when the clock offsets are estimated with a network of reference stations in POP processing. The kinematic positioning errors caused by the remaining orbit errors are below 5 cm. The POP also gives a better ambiguity fixing performance than PPP. A higher fixing rate can be achieved by POP than PPP because of the reduced effect of BDS orbit error, an average improvement of 5.1 and 3.2%, respectively can be obtained with GC and GREC observations. The ambiguity fixing can improve the kinematic positioning accuracy for both PPP and POP and their fixed solutions are compared to their float solutions. Significant improvements of 16.9, 29.7 and 20.0% for PPP with GE, GC and GREC observations, respectively, are obtained. The POP represents relatively slight improvements of 11.2, 17.6 and 13.6% with the same types of observations.

Through a real flight experiment over Antarctica, it is shown that the DD solutions are not robust for a baseline length of hundreds of kilometers. When comparing the baseline results among three antennas installed in an aircraft, it is found that some outliers in the PPP float and fixed baseline results disappear in the POP solutions. The ambiguity fixing can accelerate the convergence and overcome the fluctuations and jumps in the positional estimates. After converged, the POP fixed solutions generate the best baseline estimates with a STD of 1-3 cm.

4 Precise velocity and acceleration determination

GNSS-based velocity and acceleration determination has been used to monitor glacier melting and sea level fluctuation (Han and Rizos, 1999; Aoki et al., 2000; Zhang and Andersen, 2006; Scambos et al., 2017). It is also critical for high-accuracy and high-resolution regional gravity field modelling, for example, airborne and shipborne gravimetry (Schwarz et al., 1991; Zhang, 2007; Forsberg and Olesen, 2010; Li et al., 2019). Conventional methods for GNSS-based velocity and acceleration determination have been introduced in many studies. A common method for GNSS velocity determination is based on the Doppler effect. It has been investigated that the raw Doppler observable can be much noisier than the Doppler value obtained by differentiating the carrier-phase observable (Cannon et al., 1997; Hohensinn et al., 2018).

Another approach, related to the former one, uses the carrier-phase as an observable and numerically differentiates it to obtain both range rate and range acceleration. It uses the L1 carrier-phase observable due to its lower noise and applies DD to eliminate or minimize error sources such as satellite orbit and clock errors. This method was presented in Jekeli (1994) as well as in Jekeli and Garcia (1997), and later expanded by Kennedy (2002a). However this method is limited in practical operation due to the required ground reference stations.

The PPP method using only a standalone receiver can be much more efficient and cost-effective and does not rely on reference stations. However, satellite orbit and clock information with sufficient accuracy is required. A series of in-depth analysis and experimental studies with a standalone GPS receiver were made (van Graas and Soloviev, 2004; Serrano et al., 2004; Zhang et al., 2008; Zheng and Tang, 2016). These results show that the accuracy of velocity estimation with GPS carrier phase derived Doppler in static mode can reach a few mm/s and a few cm/s in kinematic mode. The POP method applied in velocity and acceleration determination was first shown in Salazar et al. (2011). It gave a similar performance as the RTK method during a low dynamics flight over Spain. When applied to a network in equatorial South America with baselines longer than 1,770 km, five reference stations were applied to enhance the estimation of satellite clock drifts. Results show its clear advantages in long-range scenarios when compared with the RTK solutions.

However, little research has been focused on the velocity and acceleration determination over Antarctica. Because of the special characteristics of ultra-high latitude and long-range airborne kinematic GNSS positioning, the traditional DD based velocity determination faces almost the same challenges as positioning. First, when there is a long distance between the kinematic and the reference station, the common errors cannot be completely eliminated by the methods of model correction or DD processing, thus the application of multiple reference stations should be taken into account (Fotopoulos and Cannon, 2001; He et al., 2016). This can lead to an increased number of common visible satellites and the reliability and accuracy of kinematic positioning are thus improved. However, the critical ground condition in Antarctica would make it difficult or impractical to set up nearby reference stations (optimal separation distance is less than 100 km), so DD based technique is hard to apply. In addition, the accuracy of the vertical velocity estimates using a standalone receiver under a highly dynamic flight is at the level of mm/s-cm/s with a reliable DD solution as reference, even if integrated GPS and BDS observations are used (Zheng and Tang, 2016). For airborne gravimetry applications, the accuracy of GNSS-derived vertical velocity is required to be better than 1 cm/s (Kleusberg et al., 1990; Christian and Guenter, 2003). Thus the PPP method does not always meet the requirements. Therefore, a method that can overcome the baseline limits as well as yielding high accuracy velocity solutions is required. Second, there are more visible satellites, but with lower elevation angles compared to the low-latitude regions, so lower Horizontal Dilution Of Precision (HDOP) but weaker Vertical Dilution of Precision (VDOP) direction can be achieved. However, this shortage can be compensated by applying a multi-GNSS constellation and thus the geometry of observed satellites can be improved. Therefore a method integrating GPS, GLONASS, Galileo and BDS is applied to improve the accuracy of velocity and acceleration estimates in the vertical component. A third challenge is that the Total Electron Content (TEC) in the Antarctic region has frequent fluctuation during the day. The variation of ionospheric delay may not be completely eliminated by epoch-by-epoch differencing. Also the atmospheric delays remaining in the epoch-differenced observations may also cause the velocity estimation to be biased. However in some studies (Serrano et al., 2004; Ding and Wang, 2011), it is regarded that the ionosphere and troposphere delays are highly time correlated, and after epoch-differencing over a short time interval, the residual errors can be significantly reduced or ignored compared to other error sources

such as the satellite clock offsets.

The main objective of this chapter is to investigate the POP approach in velocity and acceleration determination with GPS, GLONASS, Galileo and BDS observations over Antarctica. First, a four-system combination model as well as a combination strategy is presented. Then a static test illustrates the performances of the POP and PPP methods using different types of observations. The results using ionosphere-free LC and L1 observations are shown in order to investigate the influence of ionospheric errors on velocity estimation. Finally through the processing of two data sets of a real flight experiment over Antarctica, the reliability and robustness of the POP method is demonstrated when compared with DD and PPP. Finally, their velocity and acceleration estimates are analyzed and applied in gravimetry. In this chapter if there are no special notifications, only the vertical components of the velocity and acceleration estimates are presented as they are most critical for airborne gravimetry.

4.1 GPS/GLONASS/Galileo/BDS velocity estimation procedures

We begin with a brief, compact review of the POP algorithms in velocity estimation as presented in Salazar et al. (2011). We explain the general ideas developed in this reference. For details the interested reader is referred to the original paper.

It is then explained what has to be changed if not only GPS data are processed, as in Salazar et al. (2011), but also GLONASS, Galileo and BDS in addition.

In an inertial reference system, let:

$$\mathbf{x} = \begin{pmatrix} \xi_1 \\ \xi_2 \\ \xi_3 \end{pmatrix} \text{ and } \mathbf{y} = \begin{pmatrix} \eta_1 \\ \eta_2 \\ \eta_3 \end{pmatrix} \quad (4.1)$$

be two three-dimensional column vectors (positions). With:

$$\mathbf{x} \cdot \mathbf{y} = \xi_1 \eta_1 + \xi_2 \eta_2 + \xi_3 \eta_3, \quad \rho = |\mathbf{x}| = \sqrt{\mathbf{x} \cdot \mathbf{x}} \quad \text{and} \quad \mathbf{e} = \frac{\mathbf{x}}{|\mathbf{x}|} \quad (4.2)$$

means the scalar product of the two vectors \mathbf{x} and \mathbf{y} , the Euclidian length of \mathbf{x} and the unit vector in direction \mathbf{x} . We assume that the vector \mathbf{x} depends on the time t and has continuous derivatives up to the second order. The derivatives $\dot{\rho}$ and $\ddot{\rho}$

are obtained via elementary calculus:

$$\dot{\rho} = \frac{d}{dt} |\mathbf{x}| = \frac{\mathbf{x} \cdot \dot{\mathbf{x}}}{|\mathbf{x}|} = \mathbf{e} \cdot \dot{\mathbf{x}} \quad (4.3)$$

and:

$$\begin{aligned} \ddot{\rho} &= \frac{d}{dt} \left(\frac{\mathbf{x} \cdot \dot{\mathbf{x}}}{|\mathbf{x}|} \right) = \frac{d}{dt} \left(\frac{\mathbf{x}}{|\mathbf{x}|} \right) \cdot \dot{\mathbf{x}} + \left(\frac{\mathbf{x}}{|\mathbf{x}|} \right) \cdot \ddot{\mathbf{x}} = \left(\frac{|\mathbf{x}| \dot{\mathbf{x}} - \frac{\mathbf{x} \cdot \dot{\mathbf{x}}}{|\mathbf{x}|} \cdot \mathbf{x}}{|\mathbf{x}|^2} \right) \cdot \dot{\mathbf{x}} + \left(\frac{\mathbf{x}}{|\mathbf{x}|} \right) \cdot \ddot{\mathbf{x}} \\ &= \frac{|\dot{\mathbf{x}}|^2 - (\mathbf{e} \cdot \dot{\mathbf{x}})^2}{|\mathbf{x}|} + \mathbf{e} \cdot \ddot{\mathbf{x}} \end{aligned} \quad (4.4)$$

We replace the vector \mathbf{x} by the difference of two vectors:

$$\mathbf{x} = \mathbf{x}_m^p := \mathbf{x}^p - \mathbf{x}_m \quad (4.5)$$

which are also time-variables. The vector \mathbf{x}^p marked up with an upper index is interpreted as the position of a GNSS satellite p , and the one with the lower index \mathbf{x}_m designates the receiver number m . If, in a suggestive manner, we write

$$\rho_m^p = |\mathbf{x}_m^p| = |\mathbf{x}^p - \mathbf{x}_m| \quad \text{and} \quad \mathbf{e}_m^p = \frac{\mathbf{x}_m^p}{|\mathbf{x}_m^p|} = \frac{\mathbf{x}^p - \mathbf{x}_m}{|\mathbf{x}^p - \mathbf{x}_m|} \quad (4.6)$$

then this yields versions of Equations (4.3) and (4.4) where all variable names are replaced with their upper- and lower-indexed counterparts. We resolve them for terms that contained the first and second derivatives of the station coordinate vectors $\dot{\mathbf{x}}_m$, $\ddot{\mathbf{x}}_m$ and thus obtain (see Equation (25) in Salazar et al. (2011) and Equation 2.2.8 in Kennedy (2002a):

$$\dot{\rho}_m^p - \mathbf{e}_m^p \cdot \dot{\mathbf{x}}^p = -\mathbf{e}_m^p \cdot \dot{\mathbf{x}}_m \quad (4.7)$$

and (see Equation (17) in Salazar et al. (2011)):

$$\ddot{\rho}_m^p - \frac{|\dot{\mathbf{x}}_m^p|^2 - (\mathbf{e}_m^p \cdot \dot{\mathbf{x}}_m^p)^2}{|\mathbf{x}_m^p|} - \mathbf{e}_m^p \cdot \ddot{\mathbf{x}}^p = -\mathbf{e}_m^p \cdot \ddot{\mathbf{x}}_m \quad (4.8)$$

In both Salazar et al. (2011) and Kennedy (2002a), Equations (4.7) and (4.8) are used to construct observation equations for the velocity $\dot{\mathbf{x}}_m$ and acceleration $\ddot{\mathbf{x}}_m$ of a

receiver m .

For now, we do not look at the derivatives, but at the raw observations. What is observed instead, for GPS, is either the carrier-phase of the L_c or, if a smaller measurement noise is desired at the expense of having to deal with the ionosphere, the carrier phase of the L_1 signal alone. In general (literally quoting Equation (9) of Salazar et al. (2011)), we are confronted with the basic GNSS observation model:

$$\phi_m^p = \rho_m^p + c(dt_m - dt^p) + rel_m^p + T_m^p - \alpha_f I_m^p + b_m^p + \omega_{\phi_m}^p + \varepsilon_{\phi_m}^p \quad (4.9)$$

where, besides ρ_m^p that is already introduced, ϕ_m^p is the carrier-phase observable; dt_m and dt^p are the clock offsets of the receiver and the sender; rel_m^p is the relativistic correction, which is the transition from proper time to coordinate time and the Shapiro propagation delay; T_m^p and $\alpha_f I_m^p$ are the influence of troposphere and ionosphere delays, α_f means the ionosphere delay is a function of the frequency f ; b_m^p is the sum of carrier-phase ambiguity, UPD and receiver-dependent instrument delay; $\omega_{\phi,m}^p$ is the range distortion due to phase windup and $\varepsilon_{\phi,m}^p$ combines the rest of all the un-modelled errors.

Instead of going into details, the formal time derivatives of Equation (4.9) are essentially reduced to:

$$\dot{\phi}_m^p = \dot{\rho}_m^p + c(dt_m - dt^p) \quad (4.10)$$

$$\ddot{\phi}_m^p = \ddot{\rho}_m^p + c(d\dot{t}_m - d\dot{t}^p) \quad (4.11)$$

The rest can either be dropped or precisely modelled and subtracted in a reliable manner. The quantity b_m^p is piece-wise constant, thus their derivatives vanish (Defraigne et al., 2007; Geng et al., 2012). The expression rel_m^p and the phase windup $\omega_{\phi,m}^p$ can be precisely calculated and subtracted from the phase observations. The time variations of troposphere T_m^p and ionosphere $\alpha_f I_m^p$ are very slow compared to those of ρ_m^p , t_m and t^p , thus they may either be safely ignored, or taken care of by DD.

If the derivatives $\dot{\rho}$ and $\dot{\rho}$ in Equations (4.10) and (4.11) are substituted into Equations (4.7) and (4.8), respectively, we can obtain (see Equations (30) and (35) in Salazar et al. (2011)):

$$-\mathbf{e}_m^p \cdot \dot{\mathbf{x}}_m + cd\dot{t}_m - cd\dot{t}^p = \dot{\phi}_m^p - \mathbf{e}_m^p \cdot \dot{\mathbf{x}}^p \quad (4.12)$$

$$-\mathbf{e}_m^p \cdot \ddot{\mathbf{x}}_m + cd\ddot{t}_m - cd\ddot{t}^p = \ddot{\phi}_m^p - \frac{|\dot{\mathbf{x}}_m^p|^2 - (\mathbf{e}_m^p \cdot \dot{\mathbf{x}}_m^p)^2}{|\dot{\mathbf{x}}_m^p|} - \mathbf{e}_m^p \cdot \ddot{\mathbf{x}}^p \quad (4.13)$$

These expressions constitute design equations, albeit this time for the augmented state vector $(\dot{\mathbf{x}}_m, d\dot{t}_m, d\dot{t}^p)$ and $(\ddot{\mathbf{x}}_m, d\ddot{t}_m, d\ddot{t}^p)$. The design vector for both cases, velocity and acceleration, is a five-dimensional row $(-\mathbf{e}_m^p, c, -c)$.

There are different approaches for processing Equations (4.12) and (4.13). In Kennedy (2002a), the derivatives of the clock parameters are removed by double-differencing, solving for the receiver velocity $\dot{\mathbf{x}}_m$ and the receiver acceleration $\ddot{\mathbf{x}}_m$ alone. This method is of benefit especially if the rover with coordinate \mathbf{x}_m is not far away from the reference stations with known coordinates. In that case residual influences of the derivatives of the troposphere \dot{T}_m^p , \dot{T}_m^p and the ionosphere $\alpha_f \dot{I}_m^p$, $\alpha_f \dot{I}_m^p$ are cancelled out by the differencing process.

For the PPP method, the satellite clock drift $d\dot{t}^p$ is obtained by differentiating the IGS satellite clock products regarding time. However, the derivation process may make the clock drifts much noisier than those from estimates “on-the-fly”.

In Salazar et al. (2011), this method leaves the measurements undifferenced and explicitly solves for the derivatives of the clock offsets. This is done in quite an analogue manner as the receiver positions are adjusted instead of the velocities and the accelerations. Note that the design vectors $(-\mathbf{e}_m^p, c, -c)$ for obtaining positions are exactly the same as those for the velocities and accelerations. This feature is actually exploited by performing the adjustment of velocities and accelerations with software called GPSTk (ARL, 2017) which is originally meant for establishing the receiver positions.

Following the first equation after Equation (25) in Salazar et al. (2011), the entire

network is hooked to a reference station with index 0 which provides a reference clock:

$$\begin{aligned} d\tau_m &= dt_m - dt_0 \\ d\tau^p &= dt^p - dt_0 \end{aligned} \quad (4.14)$$

where $d\tau_m$ and $d\tau^p$ represent the receiver relative clock and the sender relative clock with respect to the reference clock, respectively. In Equations (4.12) and (4.13) both the offsets dt_m and dt^p of the GNSS receiver and sender always appear in form of the difference $dt_m - dt^p$. Therefore, they remain valid if that difference is replaced with $d\tau_m - d\tau^p$. Due to this manipulation, those equations become solvable in a unique manner.

We finish here the review of the methods as presented in Salazar et al. (2011) and Kennedy (2002a) and explain what has to be changed if not only GPS data are processed, but rather multi-GNSS data (GPS, GLONASS, Galileo and BDS). The good news is that almost everything can be taken over. The only additional item that has to be taken care of is the inter-system bias, which plays a role in adjusting the receiver position \mathbf{x}_m .

If more than one GNSS system contributes to the rover m adjustment, then Equation (4.9) changes into:

$$\phi_m^{p,X} = \rho_m^{p,X} + c(dt_m^X - dt^p,X) + rel_m^p + T_m^p - \alpha_f I_m^{p,X} + b_m^{p,X} + \omega_{\phi m}^{p,X} + \varepsilon_{\phi m}^{p,X} \quad (4.15)$$

where X runs through the GNSS systems: GPS, GLONASS, Galileo and BDS. For convenience, we introduce G, R, E and C to denote them, respectively. In multi-constellation systems, because of the different frequencies and signal structure of the individual GNSS, the ISB and IFB parameters must be considered in a combined analysis of multi-GNSS data. Here, if we do not consider the integer ambiguity resolution, the satellite- and receiver-dependent carrier-phase hardware delay biases are usually stable over time and they are considered absorbed by the ambiguity parameters (Defraigne et al., 2007; Geng et al., 2012). The satellite and receiver code biases are absorbed by the clock parameters dt^s and $dt_{r,s}$. Through this reformulation, we conclude that the receiver clock offsets are the combination of receiver clock offsets and code bias. The ambiguity is actually the one that absorbed

the satellite and receiver carrier-phase hardware delays minus the receiver code bias. When it comes to a multi-GNSS receiver, the differences of code biases for different GNSS systems inside a receiver can be written as the inter-system clock differences as the receiver code biases are absorbed by the clock. Based on this, the inter-system biases of GLONASS, Galileo and BDS with respect to GPS are set up inside the receiver:

$$\begin{aligned}
 cdt_m^R &= cdt_m^G + ISB_G^R \\
 cdt_m^E &= cdt_m^G + ISB_G^E \\
 cdt_m^C &= cdt_m^G + ISB_G^C
 \end{aligned} \tag{4.16}$$

Here, the GNSS receiver is timed to the GPS system, then in Equation (4.16) dt_m^X is exchanged for dt_m^G and we have to add the terms ISB_G^X . Thus, on the right side of Equations (4.10) and (4.11) the ISB variation rate \dot{ISB}_G^X and acceleration \ddot{ISB}_G^X should also be added, respectively. Fortunately, the ISB parameter is almost constant and its variations \dot{ISB}_G^X and \ddot{ISB}_G^X at a short sampling interval such as one second are considered as zero (Ge et al., 2008; Jiang et al., 2016). This means that the ISB parameters cause no effect on multi-GNSS velocity and acceleration determination.

4.2 Combination of different types of observations

For multi-system data processing, precise weighting of the observations from different systems is very important as the measurements of different systems have different noise levels. So, adopting an Equivalent Weight Ratio (EWR) for the combination of different types of observations is not adequate. To find the optimal weighting, Helmert variance component estimation is widely used (Koch, 1999). However, it requires a longer computation time for iteration and highly redundant measurements which are especially a challenge for systems like Galileo and BDS. Nowadays each of the four systems alone enables observations of at least four satellites for positioning, which provides very valuable *a priori* information. Here the adaptive factor is determined by the posterior variances of the overlapping parameters. The overlapping parameters to be estimated are the rover clock drift and rover velocity in three components and can be obtained by an equivalent parameter reduction principle (Xu, 2007). In practice, the adaptive factor is calculated epoch by

epoch with the following:

$$\alpha_k = \frac{1}{\sqrt{(\sigma_{R_k}^2 + \sigma_{x_k}^2 + \sigma_{y_k}^2 + \sigma_{z_k}^2)}} \quad (4.17)$$

where $\sigma_{R_k}^2$, $\sigma_{x_k}^2$, $\sigma_{y_k}^2$ and $\sigma_{z_k}^2$ are the posterior variances of the rover clock drift and the rover velocity in three components, which are obtained by the posterior unit weight variance σ_0^2 multiplied by the corresponding diagonal elements of the co-factor matrix. We can see that by applying a Posterior Weight Ratio (PWR), the contribution of a single system is adaptively adjusted by the adaptive factor determined by its inner accuracy, thus the reliability and accuracy of the combined solution are ensured in case of the outliers derived from any single system.

Since it is reported that GPS, Galileo and BDS carrier phase measurements have the same level of accuracy but not GLONASS (Yang et al., 2014; Li et al., 2015), the measurements of GPS, Galileo and BDS are assigned the same weight, and the weight for GLONASS is determined by Equation (4.17). It is suggested not to use Equation (4.17) to calculate the weight for Galileo and BDS individually, since the number of observed satellites are usually not enough to obtain reliable adaptive factors every epoch for the two systems. This may wrongly down weighted the observations of Galileo and BDS.

4.3 Static experiments over Antarctica

Two kinds of static experiments have been performed. The first fully assesses the performance of the POP method using networks of different sizes with LC and L1 observations. The second demonstrates and compares the reliability of the POP and PPP methods with multi-GNSS data.

4.3.1 Data description

The data was collected from the Antarctica IGS network, which consists of eight stations (www.igs.org/network/). The distribution of the stations is shown in Figure 4.1. Four stations of the MGEX network (<http://www.igs.org/mgex/>) are marked in red. In this experiment, the data sets from these four MGEX stations on 19 December 2015 were investigated. Table 4.1 shows the network baselines. We can see that the

shortest baseline is more than 1,000 km; it is considered difficult to obtain reliable and accurate DD solutions, thus the DD method is not involved in the computation in this experiment.

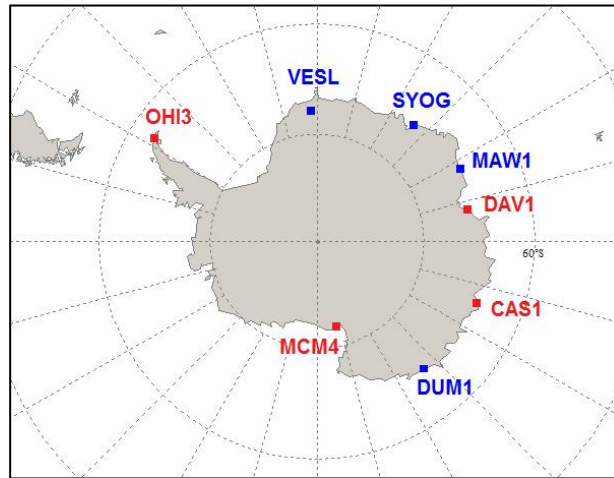


Figure 4.1 IGS station distribution over Antarctica. Four MGEX stations marked in red are used in this study. The other stations in blue are not involved in calculation as they collect neither high-rate (1 Hz) nor multi-GNSS data.

Table 4.1 Antarctica test network with the four stations shown in Figure 4.1, the baseline length is thousands of kilometres.

Station	Latitude (deg)	Longitude (deg)	Distance to DAV1 (km)
DAV1	-68.577	77.972	-
CAS1	-66.283	110.519	1399.986
MCM4	-77.838	166.669	2687.301
OHI3	-63.321	-57.902	4836.526

4.3.2 Performance assessment of the POP method using GPS data

In this experiment, the data is taken from the IGS high-rate network with one second sampling interval. DAV1 is regarded as the rover, CAS1 the master station, and MCM4 as well as OHI3 serve as the reference stations. Here we design three networks of different sizes, ranging from two to four stations. The LC and L1 observations are used to illustrate the effect of ionospheric drift on velocity and acceleration estimation. Results and statistics are shown in Figure 4.2 and Table 4.2.

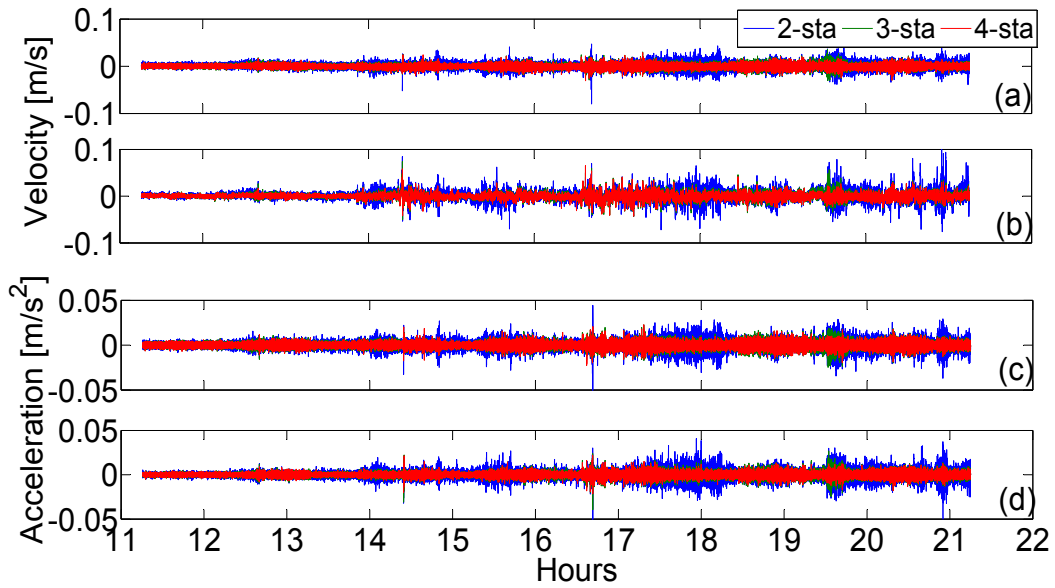


Figure 4.2 Velocity ((a), (b)) and acceleration ((c), (d)) estimates by the POP method with different networks and different types of observables. (a) and (c) are based on the LC observable, (b) and (d) are based on the L1 observable. The ionospheric drift may cause biased estimation of the velocity with L1 observable. Applying a three- or four-station network can generate more robust velocity and acceleration estimates than a two-station network.

Table 4.2 Statistics of velocity and acceleration estimates in the “Up” component as a function of network size with respect to DAV1. Master station CAS1 and the rover DAV1 are included in each network; the reference stations MCM4 and OHI3 are added to form the networks of size three and four.

Component	Network Size	Mean		RMS	
		LC	L1	LC	L1
V_U (mm/s)	2	0.62	1.07	6.91	11.13
	3	0.02	0.35	4.69	7.01
	4	-0.13	-0.27	4.24	6.21
A_U (mm/s ²)	2	8.82e-3	5.67e-3	5.17	5.08
	3	2.62e-3	-1.18e-3	3.56	3.09
	4	2.19e-3	1.01e-3	3.17	2.66

With the increase of the number of stations, regardless of using the LC or L1 observable, the RMS values of the velocity and acceleration estimates decrease. Compared to a two-station network, the improvement is significant when using a

three-station network. Taking the LC observable as an example, the RMS values of the velocity and acceleration estimates improve by 32% and 31% in the “Up” component, respectively. This improvement is mainly due to the improved geometry, and the addition of one more reference station reinforces the estimation of satellite clock drifts. However, the improvement is not significant when using a four-station network compared to a three-station. Thus, it is suggested to use a three-station network while applying the POP method for static processing in Antarctica. For real kinematic flights over the south pole, the optimal size of network still requires further investigation since the elevation maybe quite different from that of the IGS stations located along the Antarctica coast.

Figure 4.2 and Table 4.2 also show the effect of ionospheric drift on velocity and acceleration estimates and the results are comparable using LC and L1 observations. Taking the four-station network for example, it can be seen that using LC leads to a decrease in dispersion (around 51% improvement in the average value) of velocity estimates compared to L1, while there is also a magnitude improvement in RMS of about 33% for the velocity estimates. This indicates that ionospheric drift may affect the velocity determination significantly over Antarctica. On the other hand, comparison of the RMS values of the acceleration estimates derived from the LC and L1 observations suggests that the ionospheric drift rate plays a minor role in the acceleration determination. Overall, it is better to use LC for velocity and L1 for acceleration determination over Antarctica.

The POP method-based velocity and acceleration estimates can be better than 5 mm/s and 3 mm/s²; the accuracy can still be improved if multi-GNSS observations are applied. That will be shown in the next experiment.

4.3.3 Performance assessment of the POP and PPP methods using multi-GNSS data

In this experiment, data was taken from the MGEX network with a sampling interval of 30 seconds. For the POP method, the assignment of stations differed from the former test, with CAS1 as “rover”, MCM4 as “master” and DAV1 and OHI3 as “references”. This is because DAV1 collects only G/R data while CAS1, MCM4 and OHI3 all collect G/R/E/C data. For PPP, CAS1 was analyzed in kinematic mode. Figure 4.3 shows the HDOP and VDOP values of station CAS1. It can be seen that,

compared to a GPS-only system, the HDOP turns out to be much lower when using a G/R/E/C combined system. However, the VDOP does not improve significantly because of the lack of high elevation satellites over Antarctica. It should be pointed out that the DOP is only used to quantify the satellite geometry on a single station, not for a network.

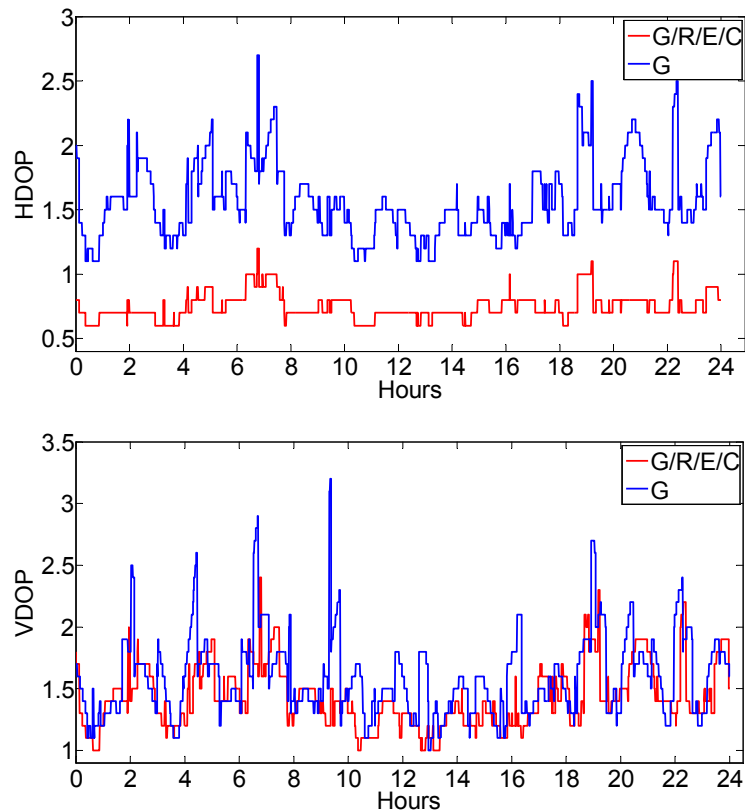


Figure 4.3 HDOP and VDOP of station CAS1. The HDOP of the G/R/E/C combined system tends to be much lower than a GPS-only system because of the improved geometry, however the improvement is not significant for VDOP.

Effectiveness and reliability of multi-GNSS velocity and acceleration determination with the POP and PPP methods are further compared and evaluated. For convenience, only the LC observable is calculated. The results are displayed in Figure 4.4 and Table 4.3. According to the analysis in Section 4.3.2, here we use a three-station network for the POP method.

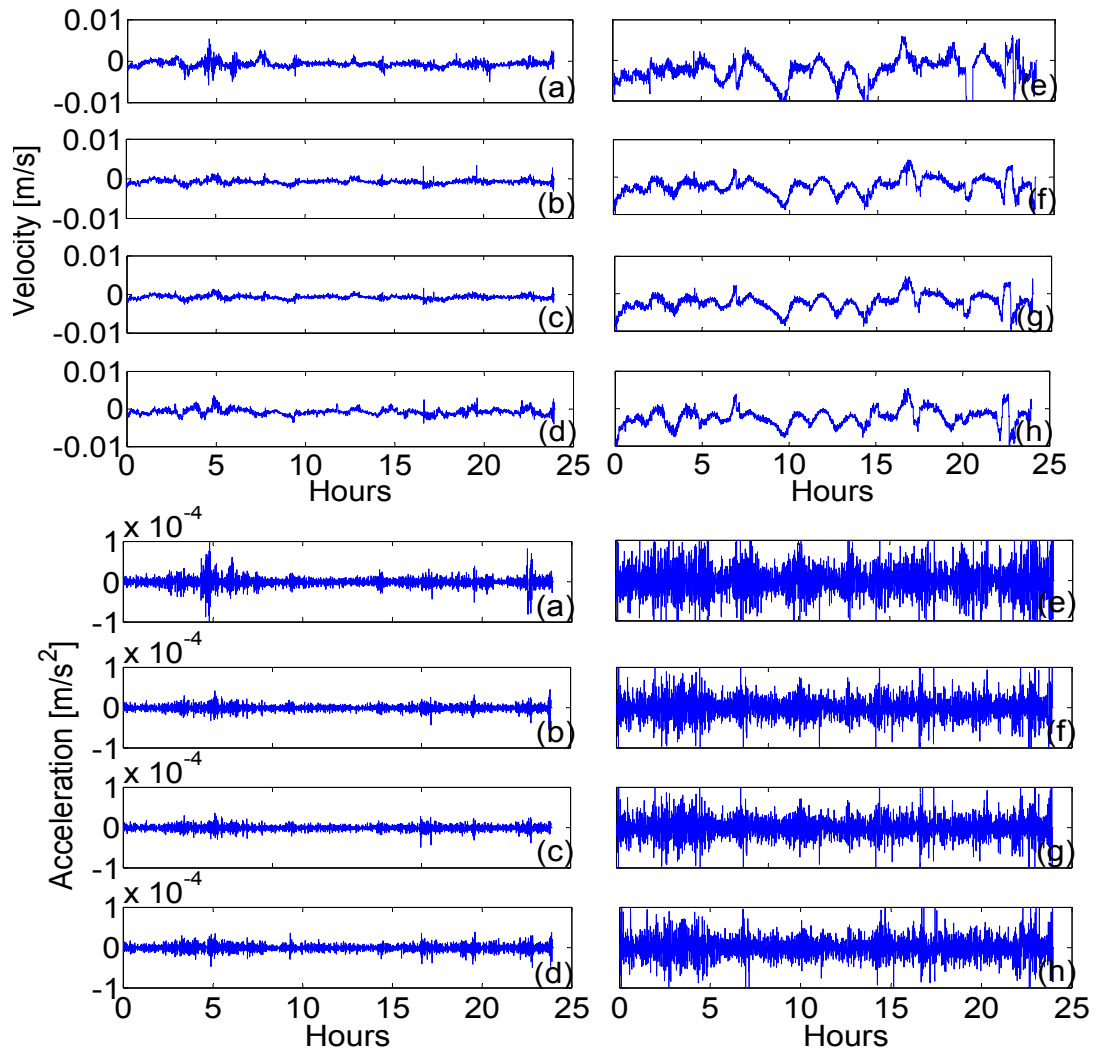


Figure 4.4 Velocity and acceleration estimates at 30 seconds interval by the POP and PPP methods from application of different GNSS systems: G (a), G/R (b), G/R/E/C with PWR (c) and G/R/E/C with EWR (d), (e)–(h) are corresponding results from PPP. It clearly shows the higher performance of the POP method with different systems.

Table 4.3 Statistics of velocity and acceleration estimates by the POP and PPP methods using different GNSS systems.

Component	System	Mean		RMS	
		POP	PPP	POP	PPP
V_U (mm/s)	G	-0.67	-2.51	1.21	4.54
	G/R	-0.72	-2.36	0.91	3.20
	G/R/E/C_PWR	-0.68	-2.34	0.82	3.16
	G/R/E/C_EWR	-0.76	-2.32	0.90	3.23
A_U (mm/s ²)	G	-5.47e-4	1.24e-4	1.72e-2	6.50e-2

G/R	-4.73e-4	1.71e-4	1.08e-2	4.48e-2
G/R/E/C_PWR	-4.79e-4	1.72e-4	9.98e-3	4.21e-2
G/R/E/C_EWR	-5.51e-4	2.05e-4	1.11e-2	4.45e-2

For the two methods, the velocity and acceleration estimates using a G/R combined system are superior to those using a GPS-only system. The accuracy is improved by 25% and 29% for velocity and 37% and 31% for acceleration. However, the improvement is not significant when adding the Galileo and BeiDou systems. One reason is that the reference station DAV1 only observes G/R data. The other is that few Galileo and BDS satellites are observed (an average number of three and six, respectively). The addition of Galileo and BDS satellites seems not to improve the VDOP of the G/R system. In addition, regarding the POP method, the results calculated from G/R/E/C combined observations with PWR are superior to that with EWR. The posterior weight can effectively adjust the contributions of different systems and the accuracy is improved by 8% and 10% for velocity and acceleration, respectively. However, the RMS does not make a difference no matter what kind of weighting approach is applied for the PPP method. This is mainly because the accuracies of velocity or acceleration estimates by the PPP method are poor and even proper weighting does not make significant improvements.

As the sampling interval is 30 seconds, compared with the experiment in Section 4.3.2 when using one second data, the measurement noise is suppressed by a magnitude of 30 when we conduct the epoch-differencing process. This is why the POP-based velocity estimates have a much higher accuracy than with one second data, and RMS values of about 1 mm/s and 0.01 mm/s² for velocity and acceleration estimates can be obtained. However, when it comes to the PPP solution, there are obvious systematic errors in the velocity estimates. When considering the calculation process of the POP and PPP solutions, the only difference is the derivation of the satellite clock drifts. As the satellite clock offsets are usually very stable or have a linear variation over one day, the derivation errors of the satellite clock offsets regarding 1 or 30 seconds should have the same magnitude, and will be significant when the measurement noise is suppressed. This equals that the resultant clock drift errors are amplified by 30 times if we assume the measurement noise does not change. It was found that the clock drift errors may cause biased estimation of the velocity.

However, as to the POP method, the satellite clock drifts are estimated with a network of reference stations, which is still robust for velocity determination. This demonstrates that the satellite clock drifts have a strong impact on velocity estimation.

Overall, comparing the RMS values shown in Table 4.3, it can be seen that the POP method is much more reliable than the PPP method when using 30 seconds data. It is thought that POP using a network of stations can provide more robust satellite clock drifts estimates, while PPP may be vulnerable to the derivation of the IGS clock products.

4.4 A real flight experiment

An application of the POP method to aircraft velocity and acceleration determination was tested. Here we also use the data from the ESA PolarGAP campaign. The data of two flights described in Chapters 2 and 3 are both processed for velocity and acceleration estimation. For the two flights, only AIR2 is used for velocity and acceleration determination, the data from the other two rovers are not necessary as the baseline information is no longer required. Besides the data from the reference stations SP2X and FD83, the GPS/GLONASS data from four IGS stations: OH13, DAV1, CAS1 and MCM4 (see Figure 4.1) were also used for POP independent calculation purposes.

4.4.1 The first data set processing

The data collected on day December 19, 2015 was applied for the first test. For the DD, PPP and POP methods, the LC carrier phase observation was used for velocity and acceleration determination. Regarding the DD method, FD83 is taken as the reference station. Its data processing was done with a software tool called HALO_GNSS (He et al., 2016). When the aircraft was parked, it was quite close to FD83. However, when it flew, the distance between them (shown in Figure 4.5) became larger. After 14:00, it is more than 100 km and up to 750 km. The velocity estimates may be greatly affected by the common errors that are not eliminated by DD processing.

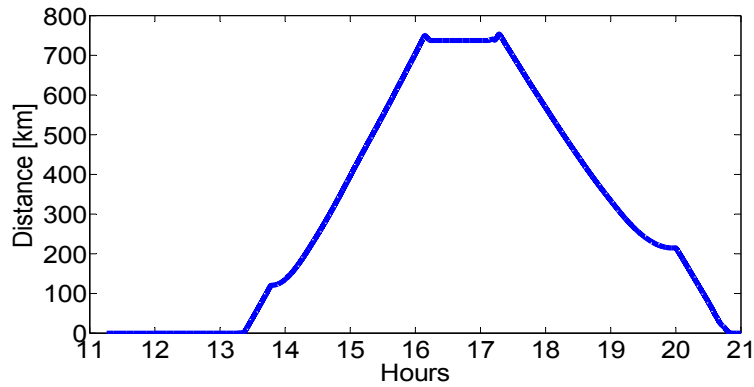


Figure 4.5 Distance between the rover and the reference station. The baseline can be as long as 750 km, which is a challenge for the application of the DD method.

It is usually very difficult to establish a “reference solution” for a kinematic experiment. However, a better way to assess the results of each method is to study during the period of time when the aircraft was parked next to the camp, which is only 55 m from the reference station FD83. This period spanned from local time 10 h 30 min to 11 h 16 min. The results from the PPP and DD methods are also calculated to make a comparison.

As Figure 4.6 shows, the vertical velocities obtained by the three methods are comparable when using a known zero reference solution during the static period. Table 4.4 presents a summary of the mean and RMS values of velocity and acceleration for the “Up” component during the static period. The RMS shows that the POP method outperforms DD and PPP in velocity estimation. It can produce velocity estimates with an accuracy of 3 mm/s. It also has better performance than the methods in van Graas and Soloviev (2004) and Salazar et al. (2011). This is because of the addition of the GLONASS observations. The acceleration estimates are similar, although the POP method again shows slight advantages.

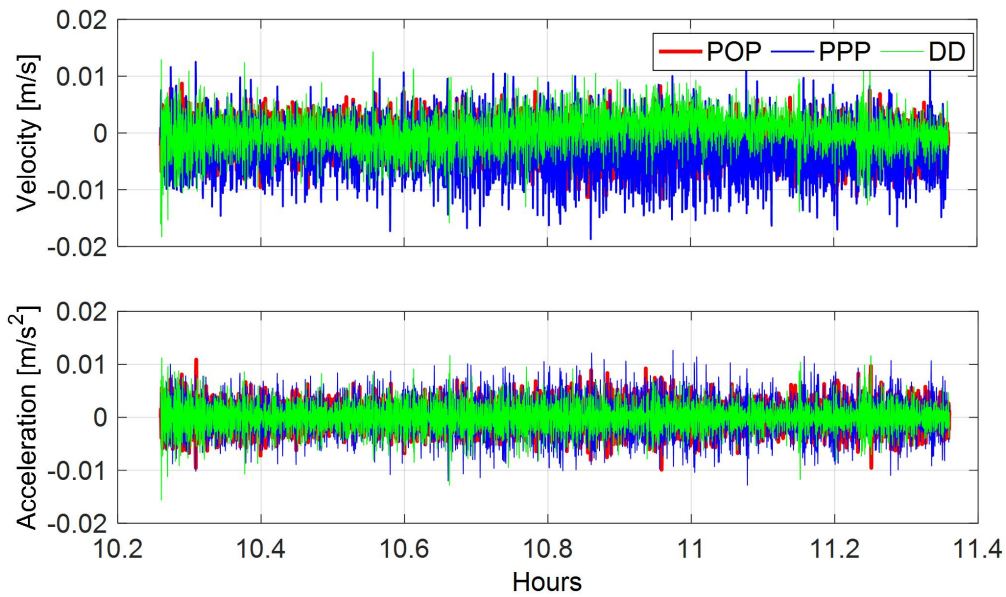


Figure 4.6 Vertical velocity and acceleration estimates during the static period.

Table 4.4 Statistics of vertical velocity and acceleration estimates for the POP, PPP and DD methods. It shows slight advantage of the POP solution over the PPP and DD solutions.

Velocity of an accuracy of 3 mm/s can be obtained.

Component		POP	PPP	DD
V_U (mm/s)	Mean	0.07	-2.98	-1.58
	RMS	3.01	5.43	3.41
A_U (mm/s ²)	Mean	0.002	-0.001	0.002
	RMS	2.54	3.65	2.74

It is rather difficult to evaluate the kinematic results. Traditionally, the differential GPS method is usually taken as an external assessment approach. For such a long range (0~750 km, see Figure 4.5), multiple reference stations that tend to have an increased number of common satellites are usually used, and it has already been successfully applied in many studies (Fotopoulos and Cannon, 2001; He et al., 2016). However, in this contribution, only one reference station is used, although there is a backup station FD83-2, but they were mounted too close together and thus the kinematic solutions may not be enhanced by using a network of these two stations.

Instead, in order to evaluate the performances of the three methods, we compare differences among their velocity and acceleration estimates. Taking the velocity solutions for analysis, Figure 4.7 plots the velocity difference for the “Up” component

during the period of the kinematic flight, Figure 4.7(a) and 4.7(b) are the differences between POP and PPP with respect to DD and Figure 4.7(c) is the difference between POP and PPP. We can see larger biases in Figure 4.7(a) and 4.7(b) than in 4.7(c). The corresponding standard deviation values of velocity differences for Figure 4.7(a), 4.7(b) and 4.7(c) are 8.06, 7.98 and 4.88 mm/s, respectively. Such comparisons show that the POP and PPP solutions agree with each other well while the DD solution seems to be less consistent with the POP or PPP solution. As in Least-Squares, usually the inner precision or the model accuracy can be evaluated by the post-fit RMS of the measurement residuals. Thus, the RMS of the velocity estimates of the three methods are calculated and their results are shown in Figure 4.7(d), 4.7(e) and 4.7(f). Starting at 14 h 30min, the distance is more than 200 km (see Figure 4.5), differences become larger than shown in Figure 4.7(a) and 4.7(b) which is in accordance with the larger RMS shown in Figure 4.7(d). This demonstrates that with the increase of the distance between the rover and the reference station, the biases in velocity estimates of the DD method also increase.

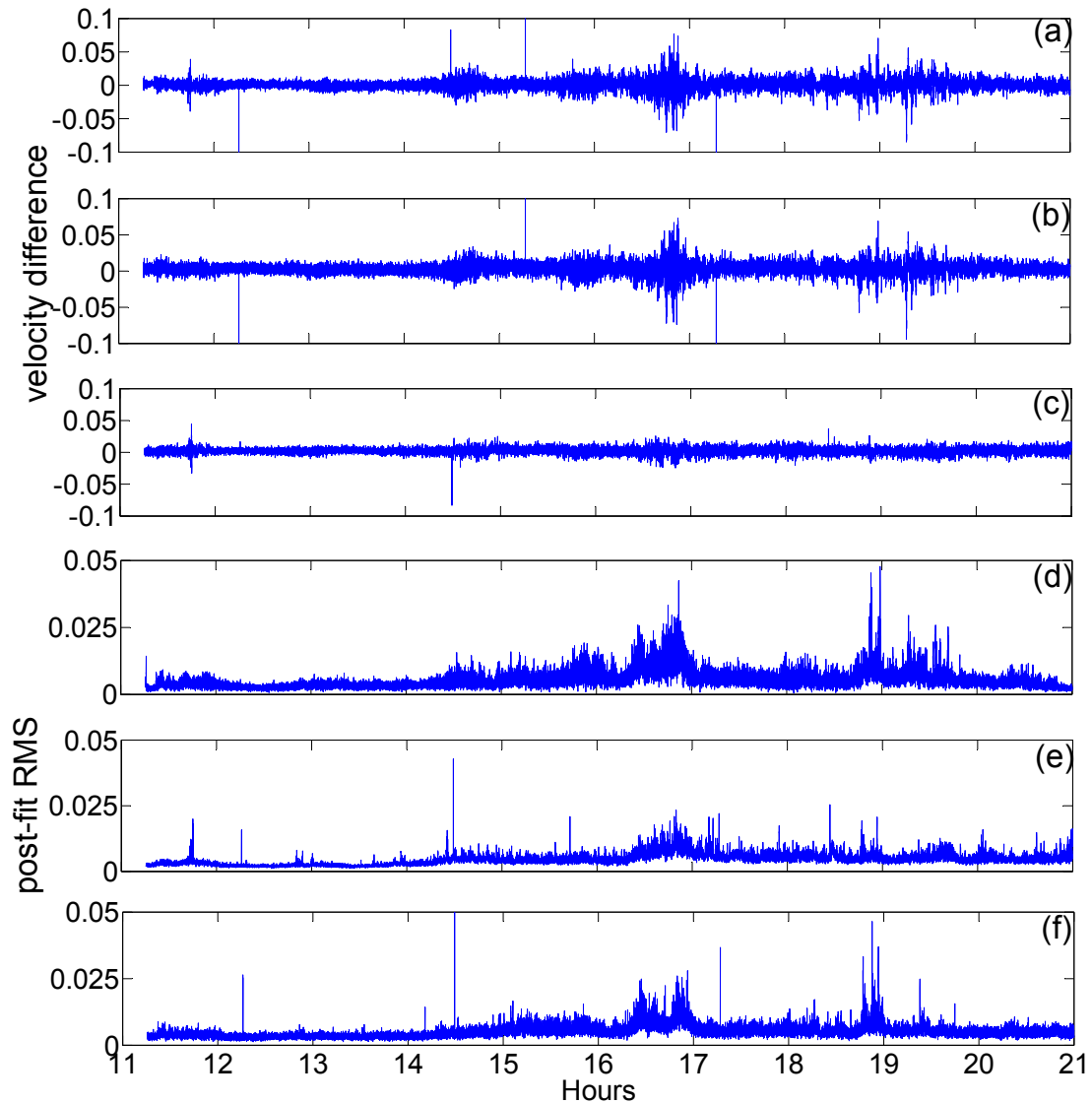


Figure 4.7 Aircraft velocity differences between POP and DD (a), PPP and DD (b), POP and PPP (c) during the kinematic flight period and epoch-by-epoch postfit RMS of DD (d), POP (e) and PPP (f) (unit: m/s). The POP and PPP solutions seem to agree with each other well while the DD solution may be biased with the increase of the baseline length.

It should be noted that the POP and PPP solutions seem to be more consistent than the results in Section 4.3.3. That is mainly because here we use one second data and the magnitude of the two kinds of satellite clock drift errors are not significant compared to the epoch-differencing errors of measurements. The kinematic velocity estimates from the two methods still show differences with STD of 4.88 mm/s, which suggests that satellite clock drifts from estimation “on-the-fly” and by derivation may still cause difference to a notable extent in the velocity determination. As already demonstrated in the static test with 30 seconds data, the estimated satellite clock drifts

tend to have a much lower noise, which is suggested for use in the kinematic velocity determination.

As the performance of acceleration is in accordance with velocity, overall, it can be concluded that for long range kinematic velocity and acceleration determination, the POP method using a network of stations tends to be more robust and reliable than the single-baseline DGPS method.

4.4.2 The second data set processing

The second data set covers two consecutive days of January 8 and 9. Only reference data of SP2X is available on the two days. It had been demonstrated in Sections 2.2.1 and 2.2.2 that there are large positioning errors at the day boundaries, here we will investigate whether the PPP derived velocity will also suffer from such influence.

The velocity and acceleration is calculated from the DD, PPP, and POP approaches based on time differentiation of the carrier phase measurements. It is difficult to establish a “true” reference for the three types of velocities and accelerations, so we investigate the differences between them. Figure 4.8 plots these differences for the vertical velocities and accelerations for the whole flight period. Generally speaking, there are large biases and outliers in the differences of the different types of positional estimates shown in Figure 2.7, while the velocity and acceleration results turn out to be much smoother. The reason is mainly that the ambiguity parameters vanish and the tropospheric delays are significantly reduced after differencing with respect to time, the residual tropospheric delays have negligible effects on the vertical velocity and acceleration estimates. However, some relatively large velocity discrepancies show up in the DD–PPP and DD–POP differences in Figure 4.8, accompanied with some fluctuations appear around 22:00 and 04:00 when the baseline length reaches its peak (see Figure 2.6). This indicates that these large discrepancies are more likely from the DD solutions which is in accordance with the result of the first flight. The acceleration results are similar with velocity. The STD values of the velocity differences shown accordingly in Figure 4.8 are 8.6, 7.8, and 3.8 mm/s, and the acceleration STD values are 3.4, 3.2, and 2.3 mm/s². This demonstrates the better agreement between the PPP and POP solutions, especially taking into account the characteristics of long-range kinematic positioning. There are almost no discrepancies

in the PPP-POP results, which indicates that the clock offset drift errors at the day boundaries cause almost no influence on the velocity estimation.

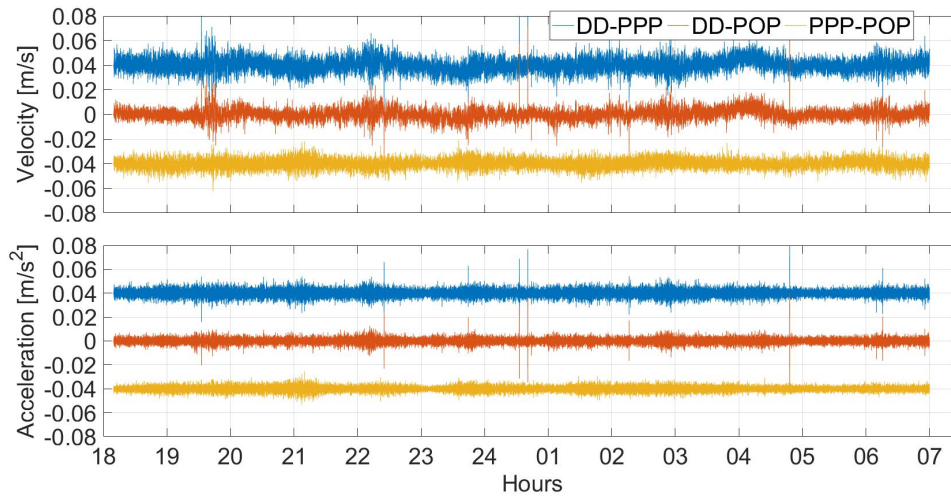


Figure 4.8 Aircraft velocity (top) and acceleration (bottom) differences between the three solutions. To show a clear visual difference, the top and bottom numerical values in each panel have been shifted by ± 0.04 , respectively.

Another way to evaluate the performances of the three methods is to investigate the velocity estimates when the aircraft was relatively stable. Figure 4.9 plots the vertical velocity estimates during the period when the aircraft was parked near the camp, only several hundred meters away from station SP2X. The RMS values for the three solutions are 2.72, 2.83, and 4.38 mm/s, respectively. The figure indicates that the vertical velocities yielded by the three methods are comparable when using a known zero velocity as a reference. The DD method produces the best estimates, which is in accordance with its high-accuracy performance in short baseline conditions. POP gives almost the same performance as DD. However, the PPP velocity estimates tend to be noisier than the others, which is most likely due to the clock offset drift noise.

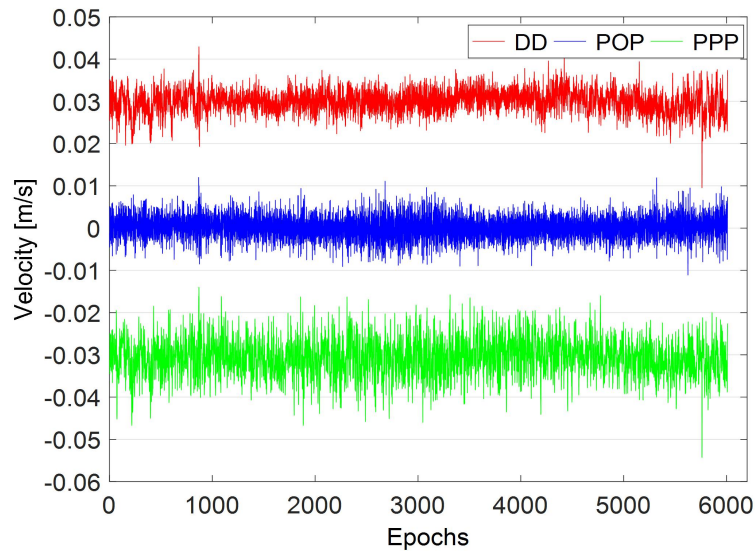


Figure 4.9 Vertical velocity of the aircraft in DD, POP, and PPP solutions during the static period since 18:00 (local time). The DD and PPP solutions have been shifted by ± 3 cm/s, respectively.

The GNSS accelerations applied in airborne gravimetry has already been well demonstrated in other regions, such as the GEOHALO campaign over Italy (He, 2015; Lu et al., 2017). In this chapter, it will be assessed over Antarctica. Unfortunately, due to the fact that the gravity data processing procedure of the PolarGAP campaign was not rigorous, the filtered gravity solutions that incorporating the GNSS vertical kinematic accelerations at different accuracy levels actually cause no differences for the final gravity results. Therefore, it is actually not necessary to compare the final gravity results with a global gravity field model. Here, we purely investigate the GNSS vertical accelerations during the static period.

In an airborne gravimetry experiment, the raw measurements from the mobile gravimeter contain not only gravity signals, but also vertical accelerations of the carrier caused by the force of inertia, which can be measured by means of GNSS. The GNSS kinematic acceleration is therefore incorporated into the gravity measurements to separate the disturbing signal. The results shown in Figure 4.9 indicate that the accuracy of the GNSS-derived vertical velocity is about 3 mm/s. The vertical acceleration is considered to be at the mm/s^2 level, which is at an order of several hundreds of mGal ($1 \text{ mGal} = 10^{-5} \text{ m/s}^2$). If we take into account that the resolution of the airborne gravity measurements is of the order of 1 mGal after low-pass filtering (Christian and Guenter, 2003; He, 2015), it is obvious that the GNSS-derived

acceleration cannot be used directly. Thus, the Fast Fourier Transform (FFT) filter was applied to extract a feasible signal from the acceleration, whereby the disturbing high-frequency noise was filtered and the low-frequency signal was retained.

The spectra of the three types of accelerations are shown in Figure 4.10. In an airborne gravimetry experiment, the FFT filter should be also applied to the gravity measurements, and the gravity signal exists within a bandwidth of 0–0.01 Hz. For low-frequency bands below 0.01 Hz, the DD accelerations have the smallest power at less than 0.5 mGal, which is reasonable since the reference station SP2X is nearby. The POP accelerations have a power of 1 mGal. However, the spectra of the PPP results are clearly larger than the others, reaching almost 2 mGal, which cannot be ignored. For DD and POP, the power of the error increases smoothly at frequencies above 0.01 Hz, but increases swiftly for PPP. This indicates that the satellite clock errors are the main sources of larger power errors in PPP accelerations.

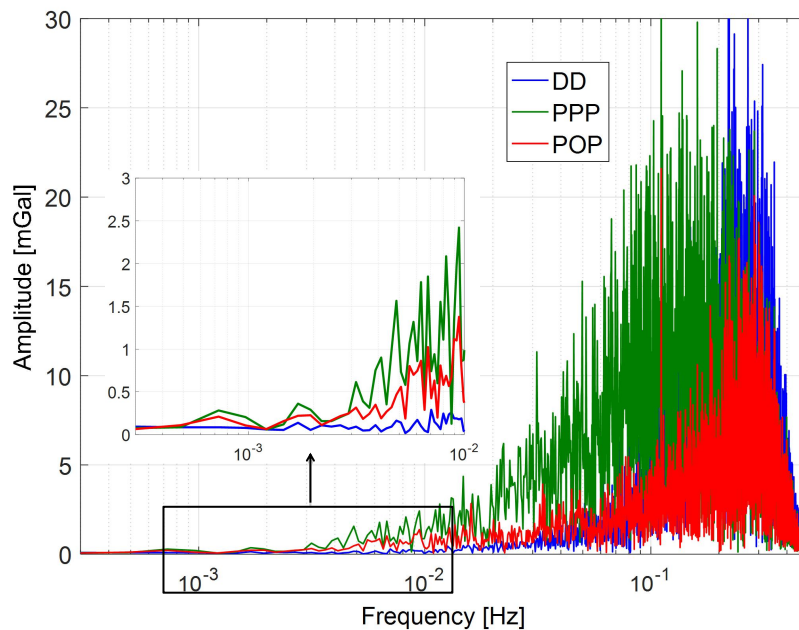


Figure 4.10 Spectra of the errors in accelerations estimated with DD, PPP, and POP methods during the static period

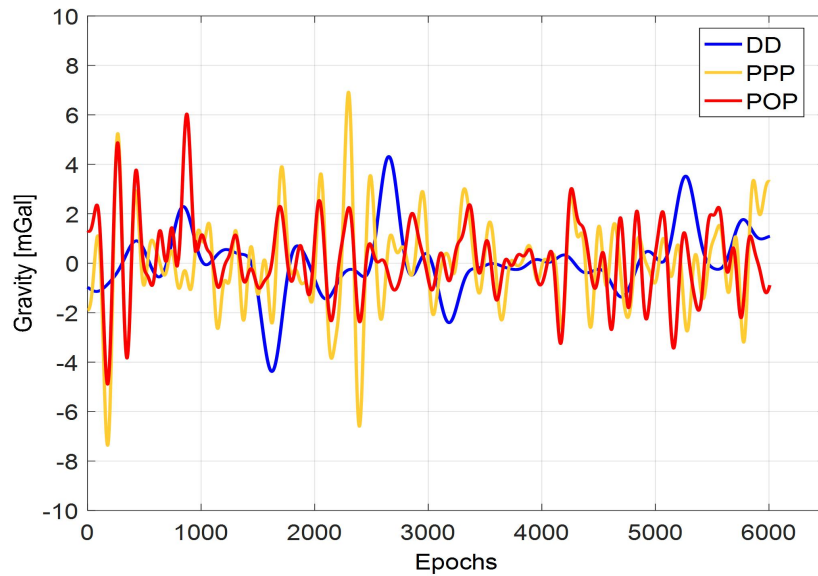


Figure 4.11 GNSS-based disturbing vertical kinematic accelerations after the application of a low-pass filter. The yellow, red, and blue results correspond to DD, POP, and PPP, respectively.

It is necessary to quantify the error in the accelerations after analyzing their power of errors. The vertical acceleration after the FFT filter with a cut-off wavelength of 200 s (Lu et al., 2017) is presented in Figure 4.11. This cut-off wavelength of 200 s is found to satisfy our requirement of 1 Hz resolution in aero-gravimetry with an aircraft speed of approximately 400 km/h, such as in the GEOHALO experiment in Italy (Lu et al., 2017). The STD values of the DD, POP, and PPP solutions are 1.30, 1.46, and 1.86 mGal, respectively. This shows that the DD solution gives the best performance, which is reasonable because the aircraft is parked close to the reference station SP2X during the static period. The value of almost 1 mGal is a realistic order of magnitude (several mGal), and is usable for separating the disturbing accelerations affecting the airborne platform.

4.5 Conclusions

In this chapter, the performance of multi-GNSS velocity and acceleration determination using DD, PPP and POP approaches over Antarctica was evaluated. The reliability and accuracy of their velocity and acceleration estimates were compared through several static tests and a real flight experiment.

The performance of the POP method for velocity and acceleration determination was evaluated using the IGS data over Antarctica. It was shown that the accuracy improvement of velocity estimation is evident using a three-station network with respect to that of a two-station network, while introducing one more station to the three-station network does not make significant improvements. However, it still needs more investigation when applying a three-station network in a flight experiment. Using the L1 observable may increase the biases as well as the RMS of velocity estimates compared to using the LC observable, which is due to the effect of ionospheric drift. The L1 observable is suggested for acceleration determination because of its lower observation noise.

Multi-GNSS velocity and acceleration determination is assessed with the POP and PPP methods. Comparisons show that regardless of POP or PPP, the accuracy was improved significantly using G/R observations with respect to that using GPS-only. However, in this study, using G/R/E/C observations do not show its advantage in the improvement of accuracy. Appropriate weighting of different types of observations is crucial. Equivalent weighting of GPS and GLONASS observations may cause a harmful effect on both velocity and acceleration estimates, whereas, posterior weighting based on their posterior variances is more reliable and robust, and can adaptively adjust the contributions of different systems. Overall, the POP method can generate higher accuracy of velocity and acceleration estimates than the PPP method.

A real flight experiment was carried out over Antarctica. Two sets of data are processed. When the aircraft was parked next to the reference station, the results showed that PPP derived velocity tended to be noisier than that of both POP and DD when comparing their solutions to a known zero-velocity reference. Comparing the results of the two kinematic flight periods, one can find the baseline length plays a significant role in the DD performance. With the increasing of the baseline length, biases as large as several cm/s could appear in the DD derived velocities. However, the POP and PPP approaches still show their advantages and reliability in long range velocity and acceleration determination. The velocity and acceleration results on two consecutive days demonstrate that the satellite clock drift errors at the day boundaries cause almost no influence on PPP velocity and acceleration estimation. It can be concluded from the two data sets processing that POP is more robust than DD with almost no biases or outliers and it will also generate smaller noise of velocities and

accelerations than PPP.

During the static period when the aircraft was parked, an accuracy of about 3 mm/s velocity can be obtained. By applying a low-pass filter, the GNSS-based disturbing kinematic vertical accelerations were found to be at the 1 mGal level, and can therefore be used to separate the disturbing kinematic accelerations affecting the airborne platform from the gravity measurements.

5 Miscellanea of velocity and acceleration determination

In this chapter, we will discuss some related topics about positioning, velocity and acceleration determination, the real-time performance, the differentiator design and the receiver clock reset.

5.1 Real-time velocity and acceleration determination

GNSS based position, velocity and acceleration are also required in real-time to satisfy many applications, such as the real-time GNSS seismology (Li et al., 2013), the automatic guidance and control of an unmanned aerial vehicle (Ding and Wang, 2011), and even in the area of athletics sports, i.e., the sport of rowing (Zhang et al., 2003). Along with the rapid development and wide applications of the airborne gravimetry, such real-time information is also demanded (Purkhauser and Pail, 2019). The acquisition of precise real-time positions has been discussed in Section 2.2.3. Here, we will focus on the real-time velocity and acceleration determination.

The most crucial aspect is the satellite velocity and acceleration derivation in real-time based on the satellite position. The satellite positions can be represented as the precise ephemeris in SP3 (Standard Product 3) format or the broadcast ephemeris with Keplerian elements. The SP3 precise ephemeris is given in Earth centered Earth fixed (ECEF) reference frame and can be directly used for post-processing. The broadcast ephemeris is usually defined in a natural orbit plane and can be used to derive the real-time satellite velocities which are important for real-time velocity and acceleration determination of a moving platform. The satellite positions in the natural orbit plane should be transformed into the ECEF system in advance.

The GPS/BDS/Galileo broadcast ephemerides are represented by the Keplerian elements, while the GLONASS is already shown as the satellite position, velocity and acceleration in the ECEF reference frame. First, the satellite positions in the natural orbit plane are calculated for GPS/BDS/Galileo, then the transformation of a satellite position from such an orbital coordinate system into the ECEF can be carried out by three rotations (Beutler, 1998; Farrell and Barth, 1999). The complexity ordinary rotation method is usually applied for determining the GPS/Galileo ECEF positions. This is the same for the BDS IGSO/MEO satellites, but not for GEO satellites. The

derivation of GEO satellite positions in ECEF from the natural orbit plane can be referred to CSNO (2013). Finally, the satellite velocity and acceleration are calculated based on the time derivative of the position closed-form formula (Zhang et al., 2005).

Zhang et al. (2006) compared the satellite velocity derived from the IGS SP3 ephemeris with that from the broadcast ephemeris calculated from the closed-form formula, and found that the accuracy of velocity derived from the broadcast ephemeris was close to those from the precise ephemeris, with differences within ± 1 mm/s for each axis component. Zheng and Tang (2017) also showed that the BDS GEO satellite velocity and clock drifts calculated from the broadcast ephemeris were comparable with that from the precise ephemeris, and the vertical velocity of a moving platform at 1 cm/s accuracy was obtained with a short baseline DD solution as reference. Therefore, the broadcast ephemeris is sufficient for real-time precise velocity determination at cm/s level.

For validation, we calculated the velocity and acceleration of IGS station “CAS1” in Antarctica with the broadcast ephemeris on day December 19, 2015. Four hours GPS and GLONASS data with a sampling interval of 1 second were processed with the PPP and POP approaches. The results are shown in Figure 5.1. We can see the velocities and accelerations are almost within ± 1 cm/s and ± 1 cm/s², respectively, accompanied with some large biases due to the poor observation quality. The POP velocities and accelerations tend to have a smaller noise than that of PPP. Overall, comparing the results with that in the static tests in Sections 4.4.1 and 4.4.2, the velocity and acceleration calculated with the broadcast ephemeris are comparable with that using the precise ephemeris.

It should be noticed that even the velocity and acceleration derived from the broadcast ephemeris are accurate enough, the derived positions are usually at sub-meter level and can hardly meet most real-time airborne gravimetry applications unless the demand of the position accuracy is not very critical. In addition, the precise ephemerides are always applied for deriving the precise position, velocity and acceleration for the calculation of the final gravity results in post-processing mode.

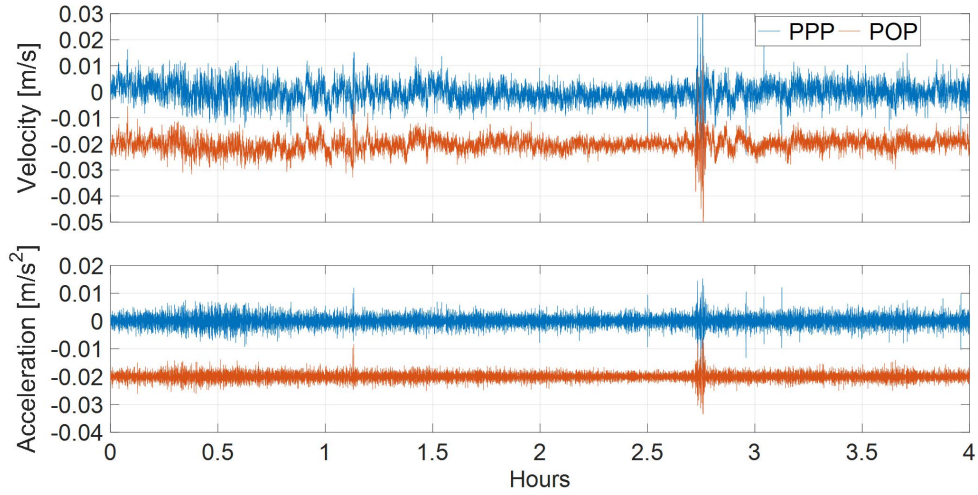


Figure 5.1 The velocity and acceleration results in the up component of IGS station “CAS1”. In order to show a visual difference, the POP numerical values are all decreased by 0.02.

5.2 Differentiator design

The derivation of the satellite velocity and acceleration from the precise ephemeris or the broadcast ephemeris all require suitable and reliable differentiators. The carrier phase measurements should also be numerically differentiated properly. Therefore, it is important to choose a reliable and practical differentiator in which the Taylor series approximation has been widely used. The differentiators used by Cannon et al. (1998) and Kennedy (2002a) were both low-order Taylor series and found performed well in geodetic applications. Such a kind of central difference approximation is expressed as:

$$y_n = \sum_{k=-N}^N c_k \cdot x_k \quad (5.1)$$

where N is the order, c_k is the coefficient of the Taylor series, x_k is the discrete numerical series, y_n is the differenced value. Instead of explaining the knowledge of signals processing, we prefer to directly apply them in velocity determination.

The 5th order Taylor series approximation was proposed and suggested to deal with the difference processing (Kennedy, 2002a; Amodio et al., 2017). Usually the sampling rate of the airborne GNSS data is 1 Hz, the bandwidth of such Taylor series appropriately covers the typical dynamics found in airborne gravimetry, which is a compromise between bandwidth, simplicity and noise suppression (Bruton et al., 2000; Kennedy, 2002a). Moreover, such an odd length ($2N + 1$) differentiating filter can

maintain an integer time property while a non-integer time delay would require interpolation (Oppenheim and Schaffer, 1999).

The impulse response of the 5th order Taylor series approximation differentiator is shown in Equation 5.2 (Beyer, 1980), where T is the sampling rate in seconds

$$h_5[n] = \frac{1}{T} \left[\frac{1}{1260} \quad \frac{-5}{504} \quad \frac{5}{84} \quad \frac{-5}{21} \quad \frac{5}{6} \quad 0 \quad \frac{-5}{6} \quad \frac{5}{21} \quad \frac{-5}{84} \quad \frac{5}{504} \quad \frac{-1}{1260} \right] \quad (5.2)$$

we can see such differentiator considers the correlations of variables at consecutive epochs. While applying the above differentiator to a discrete data set $x[n]$, a differenced signal $x'[n]$ is obtained

$$x'[i] = \sum_{j=-5}^5 h_5[j] \cdot x[i-j] \quad (5.3)$$

where i is the data number. The differencing process can be started from the second number.

Usually the Lagrange polynomial functions are used for interpolating the satellite orbit. However, it is considered that the analytical differentiation of Lagrange polynomial interpolation does not reflect the physical nature of the satellite orbit and it may cause oscillations in the satellite velocities, which is called “Runge phenomenon” (Dahlquist and Bjork, 1974). These oscillations may not cause problems when applied in positioning, but will introduce unwanted biases in the satellite velocity determination.

Two collocated IGS stations separated with a very short distance of about 3 m in Antarctica named “OHI3” and “OHI2” are chosen to test the “Runge” effect, so that almost all of the positioning errors can be eliminated in DD processing. The data was collected on day January 1, 2018 with sampling interval of 30 seconds. The GPS observation data of “OHI3” is processed in kinematic mode with “OHI2” as the reference station. Two sets of satellite velocities are calculated from the precise ephemeris by analytical differentiation of Lagrange interpolation method and Taylor series approximation filter. Then the site velocities are further calculated. Figure 5.2 shows the velocity 3D RMS results.

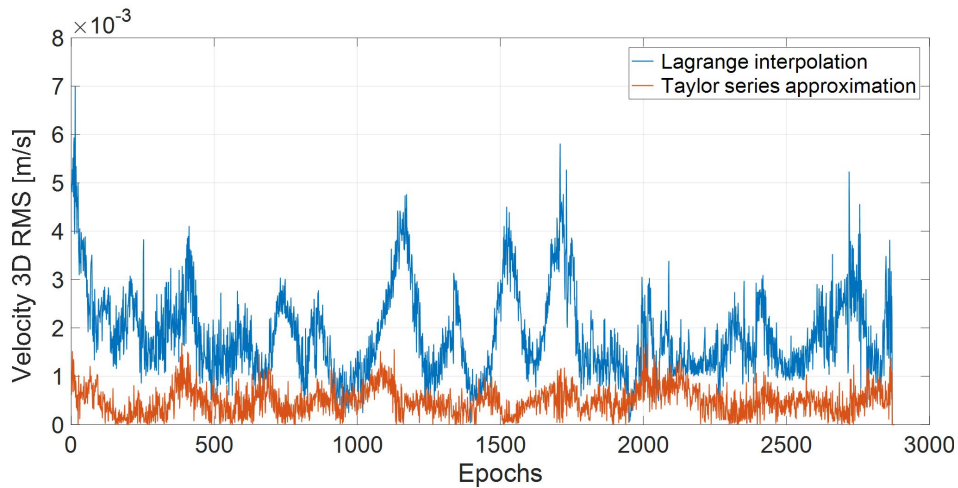


Figure 5.2 3D RMS values of velocity results for “OHI3” using the Lagrange interpolation and the Taylor series approximation.

It can be seen that there are fluctuations in the velocity results calculated with the Lagrange interpolation. The Taylor series approximation derived velocity is much more smooth and the 3D RMS values are almost below 1 mm/s. Therefore, it is significant when applying the Taylor series approximation for precise velocity determination.

5.3 Receiver clock reset

In airborne kinematic positioning, usually several different types of receivers are mounted on the aircraft. They have different mechanisms of adjusting the receiving time to synchronize with the GPS time. Generally, there are two different schemes for various GPS receivers to deal with their clock drifts. One is receiver clock steering, where the clock drift is tuned approximately to zero. The other is receiver clock reset which keeps the receiver clock time synchronized within 1 millisecond with respect to the GPS system time (Kim and Lee, 2012).

Three types of receivers named LEICA SR530, NOVATEL OEM4 and JAVAD DELTA G3T shown in Section 3.4 are used here again to illustrate the effect of clock reset. Figures 5.3 and 5.4 show the phenomenon of clock continuous steering from the LEICA and NOVATEL, meanwhile the clock millisecond jump of the JAVAD is shown in Figure 5.5.

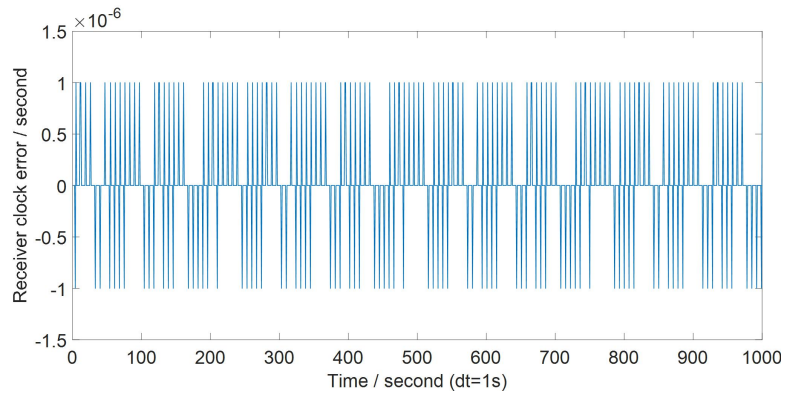


Figure 5.3 The clock continuous steering of GNSS receiver LEICA SR530

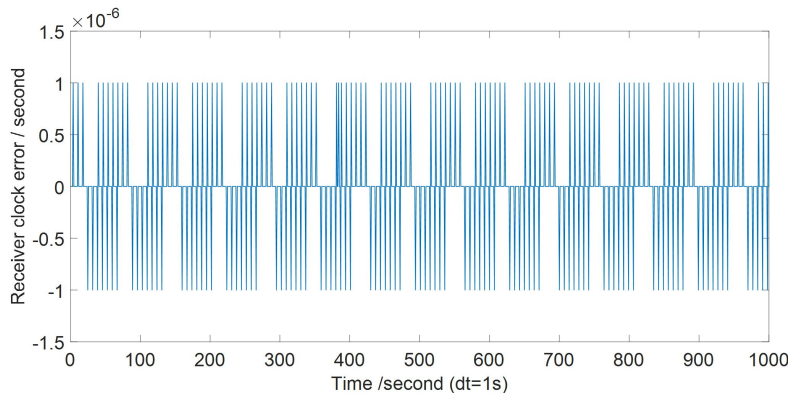


Figure 5.4 The clock continuous steering of GNSS receiver NOVATEL OEM4

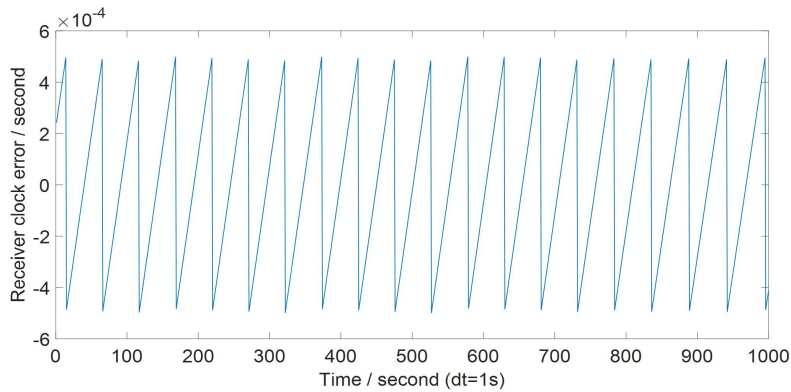


Figure 5.5 The clock millisecond jump of GNSS receiver JAVAD DELTA G3T

The clock millisecond jump of receiver JAVAD DELTA G3T will severely affect the precise positioning and velocity determination. The jumps should be corrected for both the code and carrier phase measurements for positioning, whereas only jumps in carrier phase measurements are required to be corrected for velocity and acceleration determination.

Furthermore, even if the millisecond jumps are corrected for observations from the

JAVAD type receiver, the observations of an epoch still have different time tags with that from other receivers and the time difference could reach up to more than 1 millisecond. That means the positions of the different types of receivers have different time tags, therefore they must be aligned, for example using linear interpolation to the same nominal epoch time for comparison. For instance, this is critical if we calculate and validate the distances between two collocated receivers. This is only important for receivers moving with high speed, whereas it is negligible for static or kinematic receivers with moderate speed.

In order to illustrate this impact, 1 Hz kinematic GNSS data over 10 hours collected by two receivers named AIR5 and AIR6 mounted on the HALO aircraft from the GEOHALO campaign are calculated for demonstration. Both receivers are of the JAVAD DELTA G3T type and their clock millisecond jumps are first corrected. Figure 5.6 shows the baseline lengths calculated from the estimated positions of the two receivers with and without the epoch time alignment. We can see there are periodical oscillations in the baseline lengths before interpolating, and the variations are all within 0.05 m after interpolating to the same epoch time. Therefore, the position estimates from different receivers must be interpolated to the same epoch time if their positions are all required or the constraint of baseline length is implemented in order to improve the estimation.

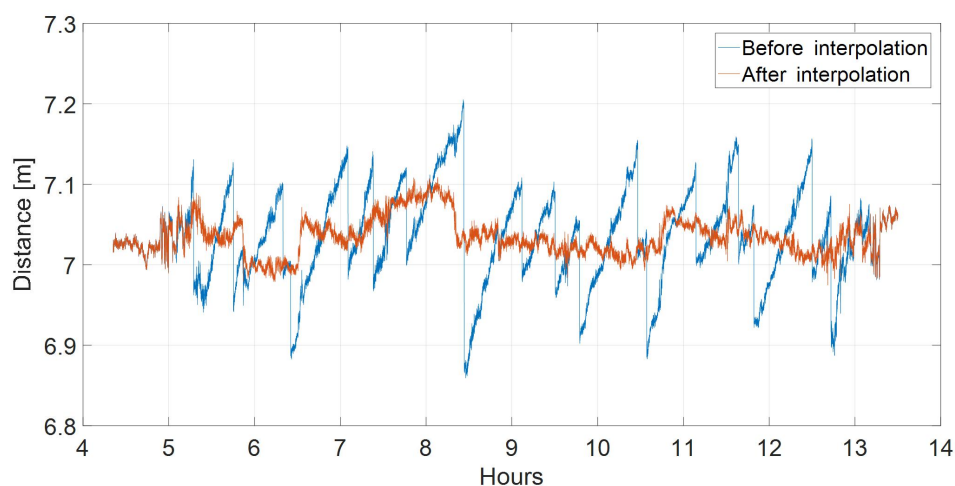


Figure 5.6 Time series of baseline length between the two GNSS receivers, calculated from the position estimates with and without interpolating to the same epoch time.

5.4 Summary

This chapter discusses miscellaneous topics about positioning, velocity and acceleration determination. First, the satellite position and velocity derived from the broadcast ephemeris for real-time precise velocity and acceleration determination is presented and the accuracy is analyzed comparable with that from the precise ephemeris. Then the 5th Taylor series approximation is introduced as the optimal differentiator to derive the satellite velocity and acceleration. Finally, the receiver millisecond jumps as well as time synchronization are discussed which is very important for receivers moving at high speed, such as the aircraft in an airborne kinematic experiment.

6 Conclusions and outlooks

The main contributions and conclusions of this thesis can be summarized as follows:

We attempt to apply an alternative approach named POP to overcome the shortcomings of the DD and PPP methods for deriving precise positions of a moving platform, especially for applications in the polar regions. Within the kinematic processing of five IGS stations in Antarctica with GPS and GLONASS data, it turns out that PPP derived positions are vulnerable to the interpolation errors of the orbits and clocks due to the discontinuities at the day boundaries. However, the POP approach which estimates the satellite clock offsets is independent of the clock behavior and the orbit errors can also be mostly absorbed by the clock estimates. It can provide more robust and accurate position estimates than PPP and an average improvement of 50% in the three coordinate components is obtained. A real flight data set covers two consecutive days is processed with DD, PPP and POP approaches. Although comparison of the three types of positional results do not suggest a clear preference for any one, with the heights generally show decimeter-level agreement, the potential of the POP approach for generating cm-level kinematic height position with sparse distributed reference stations is illustrated. It is also demonstrated that POP can be applied in real-time kinematic positioning and it can generate comparable results with post-processing. This is significant for real-time investigation of gravity measurements when applied in airborne gravimetry.

The multi-GNSS PPP and POP ambiguity resolution are performed over Antarctica with 136 globally distributed MGEX stations. First, four of the MGEX stations in Antarctica are processed in kinematic mode as moving stations. Results show that PPP and its ambiguity fixing are negatively influenced by the poor orbit quality of BDS GEO satellites. Positioning errors as large as 10 cm appear in the horizontal and vertical components of the GC solutions. However, POP can overcome such orbit errors since they can be mostly compensated by the clock estimates. POP can also achieve a higher fixing rate than PPP, an average improvement of 5.1 and 3.2%, respectively, can be obtained with GC and GREC observations. The ambiguity fixing can improve the positioning accuracy for both PPP and POP. The improvement is significant for PPP with 16.9, 29.7 and 20.0% with GE, GC and GREC observations, respectively, while the improvement for POP with the same types of observations is a

little smaller of about 11.2, 17.6 and 13.6% . Then, for the real flight experiment, it is also confirmed that POP can reduce most of large positioning errors in the PPP solutions and it becomes significant when the ambiguity fixing can accelerate the (re-)convergence for airborne kinematic positioning in the polar regions since the continuous tracking time is usually shorter than that in other regions.

A multi-GNSS POP precise velocity and acceleration determination model is presented. The performance of POP velocity and acceleration determination is validated with 1 Hz GPS data from the IGS network over Antarctica. It is found that a reference network of four stations is sufficient for the estimation of satellite clock drifts and drift rates, the accuracy of velocity and acceleration estimates is better than 5 mm/s and 3 mm/s², respectively. In a real flight experiment, usually at least two stations with one set up at the base and the other at the end of the flight are required for POP processing, some other stations can be installed along the trajectory to properly densify the network. The LC observation is required for precise velocity estimation if lower biases in the velocity are of importance; whereas the L1 observation is suggested for acceleration estimation since it has a lower observation noise than LC. Through the processing of multi-GNSS data of 30-second sampling rate, it turns out that POP yields velocity and acceleration estimates of more robustness and higher accuracy than PPP. Furthermore, including GLONASS, Galileo and BDS data can increase the accuracy of velocity and acceleration estimates of POP by 32 and 43% compared to the GPS-only solution. It is also demonstrated that appropriate weighting of different types of observations is rather important for velocity estimation. Equivalent weighting of GPS and GLONASS observations may cause a harmful effect on both velocity and acceleration estimation.

Two real flight data sets are processed with DD, PPP and POP approaches. Since there is no “reference truth” for assessing the estimated kinematic velocity and acceleration results, the differences among the results from the three approaches are calculated and analyzed. It is found that large discrepancies appear in DD–PPP and DD–POP results with the increasing of the baseline length, which indicates that the biases are more likely from the DD solutions. Meanwhile, PPP and POP generally show a good agreement in velocity and acceleration estimates. During the static period when the aircraft was parked next to one of the reference stations, the PPP derived velocities tend to be noisier than that from DD and POP. Then the

accelerations of the three approaches are derived from the corresponding velocities. After applying a low-pass filter, it is shown that POP and DD derived vertical accelerations are at the level of 1 mGal and are useful to separate the disturbing kinematic accelerations affecting the airborne platform from the gravity measurements.

Indeed, we have applied a reliable and practical method which can overcome the shortcomings of DD and PPP approaches for deriving the precise position, velocity and acceleration over Antarctica. However, there are still a number of issues worth to be investigated and implemented for better performance of GNSS to be applied in airborne gravimetry.

Due to the special gravity data processing procedure of the PolarGAP campaign, the GNSS vertical accelerations of the three processing approaches actually do not make any differences for the calculation of the final gravity results. Therefore, the GNSS vertical accelerations derived from different approaches need to be carefully compared and investigated in the future airborne gravimetry experiments to be carried out in the polar regions.

The survey data from some other sensors like laser altimetry and inertial navigation systems mounted on the aircraft can be integrated with GNSS measurements to enhance the estimation of the kinematic positions.

The low Earth orbit (LEO) satellites can track the GNSS signals, i.e., the Germany TerraSAR-X and GRACE-FO satellites, the ESA Envisat and Swarm satellites. The onboard data that observed from the GNSS satellites and terrestrial tracking data can be processed together to enhance the orbit determination for GNSS (Li et al., 2018), especially the BDS GEO satellites. Therefore, the PPP and its ambiguity fixing with BDS observations will have a better performance with the improved orbit quality of BDS.

With the completion of global coverage of BDS and Galileo systems, more satellites can be observed in polar regions which is important for the accuracy improvement of the position, velocity and acceleration especially the vertical component.

References

- Amodio, P., F. Iavernaro, F. Mazzia, M. S. Mukhametzhanov, Y. D. Sergeev (2017), A generalized Taylor method of order three for the solution of initial value problems in standard and infinity floating-point arithmetic, *Mathematics and Computers in Simulation*, 141(12), 24–39, doi: 10.1016/j.matcom.2016.03.007.
- Aoki, S., T. Ozawa, and K. Shibuya (2000), GPS observation of the sea level variation in Lützow-Holm Bay, Antarctica, *Geophysical Research Letters*, 27(15), 2285–2288, DOI: 10.1029/1999GL011304.
- ARL. (2017), The GPS Toolkit: GPSTk, (Online; October 4th, 2017), <http://www.gpstk.org/>.
- Bell, R.E., J.M. Brozena, W.F. Haxby, and J.L. LaBrecque (1990), Continental Margins of the Western Wedell Sea: Insights from airborne gravity and Geosat-derived gravity, *Contributions to Antarctic Research*, 1, 91–102.
- Bell, R.E., V.A. Childers, R.A. Arko, D.B. Lankenship, and J.M. Brozena (1999), Airborne gravity and precise positioning for geologic applications, *J. Geophys. Res.*, 104(B7), 15281–15292.
- Beutler, G. (1998), GPS Satellite Orbits, In P. J. G. Teunissen and A. Kleusberg (Ed.) *GPS for Geodesy*, Springer-Verlag Berlin Heidelberg, Berlin, Germany, pp. 43–110, ISBN:3-540-63661-7.
- Beyer, W.H. (1980), *Handbook of Mathematical Sciences*, 5th Edition, CRC Press, Florida, USA.
- Bock, H., U. Hugentobler, G. Beutler (2003), Kinematic and dynamic determination of trajectories for low Earth satellites using GPS, In: Reigber, C., H. Lühr, P. Schwintzer (eds) *First CHAMP mission results for gravity, magnetic and atmospheric studies*, Springer, Heidelberg, pp 65–69.
- Brozena, J.M., G.L. Mader, and M.F. Peters (1989), Interferometric Global Positioning System: Three-Dimensional Positioning Source for Airborne Gravimetry, *J. Geophys. Res.*, 94(B9), 12153–12162.
- Brozena, J.M., M.F. Peters, and R. Salman (1996), Arctic airborne gravity measurement program, In: Segawa, J., Fujimoto, H. and Okubu, S. (eds) *Gravity, Geoid and Marine Geodesy, Proceedings of the IAG Symposia 117*, Springer, Heidelberg, pp. 131–138.
- Bruton, A.M. (2000), Improving the accuracy and resolution of SINS/DGPS airborne gravimetry, PhD thesis, Department of Geomatics Engineering, University of Calgary, Calgary, Alberta, Canada, Report No. 20145.
- Cannon, M.E., G. Lachapelle, M.C. Szarmes, J.M. Hebert, J. Keith, and S. Jokerst (1997), DGPS kinematic carrier phase signal simulation analysis for precise velocity and position determination, *NAVIGATION, Journal of the Institute of Navigation*, 44(2), 231–246.
- Castleden, N., G.R. Hu, D.A. Abbey, D. Weihing, O. Ovstedal, C.J. Earls, and W.E. Featherstone (2005), First results from virtual reference station (VRS) and precise point positioning (PPP) GPS research at the Western Australian Centre for Geodesy, *J. GPS*, 3(1–2), 79–84.
- CSNO (2013), BeiDou navigation satellite system signal in space interface control document-open service signal, version 2.0, China Satellite Navigation Office, December 2013.
- CSNO (2018), Development of the BeiDou Navigation Satellite System, version 3.0, China Satellite Navigation Office, December 2018, available online:

<http://en.beidou.gov.cn/SYSTEMS/Officialdocument/201812/P020181227424679580428.pdf>.

- Christian, K. and W.H. Guenter (2003), GNSS based kinematic acceleration determination for airborne vector gravimetry-Methods and Results, ION GPS/GNSS 2003, Institute of Navigation, Portland, OR, USA, September 9-12, 2679–2691.
- Collins, P., F. Lahaye, P. Héroux, and S. Bisnath (2008), Precise Point Positioning with Ambiguity Resolution using the Decoupled Clock Model, In: Proceedings of ION-GNSS-2008, Savannah, Georgia, USA, September 2008, 16-19, 1315-1322.
- Colosimo, G., M. Crespi, and A. Mazzoni (2011), Real-time GPS seismology with a stand-alone receiver: a preliminary feasibility demonstration, *J. Geophys. Res.: Solid Earth*, 116(B11302), doi:10.1029/2010JB007941.
- Dahlquist, G. and A. Bjork (1974), Numerical methods, Prentice Hall, Englewood Cliffs, ISBN:0-13-627315-7.
- Defraigne, P., C. Bruyninx, and N. Guyenon (2007), GLONASS and GPS PPP for time and frequency transfer, In: Proceedings of the EFTF 2007, Geneva, Switzerland, May 29– June 1, pp 909–913.
- Ding, W. and J. Wang (2011), Precise velocity estimation with a stand-alone GPS receiver, *The Journal of Navigation*, 64(2), 311–325.
- Dong, D. and Y. Bock (1989), Global positioning system network analysis with phase ambiguity resolution applied to crustal deformation studies in California, *J. Geophys. Res.*, 94(B4), 3949–3966.
- Douša, J. (2010), The impact of errors in predicted GPS orbits on zenith troposphere delay estimation, *GPS Solut.*, 14(3), 229–239, doi:10.1007/s10291-009-0138-z.
- Farrell, J. A. and M. Barth (1999), *The Global Positioning System & Inertial Navigation*, McGraw-Hill, ISBN: 0-07-022045-X.
- Ferguson, S. and Y. Hammada (2000), Experiences with AIRGrav: Results from a New Airborne Gravimeter, In Proceedings of the IAG International Symposium in Geodesy, Geoid, and Geodynamics, July 31–August 4, Banff, Canada.
- Forsberg, R. and M.G. Sideris (1993), Geoid computations by the multi-band spherical FFT approach, *Manuscripta Geodaetica*, 18, 82–90.
- Forsberg, R., K. Hehl, L. Bastos, A. Giskehaug, and U. Meyer, Development of an airborne geoid mapping system for coastal oceanography (AGMASCO) (1997), in Proceedings of the International Symposium on Gravity, Geoid and Marine Geodesy, GRAGEOMAR, edited by J. Segawa, H. Fujimoto, and S. Okubo, The University of Tokyo, Tokyo, Sept. 30–Oct. 5, 1996, Springer-Verlag, pp. 163–170, 1997.
- Forsberg, R., A.V. Olesen, K. Keller, M. Møller, A. Gidskehaug, and D. Solheim (2001), Airborne gravity and geoid surveys in the Arctic and Baltic seas, Proceedings of International Symposium on Kinematic Systems in Geodesy, Geomatics and Navigation (KIS-2001), Banff, June 2001, pp. 586–593.
- Forsberg, R. and A.V. Olesen (2010), Airborne gravity field determination. In: Xu, G. (ed.) *Sciences of Geodesy-I*. Heidelberg, London, New York: Springer.
- Fotopoulos, G. and M.E. Cannon (2001), An overview of multi-reference station methods for cm-level positioning, *GPS Solut.*, 4(3), 1–10.
- Ge, M., G. Gendt, G. Dick, and F.P. Zhang (2005), Improving carrier-phase ambiguity resolution in global GPS network solutions, *J. Geod.*, 79(1-3), 103–110, doi:10.1007/s00190-005-0447-0.
- Ge, M., G. Gendt, M. Rothacher, C. Shi, and J. Liu (2008), Resolution of GPS carrier

- phase ambiguities in Precise Point Positioning (PPP) with daily observations, *J. Geod.*, 82(7), 389–399, doi:10.1007/s00190-007-0187-4.
- Ge, M., J. Chen, J. Douša, G. Gendt, and J. Wickert (2012), A computationally efficient approach for estimating high-rate satellite clock corrections in realtime, *GPS Solut.*, 16(1), 9–17.
- Geng, J., C. Shi, M. Ge, A.H. Dodson, Y. Lou, Q. Zhao, and J. Liu (2012), Improving the estimation of fractional-cycle biases for ambiguity resolution in precise point positioning, *J. Geod.*, 86(8), 579–589, doi:10.1007/s00190-011-0537-0.
- Geng, J., J. Guo, H. Chang (2019), Toward global instantaneous decimeter-level positioning using tightly coupled multi-constellation and multi-frequency GNSS, *J. Geod.*, 93: 977, <https://doi.org/10.1007/s00190-018-1219-y>.
- Gerlach, C., R. Dorobantu, C. Ackermann, N.S. Kjørsvik, and G. Boedecker (2010), Preliminary results of a GPS/INS airborne gravimetry experiment over the German Alps, In: *Gravity, Geoid and Earth Observation*, Springer, Berlin, Heidelberg, pp. 3–9.
- Han, S. (1997), Carrier phase-based long-range GPS kinematic positioning, PhD thesis, School of Geomatic Engineering, The University of New South Wales.
- Han, S. and C. Rizos (1999), Sea surface determination using long range kinematic GPS positioning and laser airborne depth sounder techniques, *Mar. Geod.*, 22(2), 195–203.
- Hatch, R. (1982), The synergism of GPS code and carrier measurements, In: *Proceedings of the third international symposium on satellite Doppler positioning at Physical Sciences Laboratory of New Mexico State University*, February 8–12 1982, vol 2, 1213–1231.
- He, K. (2015), DGNSS Kinematic Position and Velocity Determination for Airborne Gravimetry, Scientific Technical Report 15/04, GFZ German Research Centre for Geosciences, doi:10.2312/GFZ.b103-15044.
- He, K., G. Xu, T. Xu, and F. Flechtner (2016), GNSS navigation and positioning for the GEOHALO experiment in Italy, *GPS Solut.*, 20(2), 215–224.
- Hohensinn, R., A. Geiger, and M. Meindl (2018), Minimum Detectable Velocity Based on GNSS Doppler Phase Observables, 2018 European Navigation Conference (ENC), Gothenburg, pp. 121–128. doi: 10.1109/EURONAV.2018.8433228.
- Jekeli, C. (1994), On the computation of vehicle accelerations using GPS phase accelerations, *Proceedings of the international symposium on kinematic systems in geodesy, Geomatics and Navigation (KIS94)*, Banff, Canada, pp. 473–481.
- Jekeli, C. and R. Garcia (1997), GPS phase accelerations for moving-base vector gravimetry, *J. Geod.*, 71(10), 630–639, doi:10.1007/s001900050130.
- Jiang, N., Y. Xu, T. Xu, G. Xu, Z. Sun, and H. Schuh (2016), GPS/BDS short-term ISB modelling and prediction, *GPS Solut.*, 21(1), 163–175. doi:10.1007/s10291-015-0513-x.
- Jordan, T., C. Robinson, A. Olesen, R. Forsberg, and K. Matsuoka (2016), PolarGap 2015/16: Filling the GOCE polar gap in Antarctica and ASIRAS radar flight for CryoSat support, Data acquisition report, European Space Agency (ESA).
- Kazmierski, K., K. Sośnica, and T. Hadas (2018) Quality assessment of multi-GNSS orbits and clocks for real-time precise point positioning, *GPS Solut.*, 22(11), doi:10.1007/s10291-017-0678-6.
- Kennedy, S., A. Bruton, and K. Schwarz (2001), Improving DGPS Accelerations for Airborne Gravimetry: GPS Carrier Phase Accelerations Revisited, In *Proceedings of IAG 2001 Scientific Assembly*, September 2 – 7, Budapest,

- Hungary.
- Kennedy, S. (2002a), Acceleration estimation from GPS carrier phases for airborne gravimetry, Master's thesis, Department of Geomatics Engineering, University of Calgary, Calgary, Alberta, Canada Report No. 20160.
- Kennedy, S. (2002b), Precise acceleration determination from carrier phase measurements, Proceedings of the 15th international technical meeting of the satellite division of the Institute of Navigation, ION GPS 2002, Portland, USA, September 24–27, 962–972.
- Kim, H.S. and H.K. Lee (2012), Elimination of Clock Jump Effects in Low-Quality Differential GPS Measurements, *Journal of Electrical Engineering & Technology*, 7, 626-635.
- Kleusberg, A., D. Peyton, and D. Wells (1990), Airborne Gravimetry and the Global Positioning System, In Proceedings of IEEE 1990, pp.273-278.
- Koch, K.R. (1999), Parameter Estimation and Hypothesis Testing in Linear Models (Second, Updated and Enlarged Edition), Berlin: Springer.
- Kouba, J. and P. Heroux (2001), Precise point positioning using IGS orbit and clock products, *GPS Solut.*, 5(2), 12–28, doi:10.1007/PL00012883.
- Kouba, J. (2009), A guide to using international GNSS service (IGS) products, <http://igsceb.jpl.nasa.gov/igsceb/resource/pubs/UsingIGSProductsVer21.pdf>.
- LaCoste, L.J.B. (1967), Measurement of gravity at sea and in the air, *Rev. Geophys.*, 5, 477–526.
- Langley, R.B. (1991), The orbits of GPS satellites, *GPS world*, 2(3), 50-53.
- Laurichesse, D. and F. Mercier (2007), Integer ambiguity resolution on undifferenced GPS phase measurements and its application to PPP, ION, In: GNSS 20th international technical meeting of the satellite division, Fort Worth, USA, September 25–28 2007, 839–848.
- Leick, A., L. Rapoport, and D. Tatarnikov (2015), *GPS satellite surveying*, 4th edn, Wiley, Hoboken.
- Li, M., K. He, T. Xu, and B. Lu (2018), Robust adaptive filter for shipborne kinematic positioning and velocity determination during the Baltic Sea experiment, *GPS Solut.*, 22(81), doi:10.1007/s10291-018-0747-5.
- Li, M., T. Xu, B. Lu, and K. He (2019), Multi-GNSS Precise Orbit Positioning for airborne gravimetry over Antarctica, *GPS Solut.*, 23(2), doi: 10.1007/s10291-019-0848-9.
- Li, X., M. Ge, X. Zhang, Y. Zhang, B. Guo, R. Wang, J. Klotz, and J. Wickert (2013), Real-time high-rate co-seismic displacement from ambiguity-fixed precise point positioning: Application to earthquake early warning, *Geophys. Res. Lett.*, 40(2), 295-300, doi:10.1002/grl.50138.
- Li, X., M. Ge, X. Dai, X. Ren, M. Fritsche, J. Wickert, and H. Schuh (2015), Accuracy and reliability of multi-GNSS real-time precise positioning: GPS, GLONASS, BeiDou, and Galileo, *J. Geod.*, 89(6), 607–635.
- Li, X., X. Li, Y. Yuan, K. Zhang, X. Zhang, and J. Wickert (2017), Multi-GNSS phase delay estimation and PPP ambiguity resolution: GPS, BDS, GLONASS, Galileo, *J. Geod.*, 2017, 92(6), 579-608, doi:10.1007/s00190-017-1081-3.
- Li, X., X. Chen, M. Ge, and H. Schuh (2018), Improving multi-GNSS ultra-rapid orbit determination for real-time precise point positioning, *J. Geod.*, 93(1), 45-64, doi:10.1007/s00190-018-1138-y.
- Li, B., H. Ge, M. Ge, L. Nie, Y. Shen, and H. Schuh (2018), LEO enhanced Global Navigation Satellite System (LeGNSS) for real-time positioning services, *Advances in Space Research*, doi: 10.1016/j.asr.2018.08.017.

- Liu, Y., J. Zhu, S. Ye, and W. Song (2018), Real-Time Phase Bias Estimation for BeiDou Satellites Based on Consideration of Orbit Errors, *Remote Sens.*, 10(7), 1009, doi:10.3390/rs10071009.
- Liu, Y., S. Ye, W. Song, and Q. Li (2018), Estimating the orbit error of BeiDou GEO satellites to improve the performance of multi-GNSS PPP ambiguity resolution, *GPS Solut.*, 22(84), 101–122, doi: 10.1007/s10291-018-0751-9.
- Lou, Y., X. Gong, S. Gu, F. Zheng, and Y. Feng (2017), Assessment of code bias variations of BDS triple-frequency signals and their impacts on ambiguity resolution for long baselines, *GPS Solut.*, 21(1), 177–186.
- Lu, B., F. Barthelmes, S. Petrovic, C. Förste, F. Flechtner, Z. Luo, K. He, and M. Li (2017), Airborne gravimetry of GEOHALO mission: data processing and gravity field modeling, *J. Geophys. Res.: Solid Earth*, 122, 10586–10604, <https://doi.org/10.1002/2017JB014425>.
- Lu, B., C. Förste, F. Barthelmes, S. Petrovic, F. Flechtner, Z. Luo, B. Zhong, and H. Zhou (2019), Global gravity field model IGGT_R1C without the disturbing impact of the GOCE polar gap by combining GOCE, GRACE and polar terrestrial gravimetry data, submitted to *Journal of Geodesy*, under review.
- Malys, S. and P.A. Jensen (1990), Geodetic Point Positioning with GPS Carrier Beat Phase Data from the CASA UNO Experiment, *Geophysical Research Letters*, 17(5), 651–654.
- Mogren, S. (2019), High-Precision Gravity Measurements in Riyadh Using FGL Absolute Gravimeter, In: Sundararajan N., Eshagh M., Saibi H., Meghraoui M., Al-Garni M., Giroux B. (eds) *On Significant Applications of Geophysical Methods, Advances in Science, Technology & Innovation (IEREK Interdisciplinary Series for Sustainable Development)*, Springer, Cham.
- Montenbruck, O. and E. Gill (2000), *Satellite orbits: models, methods, applications*, Springer, Berlin Heidelberg, New York.
- Montenbruck, O., P. Steigenberger, L. Prange, Z. Deng, Q. Zhao, F. Perosanz (2017) The multi-GNSS experiment (MGEX) of the international GNSS service (IGS)—achievements, prospects and challenges, *Adv Space Res*, 59(7), 1671–1697.
- Moritz, H. (1980), *Advanced Physical Geodesy*, Wichmann Verlag, Karlsruhe, ISBN:9783879071951.
- Mostafa, M.R. (2005), Precise airborne GPS positioning alternatives for the aerial mapping practice, In: *Proceedings of FIG working week 2005 and GSDI-8*, Cairo, 16–21, April 2005.
- Moulborne, W.G. (1985), The case for ranging in GPS-based geodetic systems, In: *Proceedings first international symposium on precise positioning with the global positioning system*, Rockville, USA, April 15–19 1985, 373–386.
- Neumeyer, J., F. Barthelmes, O. Dierks, F. Flechtner, M. Harnisch, G. Harnisch, J. Hinderer, Y. Imanishi, C. Kroner, B. Meurers, S. Petrovic, C. Reigber, R. Schmidt, P. Schwintzer, S. HP, and H. Virtanen (2006), Combination of temporal gravity variations resulting from superconducting gravimeter (SG) recordings, GRACE satellite observations and global hydrology models, *J. Geod.*, 79(10–11), 573–585, <https://doi.org/10.1007/s00190-005-0014-8>.
- Novák, P., M. Kern, K.P. Schwarz, M.G. Sideris, B. Heck, S. Ferguson, Y. Hammada, and M. Wei (2003), On geoid determination from airborne gravity, *J. Geod.*, 76(9–10), 510–522.
- NRC (National Research Council) (1995), *Airborne Geophysics and Precise Positioning: Scientific Issues and Future Direction*, In *Proceedings of the Workshop on Airborne Geophysics*, July 12-14 1995, Washington, D.C.,

- National Academy Press.
- Olesen, A.V. (2002), Improved Airborne Scalar Gravimetry for Regional Gravity Field Mapping and Geoid Determination, Ph.D. dissertation, University of Copenhagen, Copenhagen.
- Oppenheim, A.V. and R.W. Schaffer (1999), Discrete-Time Signal Processing, 2nd Edition, Upper Saddle River, New Jersey, Prentice-Hall.
- Purkhauer, A. F., R. Pail (2019), Next generation gravity missions: near-real time gravity field retrieval strategy, *Geophysical Journal International*, 217(2), 1314–1333, <https://doi.org/10.1093/gji/ggz084>.
- Reussner, N. and L. Wanninger (2011), GLONASS Inter-frequency biases and their effects on RTK and PPP carrier phase ambiguity resolution, *Proceedings ION-GNSS-2011*, Institute of Navigation, Portland, OR, 712–716.
- Ruan, R. and Z. Wei (2019), Between-satellite single-difference integer ambiguity resolution in GPS/GNSS network solutions, *J. Geod.*, 93: 1367, <https://doi.org/10.1007/s00190-019-01251-z>.
- Salazar, D., M. Hernandez-Pajares, J. Juan-Zornoza, and J. Sanz-Subirana (2009), GNSS data management and processing with the GPSTk, *GPS Solut.*, 14(3), 293–299, doi: 10.1007/s10291-009-0149-9.
- Salazar, D., M. Hernandez-Pajares, J. Juan-Zornoza, J. Sanz-Subirana, and A. Aragon-Angel (2011), EVA: GPS-based extended velocity and acceleration determination, *J. Geod.*, 85(6), 329–340, doi:10.1007/s00190-010-0439-6.
- Salychev, O.S. and K.P. Schwarz (1995), Airborne Gravimetric Results obtained with the ITC-2 Inertial Platform System, In *Proceedings IAG Symposium G4 Airborne Gravity Field Determination, XXI General Assembly of the IUGG*, July 2–14, Boulder, Colorado, pp.125–141.
- Scambos, T. A., R. E. Bell, R. B. Alley, S. Anandakrishnan, D. H. Bromwich, K. Brunt,..., P. L. Yager (2017), How much, how fast?: A science review and outlook for research on the instability of Antarctica's Thwaites glacier in the 21st century, *Global and Planetary Change*, 153, 16–34, DOI: 10.1016/j.gloplacha.2017.04.008.
- Schaller, T., M. Scheinert, F. Barthelmes, C. Förste (2019), Inversion of GEOHALO aerogravimetry to infer ocean bottom topography: application to the Tyrrhenian, Ionian and Adriatic seas, *Geophysical Journal International*, 216(2), 840–850, <https://doi.org/10.1093/gji/ggy456>.
- Schlamminger, S. (2018), Gravity measured with record precision, *Nature*, 560(7720), 562 – 563, doi: 10.1038/d41586-018-06028-6.
- Schwarz, K.P., O. Colombo, G. Hein, and E.T. Knickmeyer (1991), Requirements for Airborne Vector Gravimetry, *Proceedings of the IAG Symposium G3 'From Mars to Greenland: Charting Gravity with Space and Airborne Instruments'*, Springer-Verlag, New York, pp. 273–283.
- Schwarz, K.P. and Z. Li (1997), An introduction to airborne gravimetry and its boundary value problems, In: *Geodetic Boundary Value Problems in View of the One Centimeter Geoid.*, Springer, Berlin, Heidelberg, pp. 312–358.
- Serrano, L., D. Kim, and R.B. Langley (2004), A single GPS receiver as a real-time, accurate velocity and acceleration sensor, *Proceedings of the ION GNSS*, The Institute of Navigation, Long Beach, California, September 21-24, 2021–2034.
- Teunissen, P., and S. Verhagen (2009), GNSS Carrier Phase Ambiguity Resolution: Challenges and Open Problems, In: Sideris M.G. (eds) *Observing our Changing Earth. International Association of Geodesy Symposia*, vol 133. Springer, Berlin, Heidelberg.

- Teunissen, P.J.G., and A. Khodabandeh (2019), GLONASS ambiguity resolution, *GPS Solut.*, 23(101), <https://doi.org/10.1007/s10291-019-0890-7>.
- Tian, Y., M. Ge, and F. Neitzel (2015), Particle filter-based estimation of Inter-frequency phase bias for real-time GLONASS integer ambiguity resolution, *J. Geod.*, 89(11), 1145–1158, doi:10.1007/s00190-015-0841-1.
- van Dierendonck, K.J., M.E. Cannon, M. Wei, and K.P. Schwarz (1994), Error Sources in GPS-Determined Acceleration for Airborne Gravimetry, In *Proceedings of ION Technical Meeting*, January 24-26, San Diego, CA, pp.811-820.
- van Graas, F. and A. Soloviev (2004), Precise velocity estimation using a stand-alone GPS receiver, *Navigation*, 51(4), 283–292.
- Verhagen, S (2016), GNSS Ambiguity Resolution and Validation, In: Grafarend E. (eds) *Encyclopedia of Geodesy*. Springer, Cham.
- Wang, J., C. Rizos, M.P. Stewart, and A. Leick (2001), GPS and GLONASS integration: modeling and ambiguity resolution issues, *GPS Solut.*, 5(1), 55–64.
- Wanninger, L (2012), Carrier phase inter-frequency biases of GLONASS receivers, *J. Geod.*, 86(2), 139–148.
- Wanninger, L. and S. Beer (2014), BeiDou satellite-induced code pseudorange variations: diagnosis and therapy, *GPS Solut.*, 19(4), 639–648, doi:10.1007/s10291-014-0423-3.
- Williams, S. and J.D. MacQueen (2001), Development of a versatile, commercially proven, and cost-effective airborne gravity system, *The Leading Edge*, 20(6), 651–654.
- Wübbena, G. (1985), Software developments for geodetic positioning with GPS using TI-4100 code and carrier measurements, In: *Proceedings of first international symposium on precise positioning with the global positioning system*, Rockville, USA, April 15-19 1985, 403–412.
- Xu, G. (2007), *GPS: theory, algorithms and applications*, 2nd Edn. Springer, New York.
- Yang, Y., J. Li, A. Wang, J. Xu, H. He, H. Guo, J. Shen, and X. Dai (2014), Preliminary assessment of the navigation and positioning performance of BeiDou regional navigation satellite system, *Science China Earth Sciences*, 57(1), 144–152.
- Yalvac, S., M. Berber (2018), Galileo satellite data contribution to GNSS solutions for short and long baselines, *Measurement*, 124, 173–178, <https://doi.org/10.1016/j.measurement.2018.04.020>.
- Zhang, J., K. Zhang, and R. Grenfell (2005), On Real-Time High Precision Velocity Determination for Standalone GPS Users, *Survey Review*, 40(310), 366-378.
- Zhang, J., K. Zhang, R. Grenfell, and R. Deakin (2006), GPS Satellite Velocity and Acceleration Determination Using the Broadcast Ephemeris, *Journal of Navigation*, 59, pp. 293-305.
- Zhang, J. (2007), *Precise velocity and acceleration determination using a standalone GPS receiver in real time*, PhD Thesis, RMIT University, Melbourne, Australia.
- Zhang J., K. Zhang, R. Grenfell, and R. Deakin (2008), On real-time high precision velocity determination for standalone GPS users, *Surv. Rev.*, 40(310), 366–378.
- Zhang, K., R. Grenfell, R. Deakin, Y. Li, J. Zhang, A. Hahn, C. Gore and T. Rice (2003), Towards a Low-cost, High Output Rate, Real Time GPS Rowing Coaching and Training System, *Proceedings of the ION GPS/GNSS 2003*, Portland, Oregon, USA, pp. 489-498.
- Zhang, X. and D. E (2005), Velocity of Surface Ice flow on Amery Ice Shelf

- determined with PPP, *Geo-spatial Information Science*, 8: 251, <https://doi.org/10.1007/BF0283865>.
- Zhang, X. and O.B. Andersen (2006), Surface Ice Flow Velocity and Tide Retrieval of the Amery Ice Shelf using Precise Point Positioning, *J Geodesy*, 80(171), <https://doi.org/10.1007/s00190-006-0062-8>.
- Zhang, X. and R. Forsberg (2007), Assessment of long-range kinematic GPS positioning errors by comparison with airborne laser altimetry and satellite altimetry, *J. Geod.*, 81(3), 201–211, doi:10.1007/s00190-006-0100-6.
- Zhang, X., K. Zheng, C. Lu, J. Wan, Z. Liu, and X. Ren (2017), Acceleration estimation using a single GPS receiver for airborne scalar gravimetry, *Adv. Space Res.*, 60(10), 2277-2288, <http://dx.doi.org/10.1016/j.asr.2017.08.038>.
- Zhang, X., M. Wu, W. Liu, X. Li, S. Yu, C. Lu, and J. Wickert (2017), Initial assessment of the COMPASS/BeiDou-3: new-generation navigation signals, *J. Geod.*, 91(10), 1225–1240.
- Zheng, K. and L. Tang (2016), Performance Assessment of BDS and GPS/BDS Velocity Estimation with Stand-alone Receiver, *The Journal of Navigation* 69(4), 869–882, doi:10.1017/S0373463315000958.
- Zumberge, J.F., M.B. Heflin, D.C. Jefferson, M.M. Watkins, and F.H. Webb (1997), Precise point positioning for the efficient and robust analysis of GPS data from large networks, *J. Geophys. Res.*, 102(B3), 5005–5017, doi:10.1029/96JB03860.

Acknowledgments

The completion of this thesis would not have been possible without the great help and support of a number of people and organizations.

First and foremost, I would like to express my sincere gratitude to my supervisors, Prof. Dr. Frank Flechtner, Dr. Christoph Förste, and Prof. Dr. Maorong Ge, at the German Research Centre for Geosciences (GFZ) and Prof. Dr. Tianhe Xu, at Shandong University (Weihai), for their patient guidance, valuable suggestions and continuous encouragement throughout my four years' study at GFZ as a Ph.D. student. They were always willing to share their insights and gave me suggestions and responded to my questions and queries promptly.

I feel grateful to Prof. Dr. Tianhe Xu for his continuous help and support with my work and publications. I owe a special gratitude to Prof. Dr. Maorong Ge, whose selfless and extensive support and guidance always inspire me step forward.

I would like to thank my current and former colleagues at GFZ, Dr. Svetozar Petrovic, Dr. Franz Barthelmes, Dr. Elmas Sinem Ince, Hartmut Pflug, Angelika Svarovsky, Dr. Zhiguo Deng, Dr. Kaifei He, Dr. Yan Xu, Dr. Nan Jiang, Dr. Biao Lu and many other Ph.D. students; Dr. Karl-Hans Neumayer, Dr. Rolf König, Dr. Jean-Claude Raimondo, Dr. Christian Gruber, Dipl.-Ing. Christoph Dahle, Dr. Grzegorz Michalak, Dr. Michael Murbock, Dipl.-Ing. Anton Reinhold, Patrick Schreiner, Ingbert Meyer, Karin Bogner, for their kind help to my academic study and daily life.

I am very thankful to Dr. Fausto Ferraccioli from British Antarctic Survey and Prof. Dr. René Forsberg from Danish Technical University / National Space Institute for providing the GNSS data from ESA's PolarGAP campaign, Prof. Dr. Frank Flechtner and Dr. Christoph Förste are also thanked for their help in data acquisition, which is a key to the accomplishment of my thesis.

Gratefully acknowledged is the China Scholarship Council (CSC), which had financially supported my Ph.D. research during the four years. Also many thanks to GFZ in Potsdam and outer branch in Oberpfaffenhofen and Technische Universität Berlin (TU Berlin) for hosting and supporting my work.

Finally, I would like to express my gratitude to my family for their endless understanding, support and encouragement. The person I wish to thank most is my girlfriend, Xiaoyun Xu, who fills my heart with confidence, courage and love all the time.